AD-A081 304 TORONTO UNIV DOWNSVIEW (ONTARIO) INST FOR AEROSPACE --ETC F/G 20/4
APPLICATIONS OF RANDOM-CHOICE METHOD TO PROBLEMS IN SHOCK AND D--ETC(U)
OCT 79 T SAITO, I I GLASS AFOSR-77-3303
UNCLASSIFIED UTIAS-240 AFOSR-TR-80-0144 NL

1 OF 1
AD A081304

END
DATE FILMED
4-80
DTIC

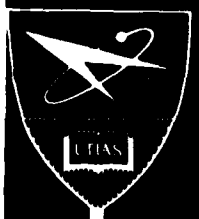

INSTITUTE
FOR
AEROSPACE STUDIES

UNIVERSITY OF TORONTO

(12) 5

APPLICATIONS OF RANDOM-CHOICE METHOD TO PROBLEMS IN SHOCK AND DETONATION-WAVE DYNAMICS

by

T. Saito and I. I. Glass

AFOSR-77-3303

October, 1979

UTIAS Report No. 240
CN ISSN 0082-5255

APPLICATIONS OF RANDOM-CHOICE METHOD

TO PROBLEMS IN SHOCK AND DETONATION-WAVE DYNAMICS

by

T. Saito and I. I. Glass

Submitted August, 1979

October, 1979

UTIAS Report No. 240
CN ISSN 0082-5255

SECURITY CLASSIFICATION (When Data Entered) Unclassified

REPORT DOCUMENTATION PAGE

READ INSTRUCTIONS BEFORE COMPLETING FORM

1. REPORT NUMBER: AFOSR-TR-80-0144	2. GOVT ACCESSION NO.
3. RECIPIENT'S CATALOG NUMBER	
4. TITLE (and Subtitle): APPLICATIONS OF RANDOM-CHOICE METHOD TO PROBLEMS IN SHOCK AND DETONATION-WAVE DYNAMICS	5. TYPE OF REPORT & PERIOD COVERED: INTERIM rept.
6. PERFORMING ORG. REPORT NUMBER: UTIAS-240	
7. AUTHOR(s): T. SAITO, I. I. GLASS	8. CONTRACT OR GRANT NUMBER(s): AFOSR-77-3303
9. PERFORMING ORGANIZATION NAME AND ADDRESS: UNIVERSITY OF TORONTO, INSTITUTE FOR AEROSPACE STUDIES, DOWNSVIEW, ONTARIO, CANADA M3H 5T6	10. PROGRAM ELEMENT, PROJECT, TASK AREA & WORK UNIT NUMBERS: 61102F, 2307/A3
11. CONTROLLING OFFICE NAME AND ADDRESS: AIR FORCE OFFICE OF SCIENTIFIC RESEARCH/NA, BLDG 410, BOLLING AIR FORCE BASE, D C 20332	12. REPORT DATE: OCTOBER 1979
	13. NUMBER OF PAGES: 57
14. MONITORING AGENCY NAME & ADDRESS (if different from Controlling Office)	15. SECURITY CLASS. (of this report): UNCLASSIFIED
	15a. DECLASSIFICATION/DOWNGRADING SCHEDULE

16. DISTRIBUTION STATEMENT (of this Report)

Approved for public release; distribution unlimited.

17. DISTRIBUTION STATEMENT (of the abstract entered in Block 20, if different from Report)

18. SUPPLEMENTARY NOTES

19. KEY WORDS (Continue on reverse side if necessary and identify by block number)

RANDOM-CHOICE METHOD (RCM)
SHOCK AND DETONATION-WAVE DYNAMICS
SHARP-FRONTED SHOCKS
CONTACT SURFACES
PLANAR AND SPHERICAL SHOCK WAVES
RAREFACTION WAVES
CONTACT SURFACES
INTERACTIONS

20. ABSTRACT (Continue on reverse side if necessary and identify by block number)

Eight applications of the Random-Choice Method (RCM) to the solution of problems in shock and detonation-wave dynamics are presented. It is shown that unlike other numerical methods, the RCM yields sharp-fronted shocks and contact surfaces without resorting to artificial and perhaps erroneous means of predicting their locations. It has been shown by examples that the RCM provides exceptionally high computational accuracy for flows involving planar and spherical shock waves, rarefaction waves and contact surfaces, as well as their interactions. In addition, the RCM can handle flows with detonations and chemical reactions involving

DD FORM 1 JAN 73 1473

UNCLASSIFIED
SECURITY CLASSIFICATION OF THIS PAGE (When Data Entered)

178920

the above transition fronts. Owing to the high accuracy of calculated values in p, ρ, u and the fact that the constant states are perfectly realized, very complex wave-interaction problems which involve small changes in physical parameters ρ, u, p, can be calculated, such as the reflection of a shock wave from the end wall of a shock tube and the subsequent interactions, or the head-on collision of a shock wave with a rarefaction wave.

Acknowledgements

We wish to acknowledge with thanks the valuable discussions with Prof. K. Takayama, Tohoku University, Sendai, Japan, while he was on sabbatical leave at this Institute. The assistance received from Dr. A. J. Chorin and Dr. G. A. Sod in providing us with their computer programs is very much appreciated.

The financial assistance received from the National Science and Engineering Research Council and from the U.S. Air Force under grant No. AF-AFOSR-77-3303 is acknowledged with thanks.

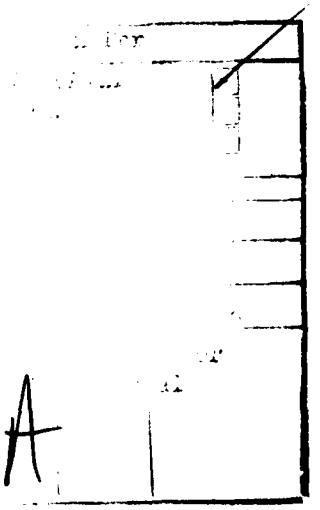

Summary

Although successful numerical methods exist for solving problems in shock and detonation-wave dynamics, there is still a real need of developing new techniques where the old methods fail to predict important flow properties. For example, it has recently been shown in Ref. 1 that existing methods fail to predict the interferometrically measured isopycnics in regular and single Mach reflections (let alone complex and double-Mach reflections, for which numerical solutions do not even exist). The purpose of the present report is to present eight applications of the Random-Choice Method (RCM) to the solution of problems in shock and detonation-wave dynamics. It is shown that unlike other numerical methods, the RCM yields sharp-fronted shocks and contact surfaces without resorting to artificial and perhaps erroneous means of predicting their locations, which depend more on art than science. It is also a very useful method in showing such fine points as the birth point of the second shock (implosion) wave at the tail of the rarefaction wave in a spherical explosion.

Despite all these advantages the RCM has yet to be developed to cope with problems such as oblique and spherical shock-wave reflections in order to compute the various isolines (pressure, density and velocity) and compare them with available interferometric or other experimental data. For example, isopycnics are much more sensitive indicators of the accuracy of a given numerical method than a comparison of shock shapes (Ref. 1). Undoubtedly, such applications of the RCM will probably take place in the near future, as the need for such numerical methods now exists.

Table of Contents

Notation

a	speed of sound
C	contact surface
D	speed of detonation wave
e	total energy per unit volume
F	function of V, from Eqs. (1), (2) and (34)
i	integer attached to the mesh point in space
I	inhomogeneous term in Eq. (34)
K	reaction rate
m	momentum per unit volume
M	molecular weight
M_ℓ	mass flow (fluid enters a wave from the left)
M_r	mass flow (fluid enters a wave from the right)
n	integer attached to the mesh point in time
p	pressure
P	sampling point
r	radial distance
S	state in Riemann problem; S_ℓ, S_r, S_*
t	time
Δt	time increment
T	temperature
u	particle velocity
U	shock velocity
v	solution of Riemann problem, see Eq. (5)
V	solution vector from Eq. (2)
w	particle velocity relative to wave front
x	space coordinate
Δx	space increment

Z	progress parameter in Eq. (66)
α	1, 2, 3 for planar, cylindrical, spherical flows, respectively
γ	specific heat ratio
ϵ	internal energy per unit mass
θ	random number $-\frac{1}{2} \leq \theta \leq \frac{1}{2}$
ρ	density

1. INTRODUCTION

Over the past two decades a number of numerical methods have been developed for the solution of flow problems in nonstationary gasdynamics involving transition fronts such as shock waves, rarefaction waves and contact surfaces. Such fronts occur in shock-tube flows, cylindrical and spherical explosions and implosions as well as in combustion with deflagration and detonation. In essence, the set of nonlinear hyperbolic partial differential equations of motion are replaced by a set of finite-difference equations which are numerically integrated for a solution. Owing to truncation errors an implicit artificial viscosity is introduced which spreads the contact-surface and shock-wave fronts over several mesh lengths. This is analogous to the action of real viscosity and heat conduction in spreading the shock transition over several mean-free-paths, and at the contact surface, due to the diffusion of heat and mass, spreading occurs with the square root of time.

Most finite-difference methods when applied to problems with discontinuities such as shock waves produce oscillations behind them. Von Neumann and Richtmyer (Ref. 5) introduced an artificial viscosity pressure term into the Lagrangian form of the gasdynamic equations to get rid of these unwanted oscillations in the solution. Since then various types of explicit or implicit artificial-viscosity terms have been used depending on the type of equations, Lagrangian or Eulerian and the type of finite-difference scheme used. Shock-wave fronts are also smeared by the artificial viscosity term, as well as the truncation error, typically over several mesh points. Moreover the artificial-viscosity term contains an arbitrary parameter which must be determined for each particular problem in order to obtain the best results. For a recent review of the subject see Ref. 4.

Unfortunately, the spreading or smearing of such fronts makes it difficult to know their positions with any precision at a given time. The development of the Random-Choice Method (RCM) by Glimm, Chorin and Sod (Refs. 2, 3 and 6), has made it possible to overcome these difficulties at the expense of some randomness in the paths of these wave fronts. For example, shock waves and contact surfaces are not spread at all and occupy zero zones. Their locations at any time are not exact but their average positions are. The physical profiles of the head and tail of rarefaction waves are perfectly sharp, whereas in other methods they come out rounded. Due to the randomness, the profiles are not smooth but on the average very close to the exact values for the rarefaction wave. In case of a shock-tube flow, the uniform states separated by the contact surface are obtained exactly without oscillations. Boundary conditions are readily handled by the RCM. The time required for the RCM may be two or threefold longer than for the other methods. However, the number of grid points are fewer for the same resolution. Consequently, the computation time can be much faster.

It is known that wave-interaction problems can be analyzed by using the method of characteristics. The solution, in this case, is computed with the aid of a grid of characteristic lines, which is constructed in the course of the computation. This method is used mainly for a detailed description of the flows. For example, the method of characteristics permits one to determine accurately the birth point of secondary shock waves in a flow at the point of intersection of the characteristics of one family. However, if a large number of such shock waves occur, difficulties would be encountered. Accordingly, the method of characteristics is usually applied to problems where the number of discontinuities is small.

The RCM does not resort to any type of finite-difference scheme to obtain the solutions for wave-interaction problems. A set of states at two adjacent mesh points i and (i + 1), at t = 0, form a Riemann problem (shock-tube problem) with the Euler type of equations of motion, namely, mass, momentum and energy. From the method of characteristics it is known that a Riemann problem has a self-similar solution which consists of four uniform states consisting of the two initial states, two final states, separated by a contact surface and a nonuniform state, the rarefaction wave. All the thermodynamic and dynamic properties can be calculated exactly from an algebraic consideration of the transition relations for shock fronts and rarefaction waves (Ref. 34). After the Riemann problem has been solved, one of the five states is chosen at random. This choice makes it possible to find a solution subsequently, at a time $\Delta t/2$, at a random point P, which is located between the mesh points i and (i + 1) as shown in Fig. 1. Although P is located in state (2), this solution is assigned to mesh point at (i + 1/2). It may appear that this is in error since the mesh point is really in state (3) in Fig. 1. However, if we realize that the mesh points are the representatives of elemental regions of the whole flow field, (i + 1/2) could have been at point P, i.e., the mesh points are not fixed in physical space. This randomness, on the average, is cancelled out and the correct solution is obtained. Although this sampling procedure gives randomness in the wave positions and the shape of the rarefaction waves, it is in reality acceptable and the calculated values are exact due to the fact that the method is free from truncation errors and artificial viscosity.

Many wave-interaction problems were investigated theoretically and experimentally at UTIAS. Finite-difference schemes with artificial viscosity were used mainly for solving the gasdynamic equations in Eulerian or Lagrangian form. In this report, the RCM is first applied to some of the practical wave-interaction problems. Although the mathematical justification of the RCM has already been shown in Refs. 2 and 3, it is important to check the usefulness and the applicability of the method to practical problems.

So far, the RCM has been applied to planar, cylindrical and spherical flows (Refs. 3 and 6) as well as to combustion flows (Ref. 7). Some very important applications of the RCM would be to pseudostationary oblique shock-wave reflection problems as well as nonstationary cylindrical and spherical shock-wave reflections. This has not been fully accomplished to date.

In Chapter 2, the RCM is described for the sake of completeness. Problems involving different gases with different values of the specific heat ratio γ were not calculated previously using the RCM. In this report the program was modified in order to make it possible to solve problems involving combinations of gases with different values of γ. The procedure is described in Appendix A. Chapter 3 deals with several examples of simple shock-tube flows solved by using the RCM. The results are compared with exact or approximate solutions. Chapter 4 extends Sod's RCM for cylindrical and spherical symmetric flows. Chorin's method for calculating reacting gas flows is also briefly described. The methods are applied to some practical examples, which required a modification of Chorin's program. Discussions and conclusions can be found in Chapter 5, and the program listings are given in Appendix B.

2. RANDOM-CHOICE METHOD (RCM)

2.1 GENERAL DESCRIPTION OF RCM

The equations for an inviscid non-heat-conducting one-dimensional flow can be written in conservation form (Ref. 3):

$$V_t + F(V)_x = 0 \tag{1}$$

where

$$V = \begin{pmatrix} \rho \\ m \\ e \end{pmatrix} \qquad F(V) = \begin{pmatrix} m \\ m^2/\rho + p \\ m(e+p)/\rho \end{pmatrix} \tag{2}$$

and the subscripts indicate differentiation. The total energy per unit volume e, may be written as

$$e = \rho\epsilon + \frac{1}{2}\rho u^2 \tag{3}$$

Assuming the gas is polytropic, the internal energy per unit mass is given by

$$\epsilon = \frac{1}{\gamma - 1}\frac{p}{\rho} \tag{4}$$

Letting Δt and Δx be time and spatial increments, respectively, the solution of the system of equations, Eq. (1), is to be evaluated at the mesh points $(i\Delta x, n\Delta t)$, and $\{(i + 1/2)\Delta x, (n + 1/2)\Delta t\}$. Letting v_i^n approximate $V(i\Delta x, n\Delta t)$ and $v_{i+1/2}^{n+1/2}$ approximate $V\{(i + 1/2)\Delta x, (n + 1/2)\Delta t\}$, it is necessary to find $v_{i+1/2}^{n+1/2}$ given v_i^n, v_{i+1}^n.

Consider an initial value problem for the system of equations given by Eq. (1), with the discontinuous initial data,

$$V(x, n\Delta t) = \begin{cases} v_{i+1}^n, & x \geq (i + 1/2)\Delta x \\ v_i^n, & x < (i + 1/2)\Delta x \end{cases} \tag{5}$$

then Eq. (1) together with Eq. (5) is called a Riemann problem. A method for solving such a Riemann problem will be described in detail in the next section. Let $v(x, t)$ denote the solution of this Riemann problem and let θ_n be a value of the random variable θ equidistributed in $[-1/2, 1/2]$. Then define $v_{i+1/2}^{n+1/2}$ by the solution of the Riemann problem at the point $\{(i + 1/2 + \theta_n)\Delta x, (n + 1/2)\Delta t\}$

$$v_{i+1/2}^{n+1/2} = v\left\{\left(i + \frac{1}{2} + \theta_n\right)\Delta x, \left(n + \frac{1}{2}\right)\Delta t\right\} \tag{6}$$

namely, at each time step the solution is first approximated by a piecewise constant; i.e., Riemann problems are formed with respect to each pair of every other mesh points. Time is then advanced exactly, and the new values on the mesh points in between those used to construct the Riemann problems are chosen by sampling (Fig. 1). The justification of this method for solving the system of equations, Eq. (1), can be found in Refs. 2 and 3.

2.2 SOLUTION OF A RIEMANN PROBLEM

The method of solving a Riemann problem is now described. Consider the system of equations given by Eq. (1) with the initial data,

$$V(x, o) = \begin{cases} S_r = (\rho_r, u_r, p_r) & x \geq 0 \\ S_\ell = (\rho_\ell, u_\ell, p_\ell) & x < 0 \end{cases} \tag{7}$$

The solution at later times will consist of three states; a left state S_ℓ, a right state S_r, a middle state S_* with $u = u_*$, $p = p_*$ and $\rho = \rho_*$ separated from S_ℓ and S_r by waves, W_r, W_ℓ, which may be either shock waves or rarefaction waves. A contact surface ($dx/dt = u_*$) separates the gas initially at $x < 0$ from the gas initially at $x \geq 0$. The values of u and p are continuous across the contact surface while ρ and other thermodynamic quantities, in general, are not. The contact surface divides S_* into two regions with differing values of densities $\rho_{*\ell}$ and ρ_{*r}, but equal constant values of u_* and p_* (Fig. 2).

Using Godunov's iterative method modified by Chorin and Sod (Refs. 3 and 6) ρ, u, p at the sample point $P(\theta\Delta x, 1/2\ \Delta t)$, $-1/2 \leq \theta \leq 1/2$, are determined as follows: Define the quantity

$$M_r = (p_r - p_*)/(u_r - u_*) \tag{8}$$

If the right wave is a shock wave, using the jump condition across the shock wave, we obtain

$$M_r = -\rho_r(u_r - U_r) = -\rho_{*r}(u_* - U_r) \tag{9}$$

where U_r is the velocity of the right shock wave. From the Rankine-Hugoniot conditions one obtains

$$M_r = (\rho_r p_r)^{1/2}\, \phi_1\left(\frac{p_*}{p_r}\right), \qquad \frac{p_*}{p_r} \geq 1 \tag{10}$$

where

$$\phi_1(\eta) = \left(\frac{\gamma + 1}{2}\,\eta + \frac{\gamma - 1}{2}\right)^{1/2} \tag{11}$$

If the right wave is a rarefaction wave, using the isentropic law $p\rho^{-\gamma}$ = constant and the constancy of the right Riemann invariant $\Gamma_r = 2(\gamma p/\rho)^{1/2}/(\gamma - 1) - u$, we find

$$M_r = (\rho_r p_r)^{\frac{1}{2}} \phi_2\left(\frac{p_*}{p_r}\right), \quad \frac{p_*}{p_r} < 1 \tag{12}$$

where

$$\phi_2(\eta) = \frac{\gamma - 1}{2\gamma^{\frac{1}{2}}} \frac{1 - \eta}{1 - \eta^{(\gamma-1)/2\gamma}} \tag{13}$$

The function

$$\phi(\eta) = \begin{cases} \phi_1(\eta) & \eta \geq 1 \\ \phi_2(\eta) & \eta < 1 \end{cases} \tag{14}$$

is continuous at $\eta = 1$, with $\phi(1) = \phi_1(1) = \phi_2(1) = \gamma^{\frac{1}{2}}$. Similarly, we define

$$M_\ell = (p_\ell - p_*)/(u_\ell - u_*) \tag{15}$$

If the left wave is a shock wave,

$$M_\ell = \rho_\ell(u_\ell - U_\ell) = \rho_{*\ell}(u_* - U_\ell) \tag{16}$$

where U_ℓ is the velocity of the left shock wave. As on the right,

$$M_\ell = (\rho_\ell p_\ell)^{\frac{1}{2}} \phi\left(\frac{p_*}{p_\ell}\right) \tag{17}$$

where $\phi(\eta)$ is defined as in Eqs. (11), (13) and (14). Eliminating u_* from Eqs. (8) and (15), we obtain

$$p_* = \frac{u_\ell - u_r + p_r/M_r + p_\ell/M_\ell}{1/M_r + 1/M_\ell} \tag{18}$$

Equations (18), (17) and (10) or (12) are three equations with three unknowns p_*, M_ℓ and M_r. These considerations lead to the following iteration procedure: Choose a starting value p_*^0 (or M_r^0, M_ℓ^0), and then compute $M_r^{\nu+1}$, $M_\ell^{\nu+1}$, $p_*^{\nu+1}$ ($\nu \geq 0$) using

$$\tilde{p}^\nu = (u_\ell - u_r + p_r/M_r^\nu + p_\ell/M_\ell^\nu)/(1/M_r^\nu + 1/M_\ell^\nu) \tag{19}$$

$$p_*^{\nu+1} = \max(\epsilon_1, \tilde{p}^\nu) \tag{20}$$

$$M_r^{\nu+1} = (\rho_r p_r)^{\frac{1}{2}} \phi(p_*^{\nu+1}/p_r) \tag{21}$$

$$M_\ell^{\nu+1} = (\rho_\ell p_\ell)^{\frac{1}{2}} \phi(p_*^{\nu+1}/p_\ell) \tag{22}$$

Since there is no guarantee that $\tilde{p}$ remains ≥ 0, Eq. (20) is needed. The iteration is stopped when

$$\max(|M_\ell^{\nu+1} - M_\ell^\nu|, \ |M_r^{\nu+1} - M_r^\nu|) \leq \epsilon_2$$

Then put

$$M_\ell = M_\ell^{\nu+1}, \ M_r = M_r^{\nu+1}, \ p_* = p_*^{\nu+1}$$

Chorin picked the value of $\epsilon_1 = 10^{-6}$, $\epsilon_2 = 10^{-6}$ in this iteration cycle. To start this iteration cycle either M_r and M_ℓ or $p*$ is needed. From the point of view of computation time, the efficiency of the RCM depends on how fast this iteration converges. Chorin obtained better results putting

$$p_*^o = (p_\ell + p_r)/2$$

as a starting value of the procedure than following the starting scheme suggested by Godunov (Ref. 8).

Godunov mentioned that the iteration may fail to converge in the presence of a strong rarefaction wave. This problem can be overcome by the following variant of Godunov's procedure. If the iteration has not converged after J iterations, Eq. (20) is replaced by

$$p_*^{\nu+1} = \zeta \max(\epsilon_1, \tilde{p}^\nu) + (1 - \zeta)p_*^\nu$$

with $\zeta = \zeta_1 = \frac{1}{2}$. In general ζ will be reset

$$\zeta = \zeta_j = \tfrac{1}{2} \zeta_{j-1}$$

after jJ iteration, j = 1, 2, 3, ... Chorin noted that the cases $j \geq 2$ had never been encountered and the number of iterations required fluctuated between 2 and 10, except at a very few points.

Knowing M_ℓ, M_r, p_*, Eqs. (8) and (15) give

$$u_* = (p_\ell - p_r + M_\ell u_\ell + M_r u_r)/(M_\ell + M_r) \qquad (23)$$

2.3 SAMPLING PROCEDURE

Having a solution in the middle state S_*, the next step is to determine the solution at each mesh point by sampling. There are four basic cases to be sampled.

1) The sampling point $P = (\theta\Delta x, \frac{1}{2}\Delta t)$ lies to the right of the contact surface whose inverse slope in the (x, t)-plane is $(dx/dt) = u_*$, and the right wave is a shock wave, i.e.,

$$\theta\Delta x \geq u_*\Delta t/2 \text{ and } p_* \geq p_r$$

As mentioned before θ is a random number uniformly distributed over the range of $[-\frac{1}{2}, \frac{1}{2}]$.

2) The sampling point P lies to the left of the contact surface and the left wave is a rarefaction wave, i.e.,

$$\theta\Delta x < u_*\Delta t/2 \text{ and } p_* < p_\ell$$

3) The sampling point P lies to the left of the contact surface and the left wave is a shock wave, i.e.,

$$\theta\Delta x < u_*\Delta t/2 \text{ and } p_* \geq p_\ell$$

4) The sampling point P lies to the right of the contact surface and the right wave is a rarefaction wave, i.e.,

$$\theta\Delta x > u_*\Delta t/2 \text{ and } p_* < p_r$$

In what follow $\bar{\rho}$, $\bar{u}$, $\bar{p}$ denote the sampled solution, and now how they are determined is explained for each case.

Case 1) From Eq. (9), the velocity of the right shock wave U_r can be obtained as

$$U_r = u_r + M_r/\rho_r \tag{24}$$

If the sampling point P lies to the right of the shock-wave line $dx/dt = U_r$, region 1 in Fig. 3,

$$\bar{\rho} = \rho_r,\ \bar{u} = u_r,\ \bar{p} = p_r$$

If the sampling point P lies to the left of the shock wave, region 2 in Fig. 3,

$$\bar{\rho} = \rho_{*r},\ \bar{u} = u_*,\ \bar{p} = p_*$$

where ρ_{*r} is obtained from Eq. (9) as

$$\rho_{*r} = -M_r/(u_* - U_r) \tag{25}$$

Case 2) The rarefaction wave is bounded on the left by the line $dx/dt = u_\ell - a_\ell$, and on the right by $dx/dt = u_* - a_*$, where a_ℓ and a_* are the sound velocities in the states S_ℓ and S_*, respectively; a_ℓ is given as

$$a_\ell = \sqrt{\gamma_\ell p_\ell/\rho_\ell} \tag{26}$$

and a_* can be found by using the Riemann invariant Γ_ℓ = constant,

$$2a_*/(\gamma_\ell - 1) + u_* = 2a_\ell/(\gamma_\ell - 1) + u_\ell = \Gamma_\ell$$

If the sampling point P lies to the left of the head of the rarefaction wave, $dx/dt = u_\ell - a_\ell$, region 5 in Fig. 3,

$$\bar{\rho} = \rho_\ell,\ \bar{u} = u_\ell,\ \bar{p} = p_\ell$$

If the sampling point P lies to the right of the tail of the rarefaction wave, $dx/dt = u_* - a_*$, region 3 in Fig. 3, set

$$\bar{\rho} = \rho_{*\ell},\ \bar{u} = u_*,\ \bar{p} = p_*$$

where $\rho_{*\ell}$ is calculated using the isentropic relation $p\rho^{-\gamma} = A$ (constant), as

$$\rho_{*\ell} = (p_*/A)^{1/\gamma_\ell} \tag{27}$$

The value of A can be calculated in the state S_ℓ as

$$A = p_*\rho_\ell^{-1/\gamma_\ell} \tag{28}$$

If the sampling point P lies inside the rarefaction wave, region 4 in Fig. 3, the slope of the characteristic $dx/dt = u - a$ is equated to the slope of the line connecting the origin and P, to obtain

$$\bar{u} - a = 2\theta\Delta x/\Delta t \tag{29}$$

Also,

$$2a/(\gamma_\ell - 1) + \bar{u} = 2a_\ell/(\gamma_\ell - 1) + u_\ell = \Gamma_\ell \tag{30}$$

Solving Eqs. (29) and (30), obtain

$$\bar{u} = \frac{2}{\gamma_\ell + 1}\left(\frac{2\theta\Delta x}{\Delta t} + a_\ell + \frac{\gamma_\ell - 1}{2}u_\ell\right) \tag{31}$$

Since $a = (\gamma_\ell\bar{p}/\bar{\rho})^{1/2}$ and $\bar{p} = A\bar{\rho}^{\gamma_\ell}$

$$\bar{\rho} = (a^2/\gamma_\ell A)^{1/(\gamma_\ell - 1)} \tag{32a}$$

$$\bar{p} = A\bar{\rho}^{\gamma_\ell} \tag{32b}$$

Cases 3 and 4 are mirror images of cases (1) and (2) and the same arguments are applied.

2.4 PRODUCTION OF RANDOM NUMBERS

The choice of a series of random numbers θ_n ($n = 1, 2, \ldots$) determines the behaviour of the solution. If θ is close to $-1/2$, the values in the left state S_ℓ propagate to the right to $[(i + 1/2)\Delta x, (n + 1/2)\Delta t]$, while, if θ is close to $1/2$, the values in the right state S_r propagate to the left. Therefore it is important to choose θ_n in such a way that they tend to be equally distributed over $[-1/2, 1/2]$ as soon as possible.

Chorin noted that it is unreasonable to choose a new value of θ for each mesh point i, at each time level n, since there is a finite probability that a given state S will propagate in both directions. Chorin overcame this problem choosing a new value of θ once for each time level rather than assigning a new value of θ for each i and n. Chorin further improved the method by making the sequence of random numbers θ_n, reach equidistribution over $[-1/2, 1/2]$ at a faster rate. This is done by combining a random number θ_n chosen from the range of $[-1/2, 1/2]$ and a pseudorandom number k_n.

Let m_1 and m_2 be two mutually prime integers ($m_1 < m_2$) then consider the sequence of integers,

$$k_{n+1} = (m_1 + k_n)(\text{mod } m_2)$$

where k_o is given, $k_o < m_2$. This will produce a series of pseudorandom numbers. For example, if $k_o = 1$, $m_1 = 3$, $m_2 = 7$, then $k_1, k_2, k_3, \ldots$ will be a repetition of a series of integers, 4, 0, 3, 6, 2, 5, 1. If we consider the following sequence:

$$\theta_n' = \frac{k_n + (\theta_n + 1/2)}{m_2} - \frac{1}{2} \qquad (n = 1, 2, \ldots)$$

θ_n' will be also in the range of $[-1/2, 1/2]$. This modified sequence of random numbers θ_n is employed in the program. The advantages of using this sequence θ_n' is described in detail in Ref. 3.

2.5 BOUNDARY CONDITIONS

Consider a solid-wall boundary at $x = b$, with the fluid to the left. The boundary conditions are imposed on the grid point closest to $x = b$, say $i_o\Delta x$. A pseudo right state S_r at $(i_o + 1/2)\Delta x$ is created by setting

$$\begin{aligned} \rho_{i_o+1/2} &= \rho_{i_o-1/2} \\ u_{i_o+1/2} &= u_{i_o-1/2} \\ p_{i_o+1/2} &= p_{i_o-1/2} \end{aligned} \qquad (33)$$

In this manner, waves can be reflected at a solid boundary.

2.6 TREATMENT OF CONTACT SURFACES

The Random-Choice Method was not applied to flow problems having combinations of gases with different specific heat ratios. In this report the program was modified to handle such problems, thereby enlarging the applicability of the RCM. The position of contact surfaces are determined during sampling procedure and consistent with the RCM. The details are given in Appendix A.

3. NUMERICAL RESULTS FOR PLANAR WAVE INTERACTIONS

The purpose of this section is to show how well the RCM works for nonstationary wave-interaction problems by using several illustrative examples. Many examples of interactions of shock waves, rarefaction waves, contact surfaces and with solid boundaries are given in Refs. 9 and 10.

In order to illustrate the usefulness of the RCM, the following examples were calculated:

1. Reflection of shock wave from end wall of a shock tube and subsequent interactions.

2. Head-on collision of a shock wave with a rarefaction wave.

3. Head-on collision of two rarefaction waves.

4. Contact-surface tailoring.

5. Shock-refraction problem at a stationary contact layer.

6. Shock-wave propagation in a varying-density field.

3.1 REFLECTION OF SHOCK WAVE FROM END WALL OF A SHOCK TUBE AND SUBSEQUENT INTERACTIONS.

The initial conditions were set in such a way that we could compare the results obtained using the RCM with those obtained by Gurke and Schwarzkopf (Ref. 11), i.e.,

diaphragm pressure ratio : $P_{41} = 27.0$

test gas - air : $\gamma_1 = 1.40$

driver gas - air : $\gamma_4 = 1.40$

Figure 4 was drawn from the data in Ref. 11. Since these results were obtained with the method of characteristics and there is no interactions between shock waves and rarefaction waves, the solutions obtained here are exact. Figure 5 shows our results obtained with the RCM for a mesh number of 720 along the axis of the shock tube. Only the region close to the end wall is displayed. Since this method does not make use of an artificial viscosity, shock waves and contact surfaces remain perfectly sharp. Owing to this outstanding feature, we can recognize as many as 68 different regions without difficulty in this particular case. The exact wave trajectories in Fig. 4 are superimposed in Fig. 5 as solid lines for ready comparison with the present results. It can be seen that the agreement in wave positions is excellent. At $t \simeq 2.5$ ms, the error in the position of the contact surface is about 6 mesh sizes, and appears to be the largest error in the region where the exact solution is presented for comparison. This error corresponds to about 0.8% of the whole mesh number, i.e., 1.3 cm for a 180-cm long shock tube. The discrepancy of the wave positions from the exact solution depends on the mesh size and was about 3% when the mesh number was 180. In Table 1, values of pressure p, density ρ, and particle velocity u, obtained by the present method are compared with the exact solution for each region. In these regions, the numerical errors in both pressure and density are of the order of 10^{-4}. Although they tend to increase as time goes on, their magnitudes are small enough to consider the numerical values as exact. In Table 2 numerically obtained values of p, ρ, u are listed for all the regions which appear on Fig. 5. In Fig. 5 and Table 2 we see that the flow patterns get more and more complex and also, as one can expect, the changes in values of ρ, u, p become smaller. For example, in regions 67 and 68, across them the changes in pressure and density are from 24.690 to 24.694, and from 8.719 to 8.721, respectively.

All the numerical computations were done using an IMB 370. It took 77.78 min to calculate this example with 720 mesh numbers and 1600 time steps. This fairly long computation time includes the time spent to calculate the solutions

at mesh points far from the end wall in which, however, there is no immediate interest. Therefore, if we could simulate wave interactions only in the region close to the end wall, significant computation time could be saved.

This can be done as follows. First, calculate the values of ρ, u, p in the regions 2 and 3 for the given initial conditions by using either Rankine-Hugoniot relations or this numerical method. Then distribute states 1, 2 and 3 as the initial conditions over the mesh points and by removing the boundary conditions at the other end wall of the shock tube so that no reflected rarefaction wave is generated there. This corresponds to a shock tube with an infinitely long high-pressure section. In the same way, one can always simulate only those wave interactions that one is interested in, that is, a larger dynamic range for the wave interactions for the same mesh number. It took 3.19 minutes to calculate the same problem with a mesh number of 180 and 300 time steps, or from t = 0 to t = 3.6 ms in this particular case. Many wave interaction patterns are seen in Fig. 5, such as the overtaking of two similarly facing shock waves, the head-on collisions among shock and rarefaction waves, the interaction of a shock or rarefaction wave with a contact surface. Some of these basic interaction problems were simulated in detail and will be discussed subsequently.

3.2 HEAD-ON COLLISION OF A SHOCK WAVE WITH A RAREFACTION WAVE

This interaction problem was investigated by Gould (Ref. 12) both analytically and experimentally. The initial conditions provided for a shock strength p_{10}, and rarefaction strength p_{20} of $p_{10} = 1.96$ and $p_{20} = 0.549$. This is achieved by putting the left diaphragm pressure ratio $p_{70} = 4.15$ and the right diaphragm pressure ratio $p_{08} = 3.26$ with $\gamma = 1.40$.

Figure 6 shows the resulting wave system for this case. As a result of the head-on collision of a forward facing shock wave (fluid particles enter the wave from the right) and a backward facing rarefaction wave (fluid particles enter the wave from the left), there appears a forward facing transmitted shock wave and a backward facing rarefaction wave. Since the shock wave increases in strength continuously during the interaction with the rarefaction wave, each fluid particle crossing the shock wave in this period of time will experience a different entropy jump thereby forming a contact layer or region. Consequently, the region between the transmitted shock wave and the transmitted rarefaction wave consists of two new uniform regions (3), (4) and a contact region. (Note that secondary interactions of characteristics within the contact layer have been neglected.) Pressure p, and particle velocity u, are the same for regions (3) and (4), but density ρ, temperature T, and entropy S, are different. The exact values of ρ, u, p in the regions (3) and (4) can be determined analytically. The wave trajectories, however, in the interaction region were determined by Gould in detail, as outlined in Ref. 12. In Fig. 6, the wave trajectories were obtained only by averaging the initial and final stage of the interaction without the detailed method of Gould. The results (circled data) obtained by the RCM are superimposed on those obtained by Gould in Fig. 6. In Table 3, the computed values of ρ, u, p are compared with those obtained by Gould. As we can see, the calculated values are correct to at least the first four digits and the error is of the order of 10^{-4}. The agreement in the wave trajectories is also very good and the error is about 1% at the most.

The computation was carried out with 180 spatial mesh points and it took 0.72 minutes to proceed through 82 time steps, which was long enough to simulate the interaction process appearing in Fig. 6.

In Table 3, as mentioned before, the pressure p and particle velocity u are the same for regions (3) and (4) but the density ρ is different. The density change across the contact region is as small as 0.19% of its absolute value.

3.3 HEAD-ON COLLISION OF TWO RAREFACTION WAVES.

This problem was solved by Steketee (Ref. 13). The computer simulation was done by assuming an experiment using a two-diaphragm shock tube. Initially the center part, which is separated by two diaphragms both from the left part and right part of the shock tube, is filled with a gas at higher pressure than the other two sections so that, after the two diaphragms are ruptured, rarefaction waves propagate into this center section and collide. The assumed initial conditions for the numerical calculations were

left section:	Ar (γ = 1.6667):	p = 0.088118,	ρ = 1.7457
centre section:	H_2 (γ = 1.4000):	p = 1.0000,	ρ = 1.0000
right section:	Ar (γ = 1.6667):	p = 0.024793,	ρ = 0.49119

This will give the forward-facing rarefaction wave strength P_{20}, of 0.59498 and the backward-facing rarefaction wave strength p_{10}, of 0.39945.

After the interaction, a uniform state appears between the two transmitted rarefaction waves. Unlike the previous case the interaction process is isentropic and no contact region will be produced. The values of ρ, u, p in this uniform region can be determined exactly. The exact values and the results obtained from the RCM are displayed in Table 4. Again the errors in this calculated values are very small. Figure 7 is the (x, t)-diagram for this interaction. The circles are the results obtained using the RCM and lines are those obtained by the method of characteristics (Ref. 13). The agreement is, in general, good especially before the interaction. The agreement of boundaries between the state (3) and transmitted rarefaction waves do not look too good. This relatively large error, typically about 3%, includes the error associated with the method of characteristics and we can expect smaller errors for the RCM itself. On the region of penetration, the characteristic lines are no longer straight, and their trajectories had to be determined graphically dividing the rarefaction waves into small segments. In Fig. 7, trajectories of characteristic lines were obtained by dividing both rarefaction waves into four segments. As far as the wave trajectories are concerned, since it is not practical to divide the rarefaction fans into too many segments, the method of characteristics is also approximate in this problem.

It took 1.72 min to compute 180 time steps with 180 spatial mesh numbers.

3.4 CONTACT-SURFACE TAILORING

In general, when a shock wave reflects at the channel end wall and collides with the oncoming contact surface, the shock wave is transmitted and either a shock wave or a rarefaction wave is reflected. However, by choosing the initial conditions properly, they provide a contact surface such that the reflected wave is a Mach wave. As a result, the gas from the end wall to the contact surface remains in a uniform or tailored state. Figure 8 shows such a condition where the wave between states (5) and (7) is a Mach wave. Since state (5) is stationary ($u_5 = 0$), states (7) and (8) are also stationary ($u_7 = u_8 = 0$) and the contact surface is brought to a complete stop. When the flow is tailored, one can get a relatively long test time in the stationary region, which is very useful for aerodynamic and chemical-kinetic studies.

Tailoring in this case was produced by using two different gases with different specific heat ratios. This problem requires a high degree of accuracy for a solution and becomes very difficult for those methods with a finite difference scheme in which contact surfaces cannot be well defined. Given the initial test gas conditions, the diaphragm pressure ratio p_{41} and the composition of the driver gas can be determined by assuming the incident shock strength p_{21} (Ref. 14). Using argon as a test gas ($\gamma_1 = 1.667$, $M_1 = 39.94$), the diaphragm pressure ratio p_{41} and the molecular weight of the driver gas (assuming a diatomic gas with $\gamma_4 = 1.400$) M_4, were calculated for $p_{21} = 12.30$. The calculated results give values for $p_{41} = 58.21$ and $M_4 = 7.251$ ($\rho_{41} = 10.57$). This driver gas can be made by mixing 79.87% of hydrogen and 20.13% of nitrogen, for example. The calculated values and the results obtained by the RCM are compared in Table 5 and in Fig. 8. It is seen the calculated values of ρ, u, p in each region are very accurate. The wave trajectories are in good agreement until the moment when the incident shock wave reflects from the end wall, where it leaves with slight delay, causing a spatial error of about 2%. Although it fluctuates back and forth one mesh size due to the randomness of the sampling procedure, the contact surface stopped after its interaction with the reflected shock wave, as expected.

It took 2.38 min to simulate 250 time steps with 180 mesh numbers.

3.5 SHOCK REFRACTION PROBLEM AT A STATIONARY CONTACT LAYER.

The interaction of a shock wave and a stationary contact surface was investigated analytically by Bitondo, Glass and Patterson (Ref. 15) and experimentally by Ford and Glass (Ref. 16). After normal reflection of a shock wave at a stationary contact surface, there are two possible cases; a transmitted shock wave, contact surface and reflected rarefaction wave, or a transmitted shock wave, contact surface and reflected shock wave, depending on the incident shock strength and the initial internal energy ratio (acoustic impedance) across the contact surface. Putting a helium layer in air (Air $\|$ He $\|$ Air), both cases occur at the two contact surfaces. In the simulation, the incident shock strength was 3.700. In this case, at the left contact surface C_ℓ (Air $\|$ He) a reflected rarefaction wave appears and at the right contact surface C_r (He $\|$ Air) a reflected shock wave results. The solution for ρ, u, p can be determined exactly and they are compared with the computed results in Table 6. The interactions are shown in Fig. 9 with the results computed by RCM. In this particular case, the shock strength was attenuated after passing through the helium layer, from a pressure ratio of 3.700 to 2.971. For further details see Ref. 16, where it is shown that other interactions soon amplify the shock wave to nearly its original strength. The order or errors both in the calculated values in the flow variables and in the wave positions are the same as the previous examples. It took 0.70 min to calculate 140 time steps of this problem with 180 mesh numbers.

3.6 SHOCK-WAVE PROPAGATION IN A VARYING-DENSITY FIELD.

When a shock wave propagates in a gas which is stationary but has a certain density distribution in the direction of the wave propagation, the shock wave changes its propagation speed and strength. For example, by cooling a vertical-channel end-wall the test gas remains at constant pressure but has a nonuniform density.

Simulation was done with the following initial conditons. The driver gas was air ($\gamma_4 = 1.400$) and test gas was helium ($\gamma_1 = 1.667$). The density distribution is uniform in the driver section. In the test section, it increases linearly such that ρ at the end wall is fourfold ρ_1 at the diaphragm position. This density change can be obtained by cooling the test gas from 298° K at the diaphragm to 74.5° K at the end wall. The initial diaphragm pressure ratio was taken as $p_{41} = 30$.

The results are displayed in Fig. 10. In this particular case, the shock strength increases from $p_{21} = 2.24$, at the moment when the diaphragm was ruptured, to $p_{21} = 3.17$, when the shock wave has propagated to the end wall of the shock tube. Correspondingly, the local shock Mach number is also increased. However, since the local speed of sound is reduced due to the density increase (temperature decrease); $a \propto \sqrt{1/\rho}$, the propagation speed of the shock wave is reduced. The particle velocities are also decreased. The wave diagram is shown in Fig. 11, where the exact solution for the case when the density ρ is initially uniform, is superimposed for comparison. As expected, the shock wave and contact surface decelerate. It took 0.503 min to calculate 200 time steps with 100 mesh numbers. It is worthwhile mentioning that this example is difficult to handle using other numerical methods. Technically, the difficulty arises from trying to keep the region ahead of the shock wave stationary until its arrival in a finite difference scheme. The method of characteristics also has difficulties to treat this problem since all the characteristics inside the nonuniform region are not straight.

4. EXTENSIONS OF RANDOM CHOICE METHOD

4.1 ONE-DIMENSIONAL SYMMETRIC FLOW

4.1.1 GENERAL DESCRIPTION

Sod developed a method of calculating one-dimensional symmetric flows such as cylindrical and spherical shock waves by combining the RCM with operator splitting. He gives some numerical results on converging shock wave problems in Ref. 6. Here, Sod's method will be applied to a spherical-explosion problem and the results will be compared with some results obtained by Brode (Ref. 26) using the artificial-viscosity method. The equations for an inviscid, non-heat-conducting, radially-symmetric flow can be written in vector form (Ref. 6):

$$V_t + F(V)_t = -I(V) \tag{34}$$

where

$$V = \begin{pmatrix} \rho \\ m \\ e \end{pmatrix} \qquad F(V) = \begin{pmatrix} m \\ m^2/\rho + p \\ m(e+p)/\rho \end{pmatrix} \qquad I(V) = (\alpha-1) \begin{pmatrix} m/r \\ m^2/\rho r \\ m(e+p)/\rho r \end{pmatrix}$$

where $\alpha = 2$, for cylindrical symmetry, $\alpha = 3$, for spherical symmetry and $\alpha = 1$, corresponds to planar cases described in Chapter 2.

Exact solutions exist for point-source explosions in the limiting case when the primary shock wave is infinitely strong (or implosions) where the pressure in front of the shock wave is negligible, by comparison to that behind it, or in the acoustic limit, when the shock is very weak (i.e., entropy changes are negligible) (Refs. 17 to 25). Although such solutions are useful whenever they are applicable, they cannot be applied to real problems of finite sources when the shock waves are neither strong nor weak. These solutions do not predict the important features of the flow that exists in an actual case such as the second shock wave and wave interactions in the vicinity of the contact surface. To obtain these features, Eq. (34) must be solved. In general, there are two major difficulties in solving Eq. (34):

1) A singularity exists at $r = 0$.

2) The momentum equation [the second component of Eq. (34)] cannot be expressed in conservation form.

Consequently, Eq. (34) has to be solved numerically. Brode (Refs. 26 - 28) was able to numerically integrate the nonlinear (inhomogeneous) partial differential equations, Eq. (34), for a number of important flow problems involving spherical explosions. Payne (Ref. 29) solved the case of a cylindrical implosion by using a similar method. Lapidus (Ref. 30) computed a cylindrical-implosion problem in Cartesian co-ordinate in two space dimensions. Although these methods have been used successfully to explain physical phenomena, they have inherent disadvantages in that the use of artificial viscosity smears out the wave fronts over several mesh numbers and to find their exact location becomes more of an art than a science.* By using Sod's method such difficulties including 1) and 2) are eliminated completely.

4.1.2 SOD'S METHOD.

In Sod's method, the first step is to remove the inhomogeneous term -I(V) from Eq. (34), using the method known as operator splitting. Thus the system

$$V_t + F(V)_x = 0 \tag{35}$$

is solved. In this system, the momentum equation can be expressed in conservation form and the RCM, described in Chapter 2, can be used to obtain solutions. Once the system of equations, Eq. (35), has been solved, the system of ordinary differential equations given by

$$V_t = -I(V) \tag{36}$$

is solved in turn.

In the program, Eq. (36) is solved using a Cauchy-Euler scheme by utilizing the solutions of Eq. (35), $\bar{V}$, to determine the inhomogeneous term -I in Eq. (36), namely, the system Eq. (36) is approximated by

$$(V_i^{n+1} - V_i^n)/\Delta t = -I(\bar{V}_i^{n+1})$$

or

$$V_i^{n+1} = V_i^n - \Delta t\ I(\bar{V}_i^{n+1}) \tag{37}$$

Since the solutions for the system Eq. (35) are only obtained at intermediate points and the scheme of Eq. (37) does not require values at $r = 0$, the singularity at the axis is eliminated. The boundary conditions are properly imposed on Eq. (35), as described in Sec. 2 - 5. There is no need to put boundary conditions on Eq. (36), since it is solved only at intermediate points.

4.1.3 EXPLOSION OF A PRESSURIZED HELIUM SPHERE.

A set of experimental results for the explosion of pressurized glass spheres

*The reader will find a fuller discussion in Ref. 38.

filled with air or helium into air may be found in Refs. 26, 31 and 32. As an example of Sod's method, one of the experimental conditions for a helium explosion was used as initial conditions for the numerical analysis,

$$\begin{aligned} &\text{diaphragm pressure ratio: } p_{41} = 18.25 \\ &\text{diaphragm density ratio: } \rho_{41} = 2.523 \\ &\text{initial particle velocities: } u_1 = u_4 = 0 \end{aligned} \tag{38}$$

At the instant of rupture, the planar-wave conditions apply, giving a shock strength $p_{21} = 6.497$. The shock wave then decelerates until it becomes a sound wave. The contact surface decelerates and its motion becomes oscillatory. The rarefaction-wave head moves at constant speed and reflects at the origin where its motion becomes complex. The tail of the rarefaction wave accelerates and an implosion (second shock) wave originates on it.

Equation (34) may be reexpressed in the following form by using the method of characteristics (Ref. 25).

Along a right running characteristics or P-wave,

$$\frac{dx}{dt} = u + a \tag{39}$$

$$\frac{\delta P}{\delta t_+} + \frac{a}{C_p}\frac{\delta S}{\delta t_+} + (\alpha - 1)\frac{au}{r} = 0 \tag{40}$$

and along a left running characteristic or Q-wave,

$$\frac{dx}{dt} = u - a \tag{41}$$

$$\frac{\delta Q}{\delta t_-} + \frac{a}{C_p}\frac{\delta S}{\delta t_-} + (\alpha - 1)\frac{au}{r} = 0 \tag{42}$$

In the present explosion case, a Q-rarefaction wave results. The values of Q in the plane case for state (4) and (3) are $2a_4/(\gamma_4 - 1)$ and $2a_3/(\gamma_4 - 1) - u_3$, respectively. In the limit for a complete rarefaction wave when $a_3 \to 0$, $u_3 \to 2a_4/(\gamma_4 - 1)$ and $Q \to -2a_4/(\gamma_4 - 1)$. Consequently, Q decreases from the head $[Q = 2a_4/(\gamma_4 - 1)]$ to the tail of the rarefaction wave. Since the Q-rarefaction wave is isentropic, Eq. (42) gives $\delta Q/\delta t_- = -(\alpha - 1)au/r$, that is, as one proceeds along a Q characteristic Q decrease. This can only happen if the characteristic accelerates in the direction of the tail of the rarefaction wave. In other words, as time goes on, the Q-rarefaction wave continues to get stronger until it is engulfed by the second shock wave.

The pressure profiles obtained by Sod's method are displayed in Fig. 12. The numerical results are drawn from the output of the computer without smoothing (except in Fig. 15, the explosion-wave diagram). The results exhibit the general characteristics of a Q-rarefaction wave for an explosion problem very well. Initially the planar rarefaction strength $p_{21} \approx 0.356$. As time goes on, the absolute values of pressures at the tail of the rarefaction wave continue to decrease until the second shock wave is generated around the time number 10 which corresponds to 26.5 μs after the glass sphere ruptures. At time number 10, the rarefaction strength is increased to 0.142. The density profiles are shown in Fig. 13. They are quite similar to the pressure profiles except for the discontinuity across the contact surface. Again, the lowered density ratios or increased rarefaction-wave strengths are observed. The formation of a second shock wave and the deceleration of the primary shock wave can be explained by considering the path of the contact surface as similar to that of a piston. The contact surface is decelerated as a result of the spherical nature of the flow and sends out ahead of itself rarefaction pulses (P-characteristics) that overtake and decay the primary shock wave. However, behind it, compression pulses (Q-characteristics) are sent out which overtake to form a second shock (implosion) wave along the tail of the rarefaction wave. (It is worth noting that in the planar case such pulses run parallel to the tail of the wave, but in cylindrical and spherical flows, they collide with the tail of the rarefaction wave.) This explains why the path of second shock is connected with the tail of the rarefaction wave. Although the second shock wave is a backward facing wave, it is initially very weak and propagates outward at first owing to the high positive particle velocity. However, as it gains strength, it overcomes this counter flow and finally implodes on the origin with unlimited strength ideally. In Figs. 12-a and 13, we can see that the strength of the primary shock wave decays as it proceeds and how the second shock wave is generated. In the foregoing figures at about 26.5 μs after rupture (time number 10), noticeable discontinuities were found that grew into a second shock wave, and were defined as the birth point of the second shock wave. The particle-velocity profiles are shown in Fig. 14. In the early stage of the explosion, all particles move outward (positive velocity). As the contact surface decelerates, compression waves (Q-characteristics) and rarefaction waves (P-characteristics) decelerate the particle velocity creating a large negative velocity range. In this particular case, it reaches almost $-0.8a_1$ (at time number 46, 120 μs after rupture). This negative particle velocity is reversed by the reflected second shock up to small positive values (time number 56). In Figs. 12, 13 and 14, the profiles of ρ, p and u have complex structures around the origin. This is mainly due to the randomness of the RCM in the rarefaction wave. Unlike similarly-facing shock waves in the planar case, the second shock wave does not overtake the primary shock wave because of the lower sound speed and the lower or even opposing particle velocity behind the primary shock wave. Therefore, the primary shock wave and the reflected second shock wave slow down continuously to become Mach waves. (It is worth noting that this is the principle behind travelling wave sonic-boom simulators; Ref. 33.)

The wave diagram is shown in Fig. 15. Isobars, isopycnics and isotachs (constant velocity lines) are shown in Figs. 16, 17 and 18, respectively. In the figures, the decreases in pressure and density behind the incident and reflected rarefaction waves are quite apparent. The pressures and densities in front of the imploding shock wave near the origin are very small. This imploding shock wave also induces large negative velocities as it approaches the origin and a line of zero particle velocity is seen. It is also apparent that the second shock wave is

produced along the tail of the rarefaction wave, propagates outward at first, then starts to implode and increases in strength to unlimited values as it hits the origin and reflects. The origin becomes a singularity and the continuum equations break-down. Transport properties would keep the thermodynamic properties finite at the implosion focus.

4.2 REACTING-GAS FLOW

4.2.1 GENERAL DESCRIPTION

The RCM was applied to reacting gas flow by Chorin (Ref. 7) and was shown to be capable of handling time-dependent detonation and deflagration waves with finite and infinite reaction rate. Chorin emphasized an important advantage of using his method since the interaction of the flow and the chemical reaction can be taken into account when the Riemann problem is solved, even when the time scales of the chemistry and the fluid flow are very different. As a result, the basic conservation laws are satisfied at the end of each time step. If the chemical reactions and the gas flow were to be taken into account in separate fractional steps, the basic conservation laws may be violated at the end of each hydrodynamic step, thus either inducing unwanted oscillations and waves, or requiring time steps small enough for all changes to be very gradual, usually a costly remedy. Chorin's main object seemed to be placed on developing the technique and to show the usefullness of the method. Thus, in his program, there is an unreasonable assumption, $\gamma_0 = \gamma_1 = \gamma$, i.e., the specific heat ratios do not change across the reaction front. Although, as he states in his paper, the case $\gamma_0 \neq \gamma_1$ is more difficult only because of additional algebra. We felt that this assumption must be improved. Here, as a first step, the program was modified to have changes in the specific heat ratio so that $\gamma_0 \neq \gamma_1$ at the detonation-wave front. The RCM was then applied to a detonation wave in a $2H_2 + O_2$ gas mixture.

4.2.2 CHAPMAN-JOUGUET DETONATION

A Chapman-Jouguet detonation is described briefly in this section for the convenience of explaining Chorin's method of calculating reacting-gas flow. The equations to be solved are (Ref. 7 and 34)

$$\rho_t + (\rho u)_x = 0 \tag{43}$$

$$(\rho u)_t + (\rho u^2 + p)_x = 0 \tag{44}$$

$$e_t + [(e + p)u]_x = 0 \tag{45}$$

where

$$e = \rho\epsilon + \frac{1}{2}\rho u^2 \tag{46}$$

$$\epsilon = \epsilon_i + q \tag{47}$$

ϵ_i is the internal energy per unit mass and expressed as,

$$\epsilon_i = \frac{1}{\gamma - 1}\frac{p}{\rho} \tag{48}$$

q is the energy of formation which can be released through chemical reaction. In this present section, it is assumed that part of q is released instantaneously in an infinitely thin reaction zone. Denoting the unburned and the burned gas with 0 and 1, respectively, we have

$$\epsilon_o = \frac{1}{\gamma_o - 1}\frac{p_o}{\rho_o} + q_o \tag{49}$$

$$\epsilon_1 = \frac{1}{\gamma_1 - 1}\frac{p_1}{\rho_1} + q_1 \tag{50}$$

Assuming that the unburned gas is on the right, and letting D be the velocity of the reacting zone, Eqs. (43) and (44) can be written in conservation form

$$\rho_1 w_1 = \rho_o w_o = -M \tag{51}$$

$$\rho_o w_o^2 + p_o = \rho_1 w_1^2 + p_1 \tag{52}$$

where

$$w_o = u_o - D, \quad w_1 = u_1 - D \tag{53}$$

From these relations one readily deduces

$$M^2 = -(p_o - p_1)/(\tau_o - \tau) \tag{54}$$

where τ is the specific volume, $1/\rho$.

Conservation of energy is expressed by

$$\epsilon_1 - \epsilon_o - \frac{1}{2}(\tau_o - \tau_1)(p_o + p_1) = 0 \tag{55}$$

Substituting Eqs. (49) and (50) into Eq. (55), we have

$$\left(p_o + \frac{\gamma_1 + 1}{\gamma_o - 1}p_1\right)\tau_1 - \left(p_1 + \frac{\gamma_1 + 1}{\gamma_o - 1}p_o\right)\tau_o + 2\Delta = 0 \tag{56}$$

where $\Delta \leq q_1 - q_o$. In the (τ_1, p_1)- plane the lines through (τ_o, p_o) tangent to the curve expressed by Eq. (56) are called the Rayleigh lines (Fig. 19). Their points of tangency, S_1 and S_2 are called the Chapman-Jouguet (CJ) points. The upper portion of the curve corresponds to detonations; the portion above S_1

to strong detonations and the portion below to weak detonations. The lower part of the curve corresponds to deflagrations. A portion of the curve is omitted as it corresponds to physically unacceptable conditions where $M^2 < 0$. The velocity and strength of a strong detonation are entirely determined by the state of the unburned gas in front of the detonation and one quantity behind the detonation just as for shock waves. Let p_o, ρ_o and u_o be given, as well as p_1, and assume the unburned gas lies to the right of the detonation, then from Eq. (56)

$$\tau_1 = \tau_o \left(\frac{\mu_1^2}{\mu_o^2} p_o + \mu_1^2 p_1 \right) \Big/ (\mu_1^2 p_o + p_1) - 2\mu_1^2 \Delta / (\mu_1^2 p_o + p_1) \qquad (57)$$

where

$$\mu_i^2 = \frac{\gamma_i - 1}{\gamma_i + 1}, \qquad i = 0, 1 \qquad (58)$$

and

$$M^2 = \rho_o (p_o - p_1)(\mu_1^2 p_o + p_1) \Big/ \left\{ \left(\frac{\mu_1^2}{\mu_o^2} - \mu_1^2 \right) p_o + (\mu_1^2 - 1) p_1 - 2\mu_1^2 \rho_o \Delta \right\} \qquad (59)$$

The states on the curve located between the CJ point S_1 and the line $\tau = \tau_o$ correspond to weak detonations. In this region, a CJ-detonation is followed by a rarefaction wave.

In what follows an explicit criterion for determining whether a detonation will be a strong detonation or a CJ-detonation is described. It is shown in Ref. 34 that at S_1, the velocity $|w_1| = a_1$ where $a_1 = (\gamma_1 p_1/\rho_1)^{1/2}$ is the sound speed, i.e., a CJ-detonation moves with respect to the burned gas with a velocity equal to the velocity of sound in the burned gas. This fact is used to determine the density ρ_{CJ}, velocity u_{CJ}, and pressure p_{CJ} behind a CJ-detonation. From Eqs. (51) and (54)

$$(p_1 - p_o)/(\tau_1 - \tau_o) = -\rho_1^2 w_1^2 = -\rho_1^2 \frac{\gamma_1 p_1}{\rho_1} \qquad (60)$$

Therefore we get

$$\tau_1 = \gamma_1 \tau_o p_1 / \{(\gamma_1 + 1) p_1 + p_o\} \qquad (61)$$

From Eqs. (56) and (61) we have,

$$p_1^2 + 2bp_1 + c = 0 \qquad (62)$$

where

$$b = -\frac{\gamma_1 - 1}{\gamma_o - 1} p_o + (\gamma_1 - 1)\rho_o \Delta \tag{63}$$

$$c = \frac{\mu_1^2}{\mu_o^2} p_o - 2\mu_1^2 \rho_o p_o \Delta \tag{64}$$

Therefore

$$p_{CJ} = p_1 = -b + (b^2 - c)^{1/2} \tag{65}$$

Given p_{CJ}, $\rho_{CJ} = \rho_1 = \tau_1^{-1}$ can be obtained from Eq. (61). Since $M = -\rho_1 w_1$ and $w_1 = -a_1$, we find

$$M = (\gamma_1 p_1 \rho_1)^{1/2} = (\gamma_1 p_{CJ} \rho_{CJ})^{1/2}$$

The velocity of the CJ-detonation wave D_{CJ} is found from

$$\rho_o(u_o - D_{CJ}) = -M$$

which yields $D_{CJ} = \{\rho_o u_o + (\gamma_1 p_{CJ} \rho_{CJ})^{1/2}\}/\rho_o$ and then

$$u_{CJ} = D_{CJ} - a_{CJ}$$

Suppose u_1, the velocity of the burned gas, is given. If $u_1 < u_{CJ}$ a CJ-detonation appears, followed by a rarefaction wave. If $u_1 = u_{CJ}$ a CJ-detonation appears alone, and if $u_1 > u_{CJ}$ a strong detonation takes place.

An outline of Chorin's method for calculating reacting-gas flows is described in the next section.

4.2.3 CHORIN'S METHOD FOR REACTING-GAS FLOWS

In this section, Eq. (47) is replaced by

$$\epsilon = \frac{1}{\gamma - 1} \frac{p}{\rho} + Zq \tag{66}$$

where Z is a progress parameter for the reaction, and q is the total available binding energy ($q \leq 0$). Z is assumed to satisfy the rate equation,

$$dZ/dt = -KZ \tag{67}$$

where

$$K = 0 \quad \text{if} \quad T = \frac{p}{\rho} \leq T_o$$
$$K = K_o \quad \text{if} \quad T = \frac{p}{\rho} > T_o \tag{68}$$

T_o is the ignition temperature and K_o is the reaction rate. Chorin has solved Eqs. (43), (44), (45), (46), (66), (67) and (68) using the RCM and has shown that a Riemann type problem can be solved even when deflagrations and detonations are included along with shock and rarefaction waves. In the present case, the initial data for a Riemann problem has the form of

$$\left.\begin{aligned} &S_\ell(\rho = \rho_\ell,\ p = p_\ell,\ u = u_\ell,\ Z = Z_\ell) \text{ for } x \leq 0 \\ \text{and} \\ &S_r(\rho = \rho_r,\ p = p_r,\ u = u_r,\ Z = Z_r) \text{ for } x > 0 \end{aligned}\right\} \tag{69}$$

When there is no chemistry ($K_o = 0$), Z = constant and Eq. (69) reduces to Eq. (7) and its solution is given in Chapter 2. In case $K_o \neq 0$, right and left waves may now be CJ or strong-detonation waves as well as shock and rarefaction waves. Chorin has incorporated these possibilities into the solution of the Riemann problem and developed a computer program to calculate this problem.

The state S_r remains a constant state; u_r and ρ_r are fixed. The energy in S_r must change at constant volume (and thus can do no work). The change δZ_r in Z_r can be found by integrating Eqs. (67) and (68), with $Z(0) = Z_r$ and $Z(\Delta t/2) = Z_r + \delta Z_r$, $\delta Z_r < 0$. The new pressure is written as

$$p_r^{new} = p_r + \delta p_r = p_r + (\gamma - 1)\, Z\, q\, \rho_r \tag{70}$$

In what follows, the superscript new, is dropped. Similarly, Z_ℓ changes to $Z_\ell + \delta Z_\ell$, and a new p_ℓ is found using the analog of Eq. (70).

In S_* the values of Z differ from the values $Z_r + \delta Z_r$, $Z_\ell + \delta Z_\ell$. Let $Z_{*\ell}$ be the value of Z to the left of the slip line ($dx/dt = u_*$) and let Z_{*r} be the value of Z to the right of the slip line. The difference in energy of formation across the right wave is $\Delta_r = \{Z_{*r} - (Z_r + \delta Z_r)\}q$, and across the left wave it is $\Delta_\ell = \{Z_{*\ell} - (Z_\ell + \delta Z_\ell)\}q$. Iteration will be carried out on the values $Z_{*\ell}$, Z_{*r}, Δ_ℓ, Δ_r. In the first iteration, Eqs. (19) to (22) are iterated with $Z_{*r} = Z_r + \delta Z_r$, $Z_{*\ell} = Z_\ell + \delta Z_\ell$, and thus $\Delta_\ell = \Delta_r = 0$. When this iteration has converged, a new pressure p_* is given, and new densities $\rho_{*\ell}$, ρ_{*r} can be found from Eqs. (9), (16) or the isentropic equation of state. New temperatures $T_{*\ell} = p_*/\rho_{*\ell}$, $T_{*r} = p_*/\rho_{*r}$, are evaluated, Eqs. (67) and (68) are solved, and new values $Z_{*\ell}$, Z_{*r}, Δ_ℓ, Δ_r are found. If $\Delta_r \geq 0$ the right wave is either a shock or a rarefaction wave, and if $\Delta_r < 0$ the right wave is either a CJ-detonation followed by a rarefaction wave or a strong detonation.

Let u_* be the velocity in S_*. Given Δ_ℓ, Δ_r, we can find the velocities u_{CJ_ℓ}, u_{CJ_r} behind possible CJ-detonations on the right and left. If $u_* \leq u_{CJ_r}$

the right wave is a CJ-detonation followed by rarefaction, and if $u_* \geq u_{CJ_r}$ the right wave is a strong detonation. The CJ state is unaffected by S_* (since it depends only on S_r) and as far as the Riemann solution is concerned it is a fixed state. If the right wave is a CJ-detonation, M_r is redefined as

$$M_r = (p_{CJ} - p_*)/(u_{CJ} - u_*)$$

where p_{CJ} is from Eq. (65) and then

$$M_r = (\rho_{CJ} p_{CJ})^{1/2} \phi_2(p_*/p_{CJ}), \quad p_*/p_{CJ} \leq 1 \tag{71}$$

ϕ_2 is defined in Eq. (13). If the right wave is a strong detonation, from Eq. (59),

$$M_r = \rho_r^{1/2} \phi_3(\rho_r \Delta_r, p_r, p_*)$$

where

$$(\phi_3)^2 = \frac{(p_r - p_*)(\mu_1^2 p_r + p_*)}{\left(\frac{\mu_1^2}{\mu_o^2} - \mu_1^2\right) p_r + (\mu_1^2 - 1) p_* - 2\mu_1^2 \rho_r \Delta_r} \tag{72}$$

Similar expressions occur on the left. A second iteration starts with M_ℓ, M_r from the previous iteration, and written out in full, appears as follows:

$$p_*^\nu = (u_\ell - u_r + p_r/M_r^\nu + p_\ell/M_\ell^\nu)/(1/M_\ell^\nu + 1/M_r^\nu) \qquad \nu \geq 0$$

$$p_*^{\nu+1} = \max(\epsilon, p_*^\nu)$$

$$u_*^\nu = (p_\ell - p_r + M_\ell^\nu u_\ell + M_r^\nu u_r)/(M_\ell^\nu + M_r^\nu)$$

where

$$(\rho_r, p_r, u_r) = (\rho_{CJ_r}, p_{CJ_r}, u_{CJ_r}) \quad \text{if right wave = CJ-detonation,}$$

$$= (\rho_r, p_r, u_r) \quad \text{otherwise,}$$

$$(\rho_\ell, p_\ell, u_\ell) = (\rho_{CJ_\ell}, p_{CJ_\ell}, u_{CJ_\ell}) \quad \text{if left wave = CJ-detonation,}$$

$$= (\rho_\ell, p_\ell, u_\ell) \quad \text{otherwise,}$$

$$M_r^{\nu+1} = \rho_r^{1/2} \phi_3(\rho_r \Delta_r, p_r, p_*^{\nu+1}) \quad \text{if right wave = strong detonation,}$$

$$= (\rho_r p_r)^{1/2} \phi(p_*^{\nu+1}/p_r) \quad \text{otherwise}$$

$$M_\ell^{\nu+1} = \rho_\ell^{1/2}\phi_3(\rho_\ell\Delta_\ell,\ p_\ell,\ p_*^{\nu+1}) \qquad \text{if left wave = strong detonation,}$$

$$= (\rho_\ell p_\ell)^{1/2}\phi(p_*^{\nu+1}/p_\ell) \qquad \text{otherwise.}$$

The iteration is stopped when it has converged, as before. New values of $Z_{*\ell}$, Z_{*r}, Δ_ℓ, Δ_r are evaluated, and the iteration is repeated. This process is stopped when Δ_ℓ, Δ_r change by less than some predetermined ϵ_3 over two successive iterations. Once S_* has been determined, the solution is sampled as described in Chapter 2. The only difference in the sampling procedure is that, if the wave is CJ-detonation, (ρ_r, p_r, u_r) are replaced by $(\rho_{CJ_r}, p_{CJ_r}, u_{CJ_r})$ in all equations which describe the flow to the left of the detonation wave. Similarly $(\rho_\ell, p_\ell, u_\ell)$ are replaced by $(\rho_{CJ_\ell}, p_{CJ_\ell}, u_{CJ_\ell})$ if the left wave is CJ-detonation wave. More details can be found in Ref. 7.

4.2.4 NUMERICAL RESULTS

In Ref. 7, Chorin has displayed numerical results in cases of a strong detonation wave, a CJ-detonation wave and a deflagration wave. However, those examples were meant to show the usefulness of the method while using only a small number of mesh points. Besides, the assumption $\gamma_0 = \gamma_1$ is quite a rough assumption from the point of view of actual applications. Here a practical case has been calculated in which the burned gas has different specific heat ratio from the unburned gas. It is assumed that a combustible gas mixture reacts in an infinitely thin reaction zone and turns into reaction products instantaneously and its composition stays the same afterward, namely, the specific heat ratio and the specific molecular weight change their values at the wave front from γ_0 to γ_1 and M_0 to M_1, respectively. A stoichiometric gas mixture of hydrogen and oxygen was chosen as an example. The data on combustion products were taken from the results obtained by Benoit (Refs. 35 and 36). Those conditions are:

unburned gas: $2H_2 + O_2$ gas mixture

$\gamma_0 = 1.40$, $M_0 = 12.0$

reaction products: H_2O (53.2%), OH (13.7%), H_2 (16.4%)

O_2 (4.9%), H (8.1%), O (3.8%)

$\gamma_1 = 1.22$, $M_1 = 14.5$

From these values, the released energy was calculated to be 22.95 K cal/mol. Under these assumptions and conditions, a CJ-detonation resulted, followed by a rarefaction wave. The pressure profiles are shown in Fig. 20. Although it takes some time for the CJ-detonation to be fully developed, the pressure profiles are quite similar once CJ-detonation is established. At the wave front, the pressure ratio p/p_0 jumps from 1 to a value of about 15 for a CJ-detonation. It then decays to a fairly constant stationary state in which p/p_0 is about 6, due to the rarefaction wave. This stationary state seems to extend from the starting position of the detonation wave to about half of the distance which the detonation

wave has travelled in the channel.

The pressure profiles of the reflected detonation wave as a shock wave at the end wall of the combustion tube is shown in Fig. 21. Since the reflected shock wave is propagating in a non-uniform state, the profiles of the reflected shock wave change accordingly. At the moment, when the detonation wave reflects at the end wall, the pressure ratio p/p_o is as high as 25 (this may be compared with the highest value of 8 for an intense planar shock wave). Later, when the reflected shock wave is propagating in the fairly uniform region p/p_o is about 12. In the sense that the data for the reaction products are needed as inputs for the computation, the program can still be improved. If a program which calculates the chemical reactions and determines the reaction products will be combined with Chorin's method, it will form a very important, useful and generalized method of calculating reacting-gas flows.

5. DISCUSSIONS AND CONCLUSIONS

It has been shown by using an extensive number of examples that the RCM provides exceptionally high computational accuracy for flows involving planar and spherical shock waves, rarefaction waves and contact surfaces, as well as their interactions. In addition, the RCM can handle flows with detonations and chemical reactions involving the above transition fronts.

Owing to the high accuracy of calculated values in p, ρ, u and the fact that the constant states are perfectly realized, very complex wave-interaction problems which involve small changes in physical parameters ρ, u, p, can be calculated, such as the reflection of a shock wave from the end wall of a shock tube and the subsequent interactions, or the head-on collision of a shock wave with a rarefaction wave.

Although, in practice, the accuracy of the wave positions is good (1 ~ 3% of the total length of the spatial zones in the examples investigated here), Glimm has recently developed "the method of tracking discontinuities", which improves this spatial error by a factor of 4 to 10 and locates the transition fronts with an accuracy of $0.05\Delta x$ to $0.5\Delta x$ (Ref. 37). This improvement must be greatly appreciated when one tries to apply the RCM to multidimensional wave-interaction problems where the number of mesh points used and the computation time are competitive.

Due to the randomness of the method, the rarefaction waves are not smooth. However, Sod states in his paper (Ref. 4) that the rarefaction wave obtained by the RCM could be smoothed out by a type of averaging and that he was considering this subject. Once this has been accomplished, it is expected that the RCM will increase its usefulness and applicability to those wave-interaction problems in which rarefaction waves are involved in a more complex manner.

There are a number of very important pseudo-stationary problems, such as oblique-shock-wave reflections (Ref. 1), which require new approaches to their numerical solutions. It is possible that the RCM may be ideally suited to the solution of regular, single-Mach, complex-Mach and double-Mach-reflection problems of oblique shock waves. A start in their direction has already been made for stationary regular and Mach oblique-shock-wave reflection by Chorin (Ref. 3). We are hopeful that complex-Mach and double-Mach reflections will be solved in the same manner and perhaps extended to similar reflections of spherical shock waves.

REFERENCES

1. Ben-Dor, G. Glass, I. I. — Nonstationary Oblique Shock-Wave Reflections: Actual Isopycnics and Numerical Experiements. A.I.A.A. J., Vol. 16, No. 11, p. 1146, 1978.

2. Glimm, J. — Solution in the Large for Nonlinear Hyperbolic Systems of Equations. Comm. Pure Appl. Math., Vol. 18, p. 697, 1965.

3. Chorin, A. J. — Random Choice Solution of Hyperbolic System. J. Comp. Phys., Vol. 22, p. 517, 1976.

4. Sod, G. A. — A Survey of Several Finite Difference Methods for Systems of Nonlinear Hyperbolic Conservation Laws. J. Comp. Phys., Vol. 27, p. 1, 1978.

5. von Neumann, J. Richtmyer, R. D. — A Method for the Numerical Calculation of Hydrodynamic Shocks. J. Appl. Phys. Vol. 21, p. 232, 1950.

6. Sod, G. A. — A Numerical Study of a Converging Cylindrical Shock. J. Fluid Mech., Vol. 83, p. 795, 1977.

7. Chorin, A. J. — Random Choice Methods with Applications to Reacting Gas Flow. J. Comp. Phys., Vol. 25, p. 253, 1977.

8. Godunov, S. K. — Finite Difference Methods for Numerical Computation of Discontinuous Solution of the Equations of Fluid Dynamics. Mat. Sbornik., Vol. 47, p. 271, 1959.

9. Glass, I. I. Patterson, G. N. — A Theoretical and Experimental Study of Shock-Tube Flows. J. Aero. Sci., Vol. 22, p. 73, 1955.

10. Glass, I. I. Hall, J. G. — Handbook of Supersonic Aerodynamics, Section 18, Shock Tubes. NAVORD Rept. 1488, Vol. 6, Bureau of Naval Weapons Publication, 1959.

11. Gurke, G. Schwarzkopf, G. — Ein Programm zum Erstellen von Wellendiagrammen fur das Einfash Membranstossrohr. Ernst-Mach-Inst., Bericht Nr. 12, 1969.

12. Gould, D. G. — The Head-On Collision of Two Shock Waves and a Shock and Rarefaction Wave in One-Dimensional Flow. UTIA Report No. 17, 1952.

13. Steketee, J. A. — On the Interaction of Rarefaction Waves in a Shock Tube. UTIA Review No. 4, 1952.

14. Kuratani, K. Tsuchiya, S. — Shock Waves in Chemistry and Physics. Shokabo, Tokyo, 1968.

15. Bitondo, D. Glass, I. I. Patterson, G. N. — One-Dimensional Theory of Absorption and Amplification of a Plane Shock Wave by a Gaseous Layer. UTIA Report No. 5, 1950.

16. Ford, C. A.
Glass, I. I.
An Experimental Study of Shock-Wave Refraction. J. Aero. Sci., Vol. 23, No. 2, pp. 189-191, 1956.

17. Taylor, G. I.
The Formation of a Blast Wave by a Very Intense Explosion. Proc. Roy. Soc., A210, p. 159, 1950.

18. Guderley, G.
Strong Spherical and Cylindrical Shock Waves in the Neighbourhood of the Center of a Sphere or the Axis of a Cylinder. Luftfahrtforschung, Vol. 19, No. 9, 1942.

19. Elsenaar, A.
A Numerical Model for a Combustion-Driven Spherical Implosion Wave. UTIAS Tech. Note No. 144, 1969.

20. Lin, S. C.
Cylindrical Shock Waves Produced by Instantaneous Energy Release. J. Appl. Phys., Vol. 25, p. 54, 1954.

21. Bethe, H. A.
Fuchs, K.
von Neumann, J.
Peierls, R.
Penney, W. G.
Shock Hydrodynamics and Blast Waves. Los Alamos Scientific Laborator Report. AECD-2860, 1944.

22. Harris, E. G.
Exact and Approximate Treatment of the One-Dimensional Blast Wave. Naval Research Laboratory Report 4858, 1956.

23. Chisnell, R. F.
The Motion of a Shock Wave in a Channel with Applications to Cylindrical and Spherical Shock Waves. J. Fluid Mech., Vol. 2, p. 286, 1957.

24. Whitham, G. B.
On the Propagation of Shock Waves Through Regions of Non-Uniform Area of Flow. J. Fluid Mech., Vol. 4, p. 337, 1958.

25. Glass, I. I.
Spherical Flows and Shock Waves. UTIA Decennial Symposium, Technical Sessions, Proceedings, Part III, p. 233, 1959.

26. Boyer, D. W.
Brode, H. L.
Glass, I.I.
Hall, J. G.
Blast from a Pressurized Sphere. UTIA Report No. 48, 1958.

27. Brode, H. L.
Numerical Solutions of Spherical Blast Waves. Rand Corp. Research Memorandum RM-1363-AEC, 1954.

28. Brode, H. L.
Blast Wave from a Sherical Charge. Phys. of Fluids, Vol. 2, No. 2, p. 217, 1959.

29. Payne, R. B.
A Numerical Method for a Converging Cylindrical Shock. J. Fluid Mech., Vol. 2, No. 2, p. 185, 1957.

30. Lapidus, A.
Computation of Radially Symmetric Shocked Flows. J. Comp. Phys., Vol. 8, p. 106, 1971.

31. Boyer, D. W. — Spherical Explosions and Implosions. UTIA Report No. 58, 1959.

32. Glass, I. I. — Aerodynamics of Blasts. Canadian Aeronautical J., Vol. 7, No. 3, 1961.

33. Glass, I. I.; Ribner, H. S.; Gottlieb, J. J. — Canadian Sonic-Boom Simulation Facilities. CASI J., Oct. 1972, pp. 235-246.

34. Courant, R.; Friedrichs, K. O. — Supersonic Flows and Shock Waves. Interscience Publishers, Inc., New York, 1948.

35. Benoit, A. — Properties of Chapman-Jouguet Detonations in Stoichiometric Hydrogen-Oxygen Mixtures Diluted with Helium and Hydrogen. UTIAS Tech. Note No. 104, 1966.

36. Benoit, A.; Glass, I. I. — An Experimental Study of Spherical Combustion Waves in a Hemispherical Chamber. Combustion and Flame, Vol. 12, No. 2, 1968, pp. 521-533.

37. Glimm, J.; Marchesin, D. — Subgrid Resolution of Fluid Discontinuities. The Rockefeller University, New York, 1979.

38. Baker, W. E. — Explosions in Air. University of Texas Press, Austin, 1973, pp. 78-117.

APPENDIX A: CONTACT SURFACE MOTION

When wave interactions are considered in a flow field which involves different gases with different specific heat ratios, it is necessary to know the positions of the contact surfaces, across which the specific heat ratios change their values. The method used here for determining the paths of contact surfaces is as follows.

In principle, as previously mentioned, solutions $\bar{\rho}$, $\bar{u}$, $\bar{p}$ are determined at points $(i\Delta x, n\Delta t)$ and $\{(i + 1/2)\Delta x, (n + 1/2)\Delta t\}$. In a real program, however, the calculation is carried out in a two-step method and there are no intermediate spatial mesh points like $(i + 1/2)\Delta x$. At the end of the first half-step, those solutions which are supposed to be placed at points $\{(i + 1/2)\Delta x, (n + 1/2)\Delta t\}$ will be stored in mesh points $\{(i + 1)\Delta x, (n + 1/2)\Delta t\}$; namely, storing positions are shifted at half-mesh intervals, $1/2\ \Delta x$, to the right. On the other hand, at the end of the second half-step, solutions are stored after being shifted $1/2\ \Delta x$ to the left. Figure A-1 illustrates this procedure. We can see that at the end of every other half time-step, the mesh points correspond to the same physical positions. Considering this procedure, we can determine the position of contact surfaces and assign the different values of the specific heat ratio γ. Suppose a contact surface was located between the i-th mesh and the (i-1)-th mesh at the beginning of the first half-step, i.e.,

$$\left.\begin{aligned} \gamma(i) &= \gamma_1 \\ \gamma(i-1) &= \gamma_2 \end{aligned}\right\} \quad \text{at } t = n\Delta t$$

and one of the regions to the left of the contact surface was chosen by sampling. Then, as described before, the solution which is associated with this region will be given to the i-th mesh point. This means that the contact surface has moved one mesh to the right, namely, from the mesh (i-1) to the mesh i. When sampling point P lies to the right of the contact surface, the solution associated with one of the regions having the specific heat ratio γ_1 will be assigned to the mesh i. This situation corresponds to a situation where the contact surface did not move at all because the distribution of γ is the same as before. In the second half-step, the movement of a contact surface is determined in the same manner as in the first half-step, except that, in this case, the movement of a contact surface is either one mesh to the left or stays in the same position. Figure A-2 and Table A-1 illustrate the propagation of a contact surface.

APPENDIX B: PROGRAM LISTINGS

In the program, all dependent thermodynamic and dynamic values are made nondimensional as follows

$$\bar{p} = \frac{p}{p_1}, \qquad \bar{\rho} = \frac{\rho}{\rho_1}, \qquad \bar{u} = \frac{\sqrt{\gamma_1}\, u}{a_1}$$

The independent variables of time and distance are also made nondimensional so that

$$\bar{t} = \frac{a_1 t}{\sqrt{\gamma_1}\, L} \quad \text{and} \quad \bar{x} = \frac{x}{L}$$

where L is the total length of a shock tube or the radius of an initial cylindrical or spherical charge. The program consists of one main program and five subroutines. Their functions will be described briefly.

Initial conditions; type of flow such as plane, cylindrical or spherical; how and how often the output should be printed; mesh number; when to stop the calculation; the boundary conditions are put into the main program. The main program determines the time increment DT(Δt) , and spatial increment DX(Δx), in such a way that the Courant condition is satisfied, though the method itself is stable, even if the Courant condition is violated. A random number XI(θ_n'), is determined at each half-time step with the aid of the SUBROUTINE RANDU which is designed by IBM to generate random number, YFL over (0, 1). Then, at each mesh point, the Riemann problem is solved calling the SUBROUTINE GLIMM. It solves the Riemann problem receiving the two initial state S_ℓ and S_r from the main program and does the sampling according to the random number X1. In the course of solving the Riemann problem, FUNCTION FAI which corresponds to the function ϕ in Eqs. (11), (13) and (17) in Chapter 2 is used. By putting the sampled solutions into each mesh, the first half-step is finished. Repeating the same procedure for the second half-step, one time step is finished and the solutions for a planar waves are obtained. Boundary conditions are taken into consideration when S_ℓ and S_r are chosen in the main program. The results are printed calling the SUBROUTINE STTOUT. If either a cylindrical or spherical flow is needed to be solved, Eq. (36) in Sec. 4.1.2 is solved after the planar case has been solved. This is done calling SUBROUTINE INHOM.

LISTING OF THE COMPUTER PROGRAM

```
      C           RANDOM CHOICE METHOD   VARIATION  2.
      C             PROGRAM FOR EXPLOSION OF A PRESSURIZED HELIUM SPHERE
    1       COMMON//DT,RL,UL,PL,R,U,P,E,RR,UR,PR,XI,Y,GAMMAL,GAMMAR
    2       COMMON/OUT/TIME,N,DX,RHO(301),PRE(301),UX(301),ENG(301),GAMMA(301)
    3       COMMON/RAD/ETA
    4       INTEGER TSTP
    5       NSTOP=320
    6       NPRINT=5
    7       N=180
    8       NP1=N+1
    9       NHALF=34
   10       NHALP1=NHALF+1
   11       DX=1./FLOAT(N)
   12       DT=0.01
   13       TIME=0.
   14       VMAX=0.
   15       NCNTCT=NHALP1
   16       NINCRS=0
   17       GAMMRI=1.400
   18       GAMMLI=1.667
   19       K1=11
   20       K2=7
   21       NU=2
   22       SIGMA=.5
   23       ETA=3.
      C     SET INITIAL CONDITIONS
   24       DO 83 I=1,NP1
   25       IF(I.GE.NCNTCT) GO TO 11
   26       GAMMA(I)=GAMMLI
   27       GO TO 83
   28    11 GAMMA(I)=GAMMRI
   29    83 CONTINUE
   30       PL=18.25
   31       RL=2.523
   32       UL=0.
   33       PR=1.
   34       RR=1.
   35       UR=0.
   36       DO 15 I=1,NHALF
   37       RHO(I)=RL
   38       PRE(I)=PL
   39       UX(I)=UL
   40    15 CONTINUE
   41       DO 16 I=NHALP1,NP1
   42       RHO(I)=RR
   43       PRE(I)=PR
   44       UX(I)=UR
   45    16 CONTINUE
      C     BEGIN TIME STEP
   46       IX=123456789
   47       DO 100 TSTP=1,NSTOP
   48       DO 8 I=2,N
   49       VMAX1=ABS(UX(I))+SQRT(GAMMA(I)*PRE(I)/RHO(I))
```

```
      IF(VMAX1 .GT. VMAX)  VMAX=VMAX1
    8 CONTINUE
      DTT=SIGMA*DX/VMAX
      IF(DTT .LT. DT) DT=DTT
      TIME=TIME+2.*DT
C     COMPUTE FIRST HALF STEP
C     GENERATE RANDOM SI USING CHORIN'S METHOD
      NU=MOD(NU+K2,K1)
      CALL RANDU(IX,IY,YFL)
      SI=(YFL+FLOAT(NU))/FLOAT(K1)
C     XI LIES BETWEEN -DX/2 AND DX/2
      XI=SI*DX-0.5*DX
      DO 40 I=2,NP1
      RR=RHO(I)
      UR=UX(I)
      PR=PRE(I)
      GAMMAL=GAMMA(I-1)
      GAMMAR=GAMMA(I)
      IF(I .EQ. 2.) GO TO 43
      RL=RIM1
      PL=PIM1
      UL=UIM1
      GO TO 44
C     BOUNDARY CONDITION AT AXIS R=0.
   43 RL=RR
      UL=-UR
      PL=PR
C     COMPUTE FIRST HALF STEP OF GLIMM
   44 CALL GLIMM
      IF(I.NE.NCNTCT) GO TO 35
      NINCRS=1
      IF(XI.GE.Y) NINCRS=0
   35 RIM1=RHO(I)
      RHO(I)=R
      PIM1=PRE(I)
      PRE(I)=P
      UIM1=UX(I)
      UX(I)=U
   40 CONTINUE
      NCNTCT=NCNTCT+NINCRS
      DO 75 I=1,NP1
      IF(I.GE.NCNTCT) GO TO 4
      GAMMA(I)=GAMMLI
      GO TO 75
    4 GAMMA(I)=GAMMRI
   75 CONTINUE
C     COMPUTE SECOND HALF STEP
C     GENERATE RANDOM SI USING CHORIN'S METHOD
      NU=MOD(NU+K2,K1)
      CALL RANDU(IX,IY,YFL)
      SI=(YFL+FLOAT(NU))/FLOAT(K1)
C     XI LIES BETWEEN -DX/2 AND DX/2
      XI=SI*DX-0.5*DX
      DO 60 I=1,N
      RL=RHO(I)
      PL=PRE(I)
      UL=UX(I)
      GAMMAL=GAMMA(I)
      GAMMAR=GAMMA(I+1)
      IF(I .EQ. N) GO TO 63
```

```
102           RR=RHO(I+1)
103           PR=PRE(I+1)
104           UR=UX(I+1)
105           GO TO 64
      C       BOUNDARY CONDITION AT R=1.
106        63 RR=RL
107           UR=-UL
108           PR=PL
      C       COMPUTE SECOND HALF STEP OF GLIMM
109        64 CALL GLIMM
110           NCNTM1=NCNTCT-1
111           IF(I.NE.NCNTM1) GO TO 55
112           NINCRS=-1
113           IF(X(I).LT.Y) NINCRS=0
114        55 RHO(I)=R
115           PRE(I)=P
116           UX(I)=U
117        60 CONTINUE
118           NCNTCT=NCNTCT+NINCRS
119           DO 70 I=1,NP1
120           IF(I.GE.NCNTCT) GO TO 3
121           GAMMA(I)=GAMMLI
122           GO TO 70
123         3 GAMMA(I)=GAMMRI
124        70 CONTINUE
125           CALL INHOM
126           IF(MOD(TSTP,NPRINT).EQ.0) CALL STTOUT
127       100 CONTINUE
128           STOP
129           END
```

```
130           SUBROUTINE GLIMM
131           COMMON//DT,RL,UL,PL,R,U,P,E,RR,UR,PR,XI,Y,GAMMAL,GAMMAR
132           REAL ML,MR,MLP1,MRP1
133           EPS=1.0E-6
134           IT=0
135           ITSTOP=20
      C       CONSTRUCTION OF RIEMANN PROBLEM
      C       ALFA IS THE CONVERGENCE FACTOR
      C       INITIAL ML AND MR
136           ALFA=1.
137           ALFAM=1.-ALFA
138           ML=100.
139           MR=100.
140           COEFL=SQRT(PL*RL)
141           COEFR=SQRT(PR*RR)
142           PSTAR=.5*(PL+PR)
      C       SOLVE RIEMANN PROBLEM USING GODUNOV'S ITERATIVE METHOD
143        10 IT=IT+1
      C       IF PSTAR IS LESS THAN EPS THEN PSTAR IS SET EQUAL
      C       TO 1.0E-6 TO PREVENT PSTAR FROM BECOMING NEGATIVE.
144           IF(PSTAR.LT.EPS) PSTAR=EPS
      C       COMPUTE MR AND ML AT STEP Q+1
145           MLP1=COEFL*PHI(PSTAR/PL,GAMMAL)
146           MRP1=COEFR*PHI(PSTAR/PR,GAMMAR)
147           DIFML=ABS(MLP1-ML)
148           DIFMR=ABS(MRP1-MR)
149           ML=MLP1
150           MR=MRP1
      C       COMPUTE NEW PRESSURE PSTAR
151           PSTARP=PSTAR
152           PSTAR=(UL-UR+PR/MR+PL/ML)/(1./ML+1./MR)
153           PSTAR=ALFA*PSTAR+ALFAM*PSTARP
154           IF(IT .LE. ITSTOP) GO TO 30
155           IF(ABS(PSTAR-PSTARP) .LT. EPS) GO TO 40
156           IF(DIFML*DIFMR .LT. EPS) GO TO 40
157           ALFA=ALFA/2.
158           ALFAM=1.-ALFA
159           IF(ALFAM .LT. EPS) GO TO 40
160           IT=0
161        30 IF(DIFML .GT. EPS) GO TO 10
162           IF(DIFMR .GT. EPS) GO TO 10
      C       COMPUTE USTAR AT END OF GODUNOV ITERATION
163        40 USTAR=(PL-PR+MR*UR+ML*UL)/(ML+MR)
      C       BEGIN GLIMM'S METHOD
164           IREGL=1
165           IF(PSTAR .LT. PL) IREGL=2
166           IREGR=1
167           IF(PSTAR .LT. PR) IREGR=2
168           X=USTAR*DT
169           Y=X
```

```
      IF(XI .GE. X) GO TO 200
C     LEFT SIDE
      IF(IREGL .EQ. 2) GO TO 110
C     COMPUTE LEFT SHOCK SPEED
      U=UL-ML/RL
      X=U*DT
      IF(XI .GE. X) GO TO 100
C     LEFT OF LEFT SHOCK
      R=RL
      U=UL
      P=PL
      GO TO 500
C     RIGHT OF LEFT SHOCK
  100 R=ML/(USTAR-U)
      U=USTAR
      P=PSTAR
      GO TO 500
C     COMPUTE SOUND SPEED IN LEFT STATE
  110 CL=SQRT(GAMMAL*PL/RL)
      X=(UL-CL)*DT
      IF(XI .GE. X) GO TO 120
C     LEFT OF LEFT FAN
      R=RL
      U=UL
      P=PL
      GO TO 500
C     COMPUTE CONSTANT OF ISENTROPIC LAW - A
  120 A=PL/(RL**GAMMAL)
C     COMPUTE DENSITY IN STATE STAR  *
C     COMPUTE SOUND SPEED IN STATE STAR  *
      RSTAR=(PSTAR/A)**(1./GAMMAL)
      CSTAR=SQRT(GAMMAL*PSTAR/RSTAR)
      X=(USTAR-CSTAR)*DT
      IF(XI .GE. X) GO TO 130
C     IN LEFT FAN
      U=(2./(GAMMAL+1.))*(XI/DT+CL+0.5*(GAMMAL-1.)*UL)
      RINT=CL+0.5*(GAMMAL-1.)*(UL-U)
      R=(RINT*RINT/(A*GAMMAL))**(1./(GAMMAL-1.))
      P=A*(R**GAMMAL)
      GO TO 500
C     RIGHT OF LEFT FAN
  130 R=RSTAR
      U=USTAR
      P=PSTAR
      GO TO 500
C     RIGHT SIDE
  200 IF(IREGR .EQ. 2) GO TO 220
C     COMPUTE RIGHT SHOCK SPEED
      U=UR+MR/RR
      X=U*DT
      IF(XI .GE. X) GO TO 210
C     LEFT OF RIGHT SHOCK
      R=-MR/(USTAR-U)
      U=USTAR
      P=PSTAR
      GO TO 500
C     RIGHT OF RIGHT SHOCK
  210 R=RR
      U=UR
      P=PR
```

```
215         GO TO 500
      C     COMPUTE CONSTANT OF INSENTROPIC LAW - A
216     220 A=PR/(RR**GAMMAR)
      C     COMPUTE DENSITY IN STATE STAR  *
217         RSTAR=(PSTAR/A)**(1./GAMMAR)
      C     COMPUTE SOUND SPEED IN STATE STAR  *
218         CSTAR=SQRT(GAMMAR*PSTAR/RSTAR)
219         X=(USTAR+CSTAR)*DT
220         IF(XI .GE. X) GO TO 230
      C     LEFT OF RIGHT FAN
221         R=RSTAR
222         U=USTAR
223         P=PSTAR
224         GO TO 500
      C     COMPUTE SOUND SPEED IN RIGHT STATE
225     230 CR=SQRT(GAMMAR*PR/RR)
226         X=(UR+CR)*DT
227         IF(XI .GE. X) GO TO 240
      C     IN RIGHT FAM
228         U=(2./(GAMMAR+1.))*(XI/DT-CR+0.5*(GAMMAR-1.)*UR)
229         RINT=CR+0.5*(GAMMAR-1.)*(U-UR)
230         R=(RINT*RINT/(A*GAMMAR))**(1./(GAMMAR-1.))
231         P=A*(R**GAMMAR)
232         GO TO 500
      C     RIGHT OF RIGHT FAN
233     240 R=RR
234         U=UR
235         P=PR
236     500 CONTINUE
237         RETURN
238         END
```

```
      SUBROUTINE RANDU(IX,IY,YFL)
      IY=IX*65539
      IF(IY)5,6,6
    5 IY=IY+2147483647+1
    6 YFL=IY
      YFL=YFL*.4656613E-9
      IX=IY
      RETURN
      END

      SUBROUTINE STTOUT
      COMMON//DT,RL,UL,PL,R,U,P,E,RR,UR,PR,XI,Y,GAMMAL,GAMMAR
      COMMON/OUT/TIME,N,DX,RHO(301),PRE(301),UX(301),ENG(301),GAMMA(301)
      WRITE(6,10000) TIME
10000 FORMAT(1H1,7H TIME = ,F11.7)
      WRITE(6,10001)
10001 FORMAT(1H0,3H  X,4X,5HDENSE,4X,3HVEL,5X,4HPRES,3X,3HGAM/)
      DO 20 I=2,61
      KT1=I-1
      RT1=RHO(I)
      UT1=UX(I)
      PT1=PRE(I)
      G1=GAMMA(I)
      KT2=I+59
      RT2=RHO(I+60)
      UT2=UX(I+60)
      PT2=PRE(I+60)
      G2=GAMMA(I+60)
      KT3=I+119
      RT3=RHO(I+120)
      UT3=UX(I+120)
      PT3=PRE(I+120)
      G3=GAMMA(I+120)
      PRINT5,KT1,RT1,UT1,PT1, G1,KT2,RT2,UT2,PT2, G2,KT3,RT3,UT3,PT3, G3
    5 FORMAT(1H ,3(I4,4F8.3,4X))
   20 CONTINUE
      RETURN
      END
```

```
276           FUNCTION PHI(X,GAMMA)
277           EPS=1.0E-6
278           IF(ABS(1.-X) .GT. EPS) GO TO 100
279           PHI=SQRT(GAMMA)
280           RETURN
281       100 COEF1=0.5*(GAMMA+1.)
282           COEF2=0.5*(GAMMA-1.)
283           COEF3=COEF2/GAMMA
284           IF(X .GE. 1.) GO TO 200
285           PHI=COEF2*(1.-X)/(SQRT(GAMMA)*(1.-(X**COEF3)))
286           RETURN
287       200 PHI=SQRT(COEF1*X+COEF2)
288           RETURN
289           END

290           SUBROUTINE INHOM
291           COMMON//DT,RL,UL,PL,R,U,P,E,RR,UR,PR,XI,Y,GAMMAL,GAMMAR
292           COMMON/OUT/TIME,N,DX,RHO(301),PRE(301),UX(301),ENG(301),GAMMA(301)
293           COMMON/RAD/ETA
294           REAL MOM
295           NP1=N+1
296           DO 100 I=2,NP1
297           G=GAMMA(I)
298           X=FLOAT(I-1)*DX
299           R=RHO(I)
300           P=PRE(I)
301           U=UX(I)
302           E=P/(G-1.)+0.5*R*U*U
303           DEN=R-DT*(ETA-1.)*R*U/X
304           MOM=R*U*(1.-DT*(ETA-1.)*U/X)
305           E=E-DT*(ETA-1.)*U*(E+P)/X
306           RHO(I)=DEN
307           UX(I)=MOM/DEN
308           PRE(I)=(G-1.)*(E-0.5*MOM*MOM/DEN)
309       100 CONTINUE
310           RETURN
311           END
```

TABLE 1. COMPARISON OF PRESENT CALCULATION WITH REF. 11

Region	REF. 11			PRESENT RESULTS		
	ρ	p	u	ρ	p	u
1	1.000	1.000	0.000	1.000	1.000	0.000
2	2.555	4.161	1.172	2.555	4.160	1.172
3	7.100	4.161	1.172	7.098	4.160	1.172
4	27.000	27.000	0.000	27.000	27.000	0.000
5	5.587	13.221	0.000	5.586	13.217	0.000
6	6.701	17.063	0.286	6.698	17.055	0.286
7	17.997	17.063	0.286	17.987	17.055	0.286
8	7.985	21.823	0.000	7.981	21.812	0.000
9	8.324	23.133	0.069	8.320	23.120	0.069
10	22.349	23.133	0.069	22.335	23.120	0.069
11	8.675	24.509	0.000	8.670	24.494	0.000
12	8.761	24.852	0.017	8.757	24.837	0.017
13	23.523	24.852	0.017	23.507	24.37	0.017
14	8.849	25.200	0.000	8.844	25.184	0.000

TABLE 2. VALUES OF ρ, p AND u FOR REGIONS IN FIG. 5

Region	ρ	p	u	Region	ρ	p	u
2	2.555	4.160	- 1.172	36	8.886	25.353	0.000
3	7.098	4.160	- 1.172	37	8.818	25.083	+ 0.013
5	5.586	13.217	0.000	38	8.824	25.103	+ 0.012
6	6.698	17.055	- 0.286	39	23.686	25.103	+ 0.012
7	17.987	17.055	- 0.286	40	23.670	25.079	+ 0.013
8	7.981	21.812	0.000	41	23.665	25.073	+ 0.013
9	8.320	23.120	- 0.069	42	23.663	25.072	+ 0.013
10	22.335	23.120	- 0.069	43	23.662	25.071	+ 0.013
11	22.104	22.790	- 0.058	44	22.414	25.071	+ 0.013
12	20.939	22.790	- 0.058	45	22.355	24.979	+ 0.015
13	8.670	24.494	0.000	46	8.819	25.084	+ 0.013
14	8.757	24.837	- 0.017	47	23.673	25.084	+ 0.013
15	23.507	24.837	- 0.017	48	23.669	25.079	+ 0.013
16	23.269	24.487	- 0.007	49	23.668	25.078	+ 0.013
17	23.251	24.463	- 0.006	50	23.666	25.076	+ 0.013
18	22.025	24.463	- 0.006	51	8.751	24.814	0.000
19	21.965	24.373	- 0.003	52	8.756	24.835	- 0.001
20	21.631	24.373	- 0.003	53	8.752	24.816	- 0.000
21	8.844	25.184	0.000	54	8.735	24.752	+ 0.003
22	8.865	25.269	- 0.004	55	23.449	24.752	+ 0.003
23	23.798	25.269	- 0.004	56	23.445	24.746	+ 0.003
24	23.558	24.913	+ 0.006	57	23.442	24.745	+ 0.003
25	23.541	24.889	+ 0.007	58	8.761	24.855	0.000
26	23.535	24.883	+ 0.007	59	8.757	24.837	+ 0.001
27	22.294	24.883	+ 0.007	60	8.741	24.772	+ 0.004
28	22.235	24.792	+ 0.010	61	8.742	24.777	+ 0.003
29	8.798	24.999	+ 0.008	62	23.466	24.777	+ 0.003
30	23.616	24.999	+ 0.008	63	23.462	24.771	+ 0.004
31	23.599	24.975	+ 0.009	64	8.732	24.818	0.000
32	23.594	24.969	+ 0.009	65	8.736	24.754	+ 0.003
33	23.592	24.968	+ 0.010	66	8.737	24.759	+ 0.003
34	22.348	24.968	+ 0.010	67	8.719	24.690	0.000
35	22.289	24.876	+ 0.013	68	8.721	24.694	- 0.000

TABLE 3. COMPARISON OF PRESENT CALCULATIONS WITH REF. 12

Region	REF. 12			PRESENT RESULTS		
	ρ	p	u	ρ	p	u
0	1.00000	1.00000	0.00000	1.0000	1.0000	0.0000
1	1.60300	1.96000	0.50789	1.603	1.960	0.5079
2	0.64340	0.53935	0.42207	0.6435	0.5393	0.4217
3	1.07360	1.12217	0.93126	1.074	1.122	0.9314
4	1.07630	1.12217	0.93126	1.076	1.122	0.9314
5	2.42830	1.96000	0.50789	2.428	1.960	0.5079
6	0.45660	0.53935	0.42207	0.4565	0.5393	0.4217
7	4.41850	4.1485	0.00000	4.1485	4.1485	0.0000
8	0.30659	0.30659	0.00000	0.30659	0.30659	0.0000

TABLE 4. HEAD-ON COLLISION OF TWO RAREFACTION WAVES

Region	METHOD OF CHARACTERISTICS			PRESENT NUMERICAL RESULTS		
	ρ	p	u	ρ	p	u
1	0.49119	0.024793	0.0000	0.49119	0.024793	0.000
2	1.5984	0.3995	0.6145	1.598	0.399	0.614
3	0.5192	0.3995	0.6145	0.519	0.399	0.614
4	1.0000	1.0000	0.0000	1.000	1.000	0.0
5	0.6901	0.5950	- 0.3576	0.690	0.595	- 0.358
6	4.5474	0.5950	- 0.3576	4.547	0.595	- 0.358
7	1.7457	0.088118	0.0000	1.7457	0.088118	0.000
8	0.3393	0.2202	0.2569	0.339	0.220	0.257

TABLE 5. CONTACT-SURFACE TAILORING

Region	EXACT SOLUTIONS			PRESENT NUMERICAL RESULTS		
	ρ	p	u	ρ	p	u
1	1.000	1.000	0.000	1.000	1.000	0.000
2	3.100	12.310	2.140	3.079	12.310	2.141
3	3.484	12.310	2.140	3.484	12.310	2.141
4	10.568	58.207	0.000	10.568	58.207	0.000
5	6.907	54.982	0.000	6.860	54.976	0.000
7	6.907	54.982	0.000	6.860	54.976	0.000
8	9.253	54.982	0.000	9.251	54.976	0.000

TABLE 6. SHOCK-WAVE REFRACTION AT A STATIONARY CONTACT LAYER

Region	EXACT SOLUTIONS			PRESENT NUMERICAL RESULTS		
	ρ	p	u	ρ	p	u
1	0.13823	1.0000	0.0000	0.138	1.000	0.0
2	0.2183	2.1965	1.5058	0.218	2.196	1.505
3	1.6481	2.1965	1.5058	1.648	2.196	1.505
4	2.3920	3.7000	1.0594	2.392	3.700	1.059
5	1.0000	1.0000	0.0000	1.000	1.000	0.0
6	1.0000	1.0000	0.0000	1.000	1.000	0.0
7	2.0988	2.9717	0.8587	2.099	2.971	0.859
8	0.2560	2.9717	0.8587	0.261	2.971	0.859

TABLE A-1 RELATION BETWEEN SAMPLED REGION IN FIG. A-2 AND CONTACT-SURFACE MOVEMENT

	SAMPLED REGION	MOVEMENT OF CONTACT SURFACE
First-half step	A	+ 1
	B	0
Second-half step	C	0
	D	- 1

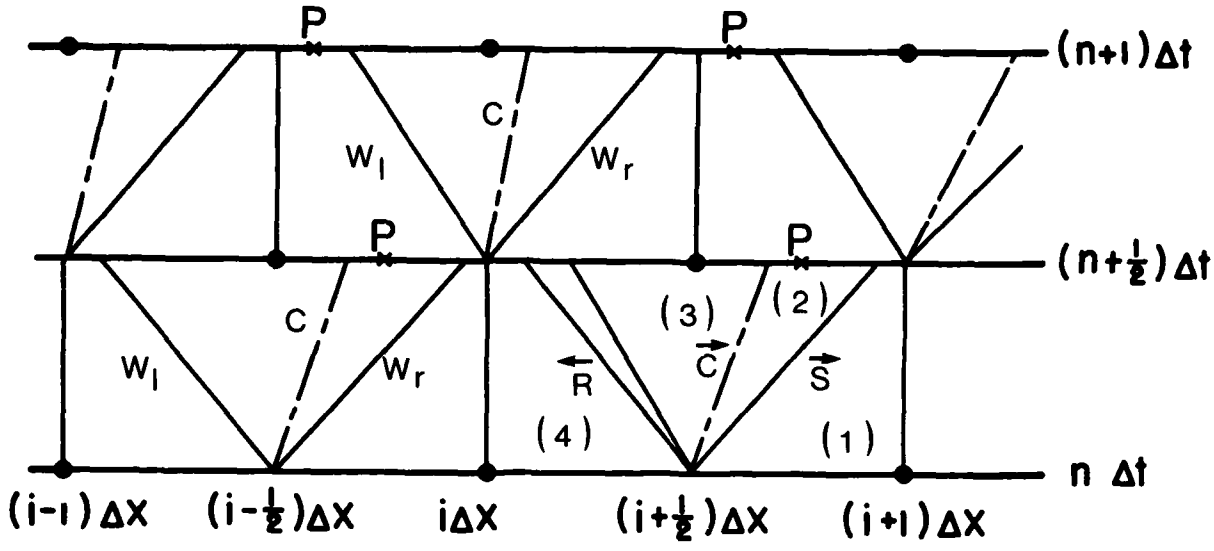

FIG. 1 GRID CONSTRUCTION FOR RANDOM-CHOICE METHOD AND SEQUENCE OF SAMPLING PROCEDURE.

● - GRID POINTS WHERE SOLUTIONS ARE SOUGHT; W_ℓ, W_r - LEFT OR RIGHT RUNNING WAVES; C - CONTACT SURFACE; P - SAMPLING POINT.

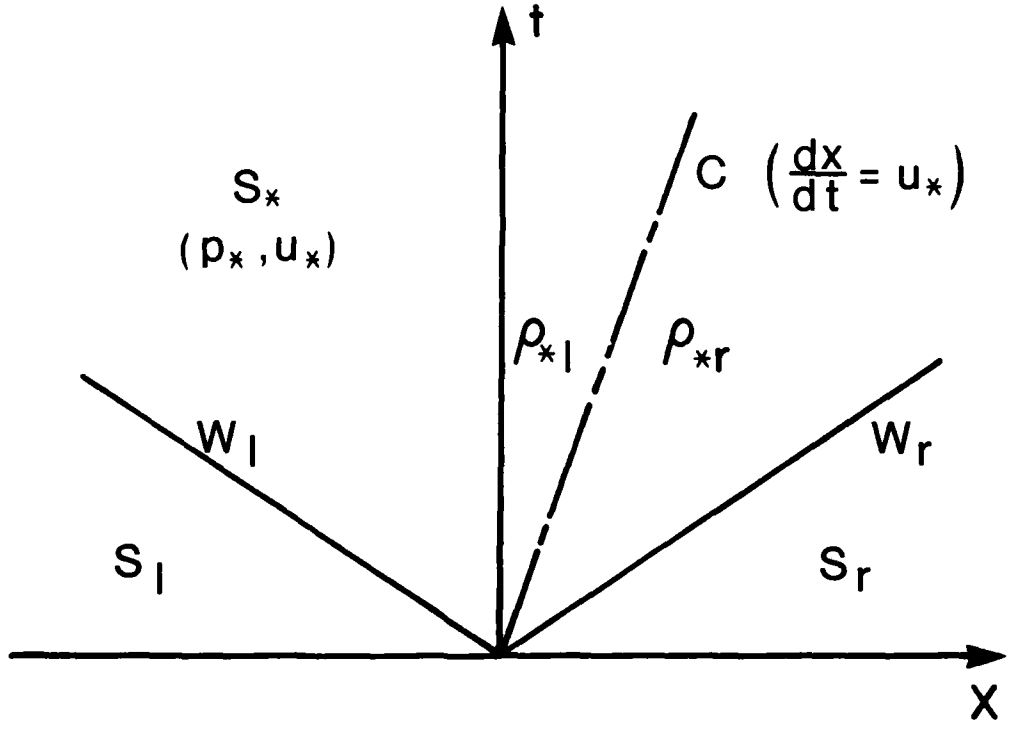

FIG. 2 SOLUTION OF A RIEMANN PROBLEM IN (x-t)-PLANE.

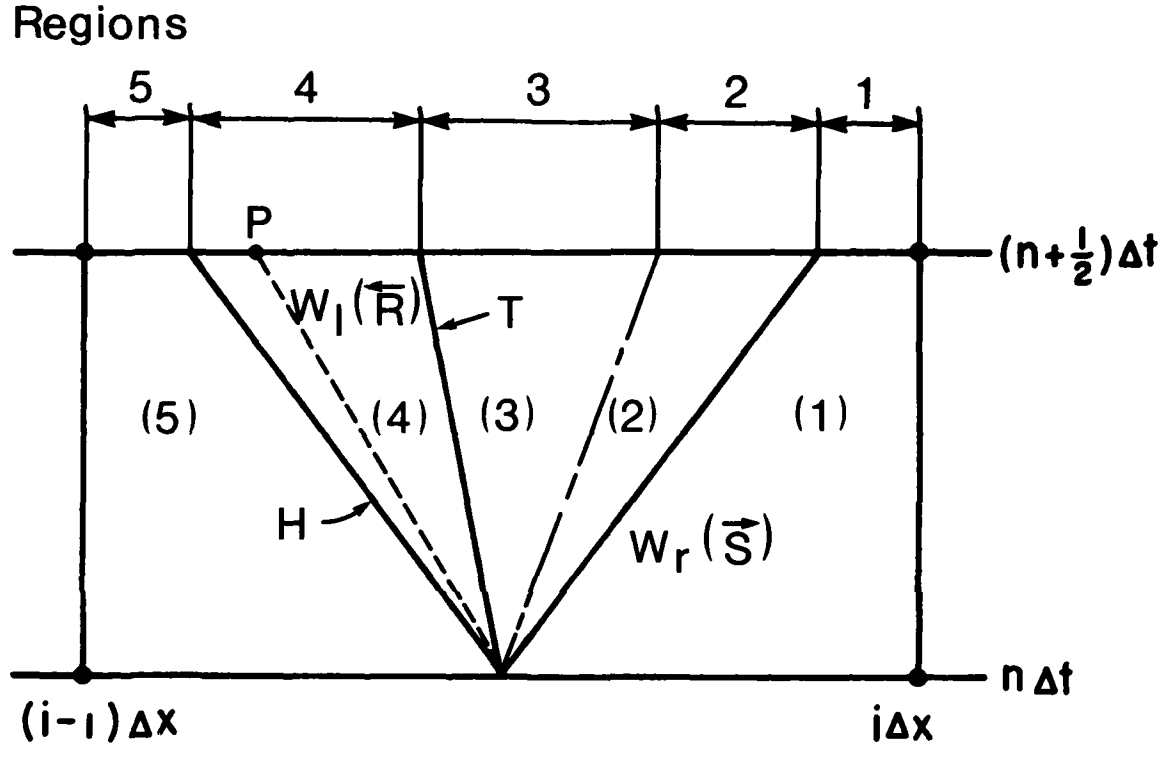

FIG. 3 FIVE DIFFERENT SOLUTIONS OF A RIEMANN PROBLEM CORRESPONDING TO THE SAMPLED REGION OR STATE.

W_ℓ = R - RAREFACTION WAVE; H - HEAD, T - TAIL; C - CONTACT SURFACE; W_r = S - SHOCK WAVE.

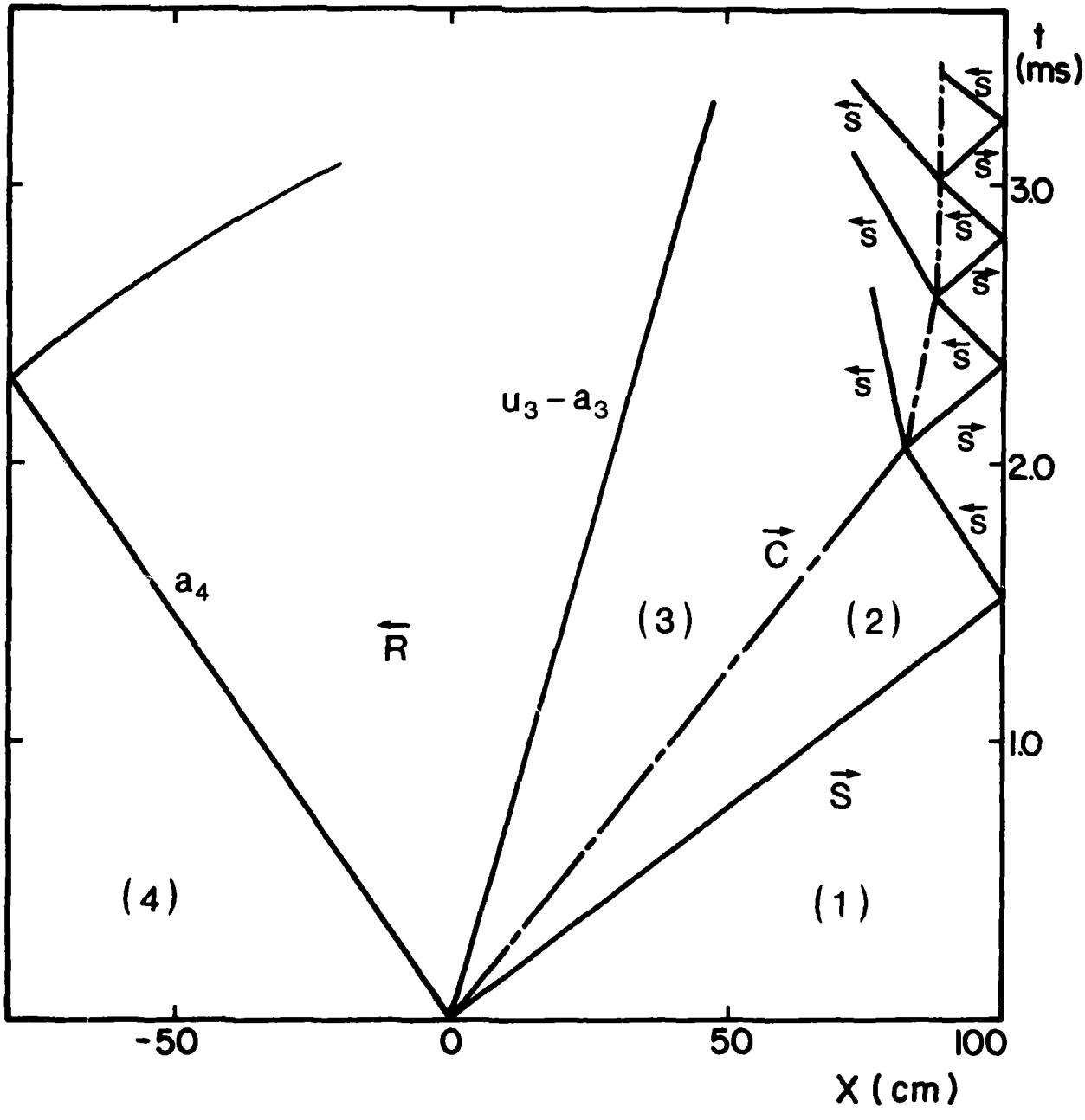

FIG. 4 WAVE DIAGRAM IN (x, t)-PLANE (REF. 11).

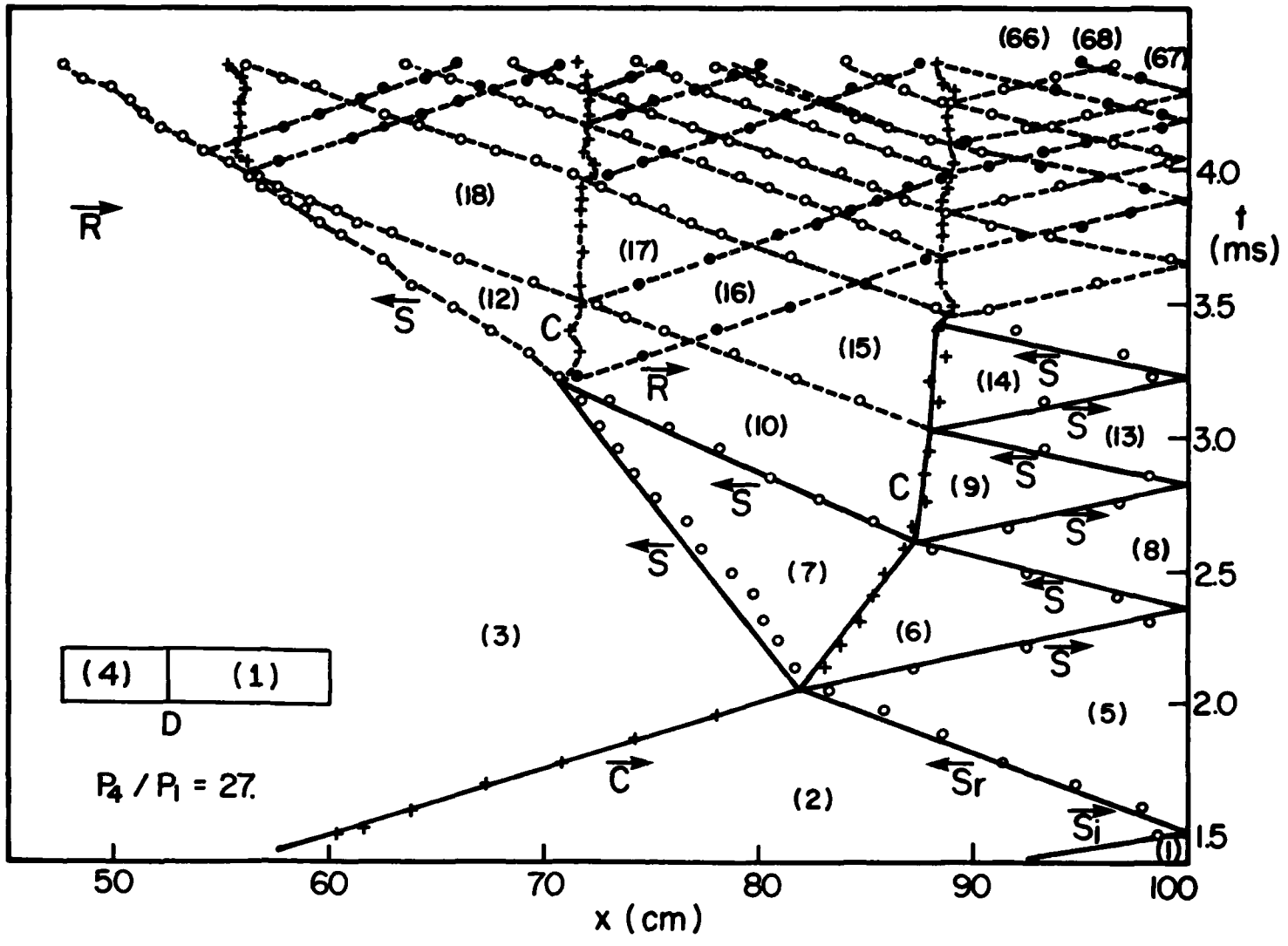

FIG. 5 DIAGRAM OF (x, t)-PLANE SHOWING A PLANE-SHOCK-WAVE REFLECTION FROM THE END WALL OF A SHOCK TUBE AND ITS SUBSEQUENT INTERACTIONS. p_4, p_1 - INITIAL PRESSURES; D - DIAPHRAGM, ——— FROM REF. 11.

PRESENT NUMERICAL VALUES: O O O SHOCK WAVES: ● ● ● RAREFACTION WAVES; + + + CONTACT SURFACES.

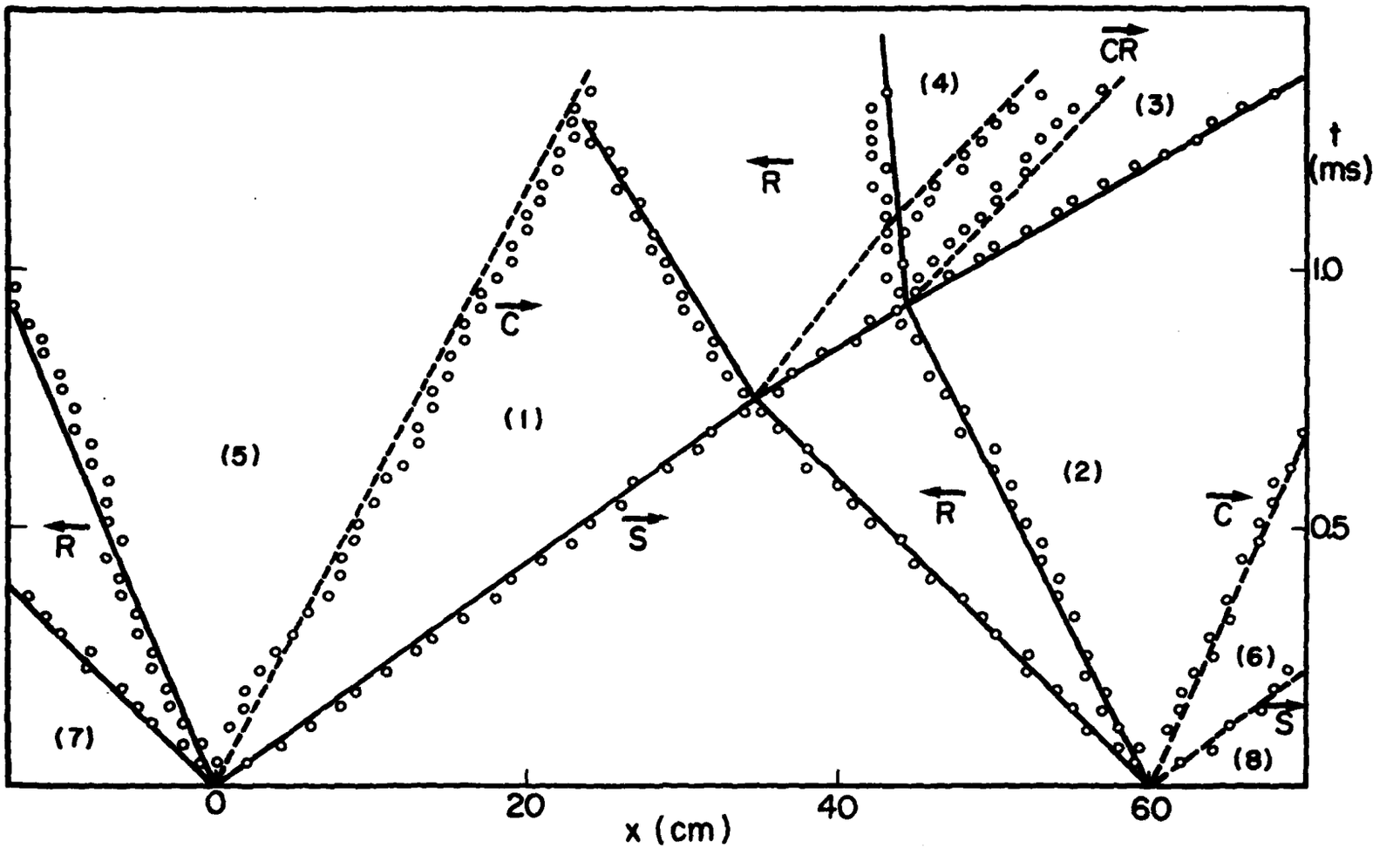

FIG. 6 HEAD-ON COLLISION OF A SHOCK WAVE WITH A RAREFACTION WAVE. O O O PRESENT NUMERICAL VALUES. FROM REF. 12: ━━━ SHOCK WAVES; ——— RAREFACTION WAVES; --- CONTACT SURFACES.

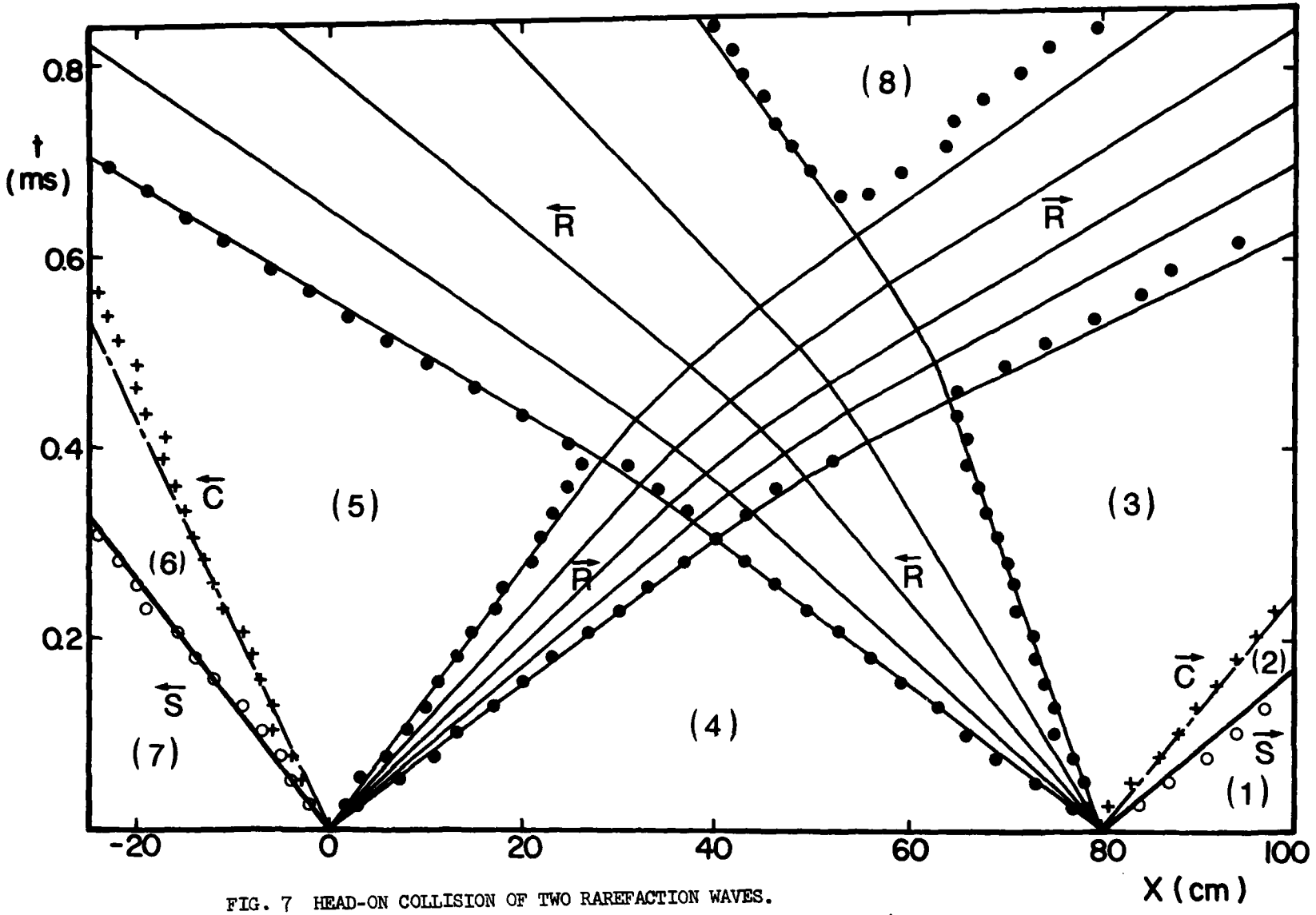

FIG. 7 HEAD-ON COLLISION OF TWO RAREFACTION WAVES.

INITIAL DIAPHRAGM PRESSURE RATIOS: $p_4/p_1 = 40.33$, $p_4/p_7 = 11.35$.

——— FROM REF. 13.

PRESENT NUMERICAL VALUES: O O O SHOCK WAVES; ● ● ●RAREFACTION WAVES; + + + CONTACT SURFACES.

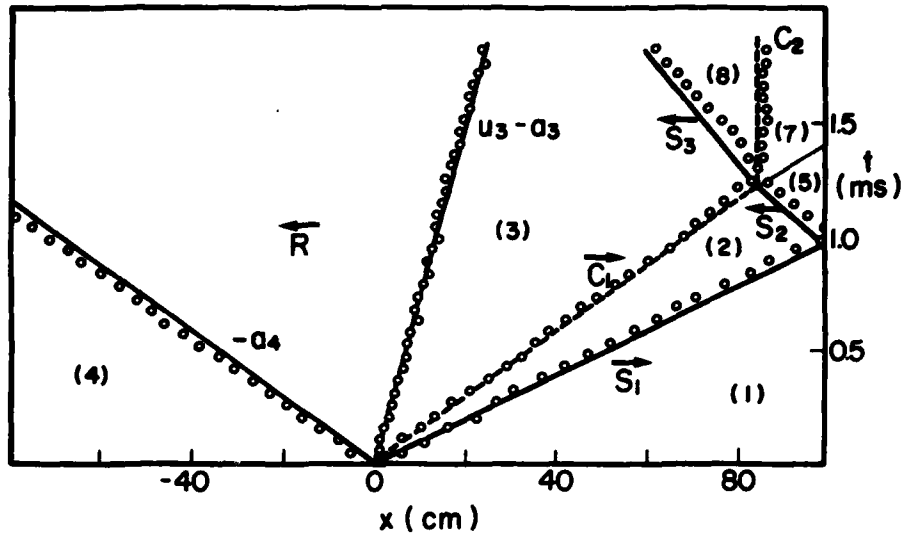

FIG. 8 NUMERICAL CONTACT-SURFACE TAILORING.

INITIAL CONDITIONS: $p_4/p_1 = 58.207$
$\gamma_1 = 1.400$, $a_1 = 322.000$ m/s
$\gamma_4 = 1.667$, $a_4 = 692.548$ m/s

WAVE SPEEDS: $M_s \equiv S_1/a_1 = 3.1698$, $M_c \equiv C_1/a_1 = 2.1404$
$M_3 \equiv (u_3-a_3)/a_1 = 0.41775$, $M_4 \equiv S_2/a_1 = -1.74315$
$M_{rs} \equiv S_2/a_1 = -1.74315$, $M_{ts} \equiv S_3/a_1 = -1.26913$

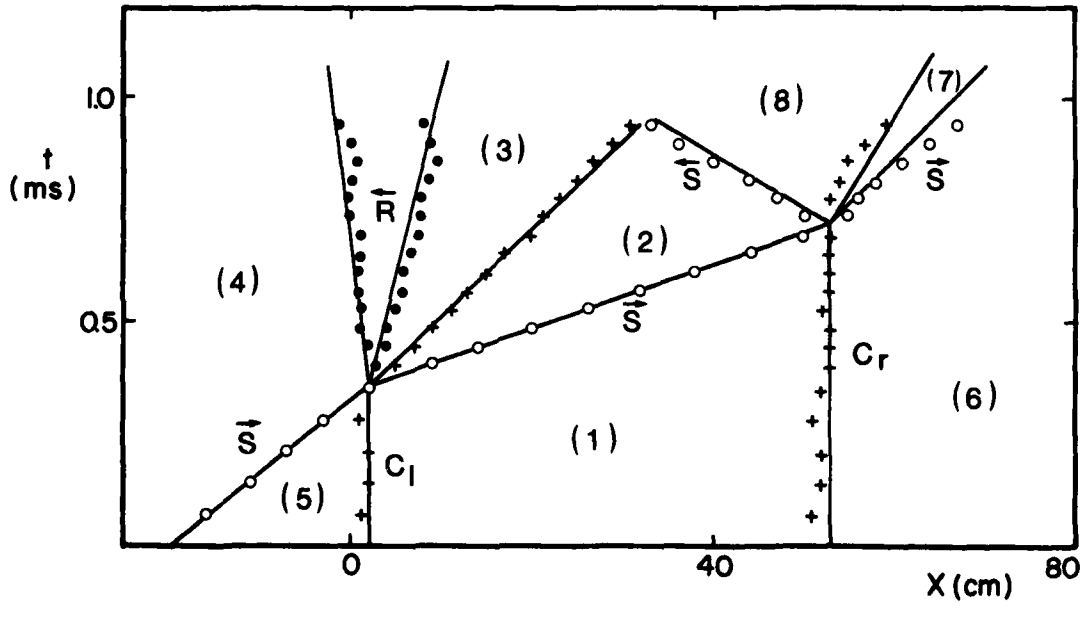

FIG. 9 SHOCK-WAVE REFRACTION AT A STATIONARY CONTACT LAYER.
INCIDENT SHOCK STRENGTH $p_2/p_1 = 3.70$. ——— FROM REF. 15.
PRESENT NUMERICAL VALUES: O O O SHOCK WAVES; ● ● ● RAREFACTION WAVES; + + + CONTACT SURFACES.

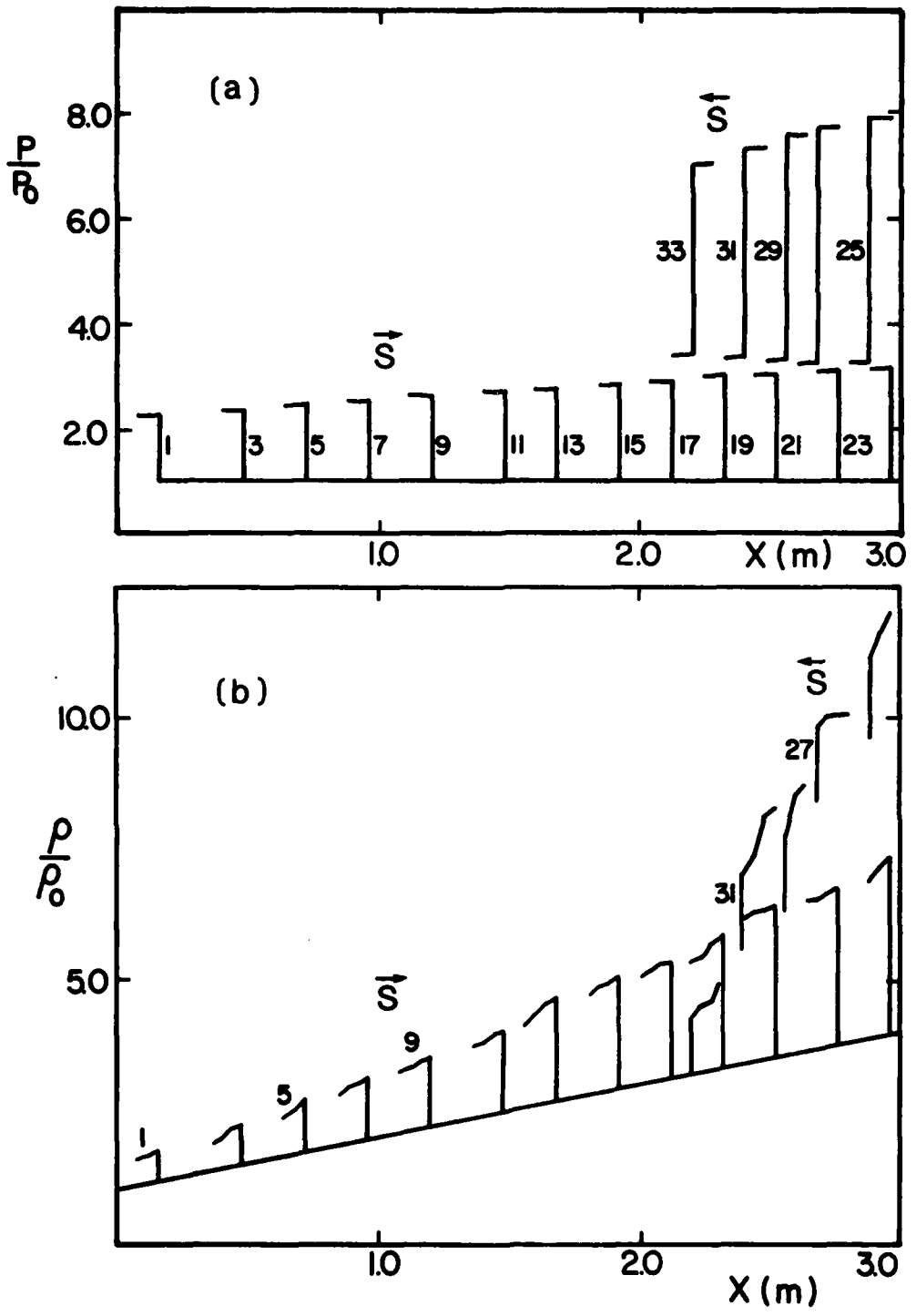

FIG. 10 PROFILES AT FIXED TIMES FOR A SHOCK WAVE MOVING IN A VARIABLE DENSITY STATE (a) PRESSURE, (b) DENSITY.

TIME NUMBERS: 1 - 0.132 ms, 3 - 0.362 ms, 5 - 0.591 ms, 7 - 0.820 ms, 9 - 1.05 ms, 11 - 1.28 ms, 13 - 1.51 ms, 15 - 1.74 ms, 17 - 1.96 ms, 19 - 2.19 ms, 21 - 2.42 ms, 23 - 2.65 ms, 25 - 2.87 ms, 27 - 3.10 ms, 29 - 3.33 ms, 31 - 3.55 ms, 33 - 3.78 ms.

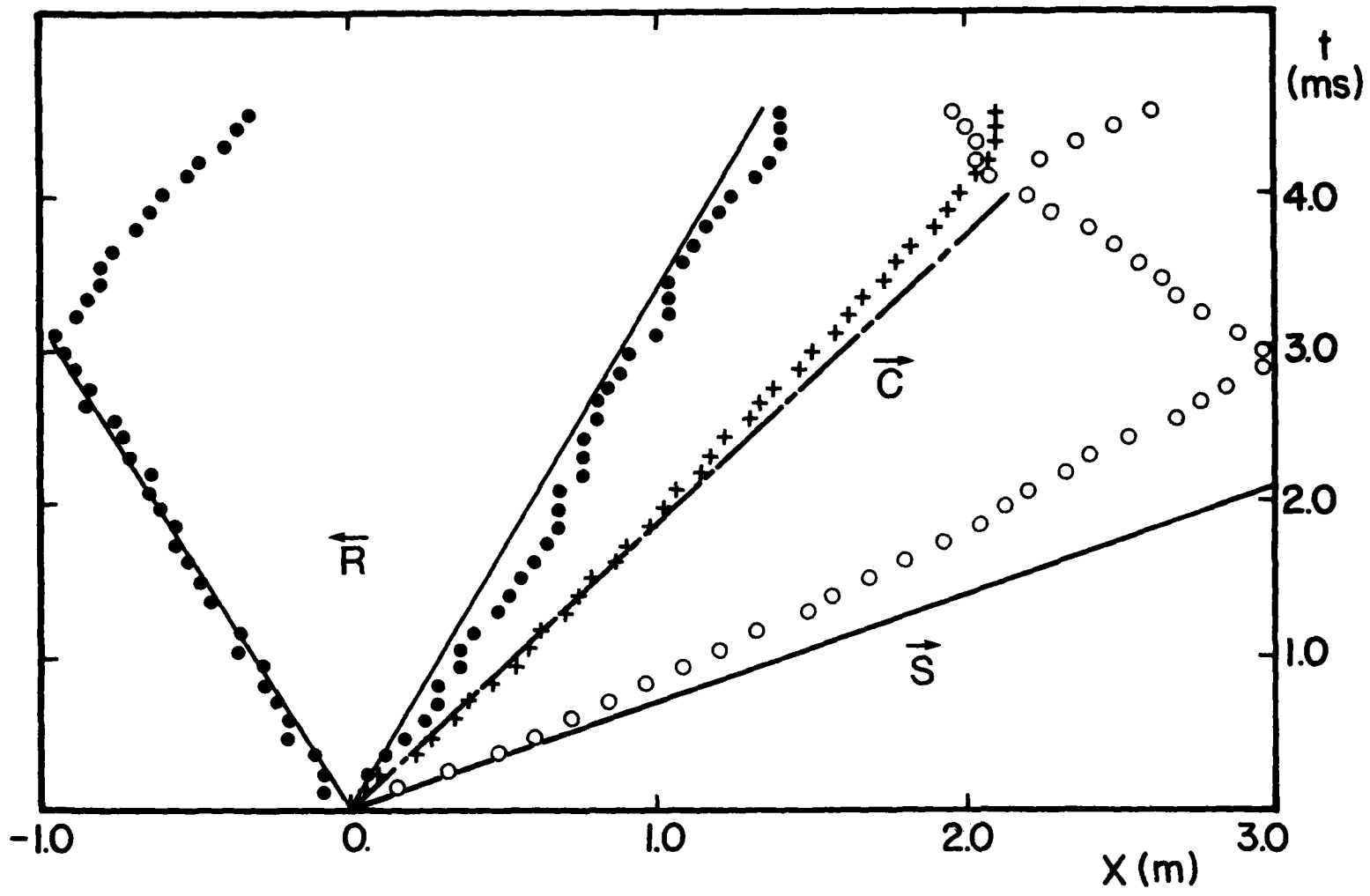

FIG. 11 WAVE DIAGRAM IN (x, t)-PLANE FOR NONUNIFORM DENSITY CHANNEL STATE IN A SHOCK TUBE.
——— WAVE DIAGRAM FOR UNIFORM DENSITY FIELD.

PRESENT NUMERICAL RESULTS: O O O SHOCK WAVES; ● ● ● RAREFACTION WAVES;
+ + + CONTACT SURFACES.

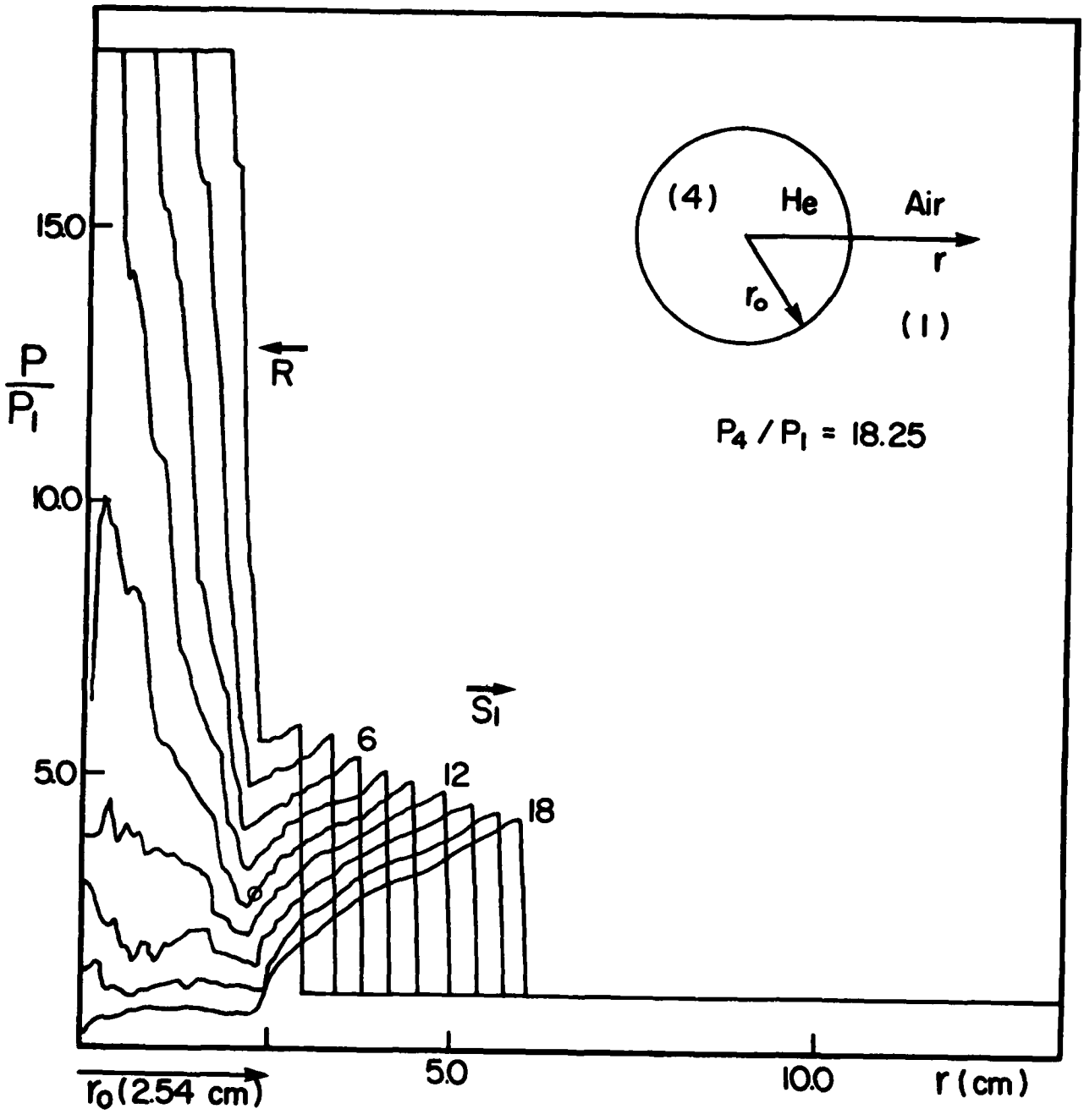

FIG. 12-a EXPLOSION OF A HELIUM SPHERE. PRESSURE PROFILES vs RADIUS FOR FIXED TIMES. $\gamma_1 = 1.400$, $\gamma_4 = 1.667$, DIAPHRAGM PRESSURE RATIO 18.25; SHOCK MACH NUMBER $M_s = 2.39$, PRESSURE RATIO $P_{21} = 6.50$, DENSITY RATIO $\rho_{21} = 3.20$, PARTICLE VELOCITY $U_{21} = 1.64$; THE FOREGOING ARE THE INITIAL CONDITIONS FOR THE PLANAR (SHOCK TUBE) CASE. ° BIRTH POINT OF SECOND SHOCK. TIME NUMBERS: 6 - 16 μs, 12 - 31.7 μs, 18 - 47.2 μs.

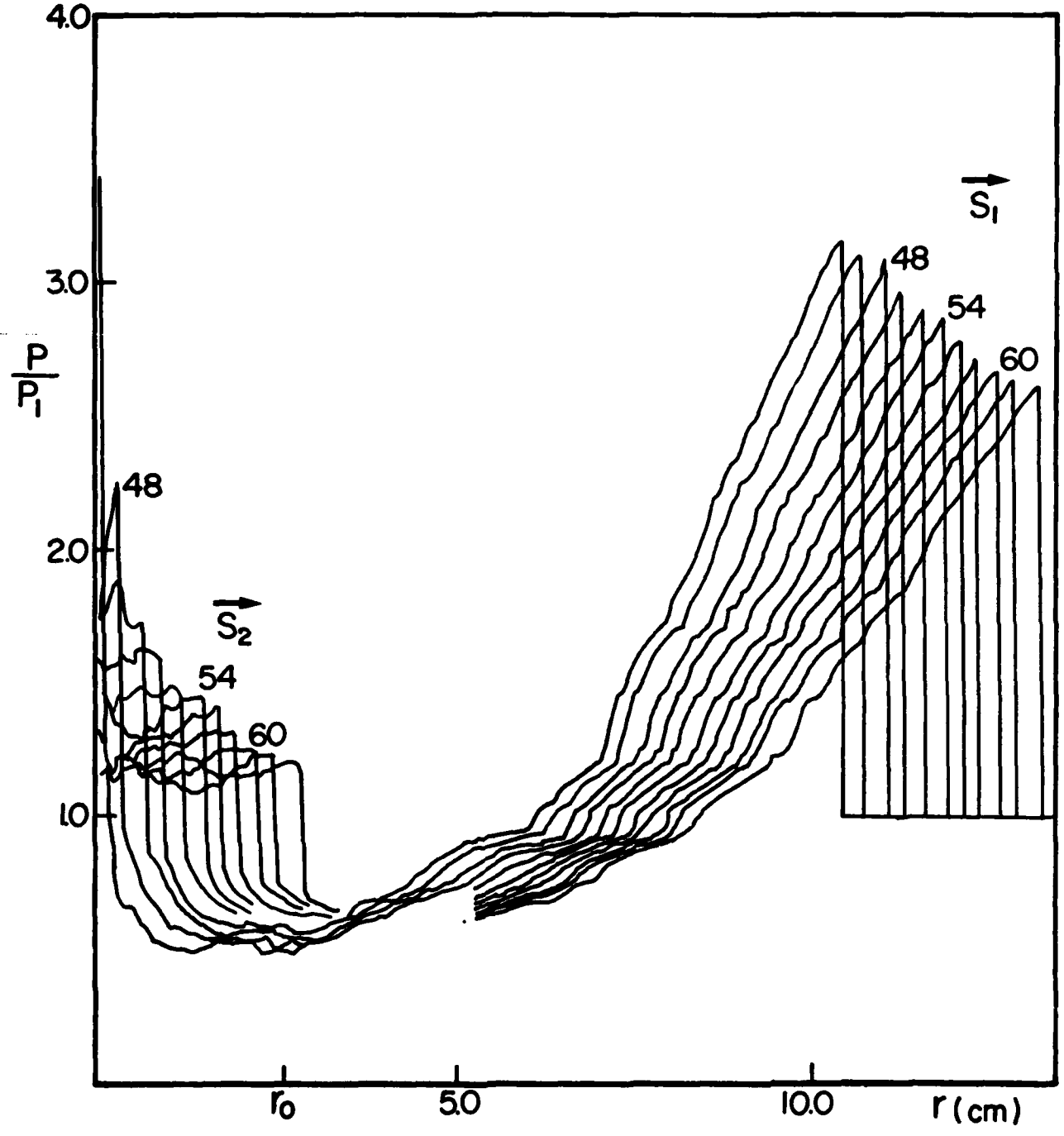

FIG. 12-b EXPLOSION OF A HELIUM SPHERE. PRESSURE PROFILES vs RADIUS FOR FIXED TIMES AFTER SECOND SHOCK WAVE IS REFLECTED. TIME NUMBERS: 48 - 125. μs, 54 - 140. μs, 60 - 156. μs.

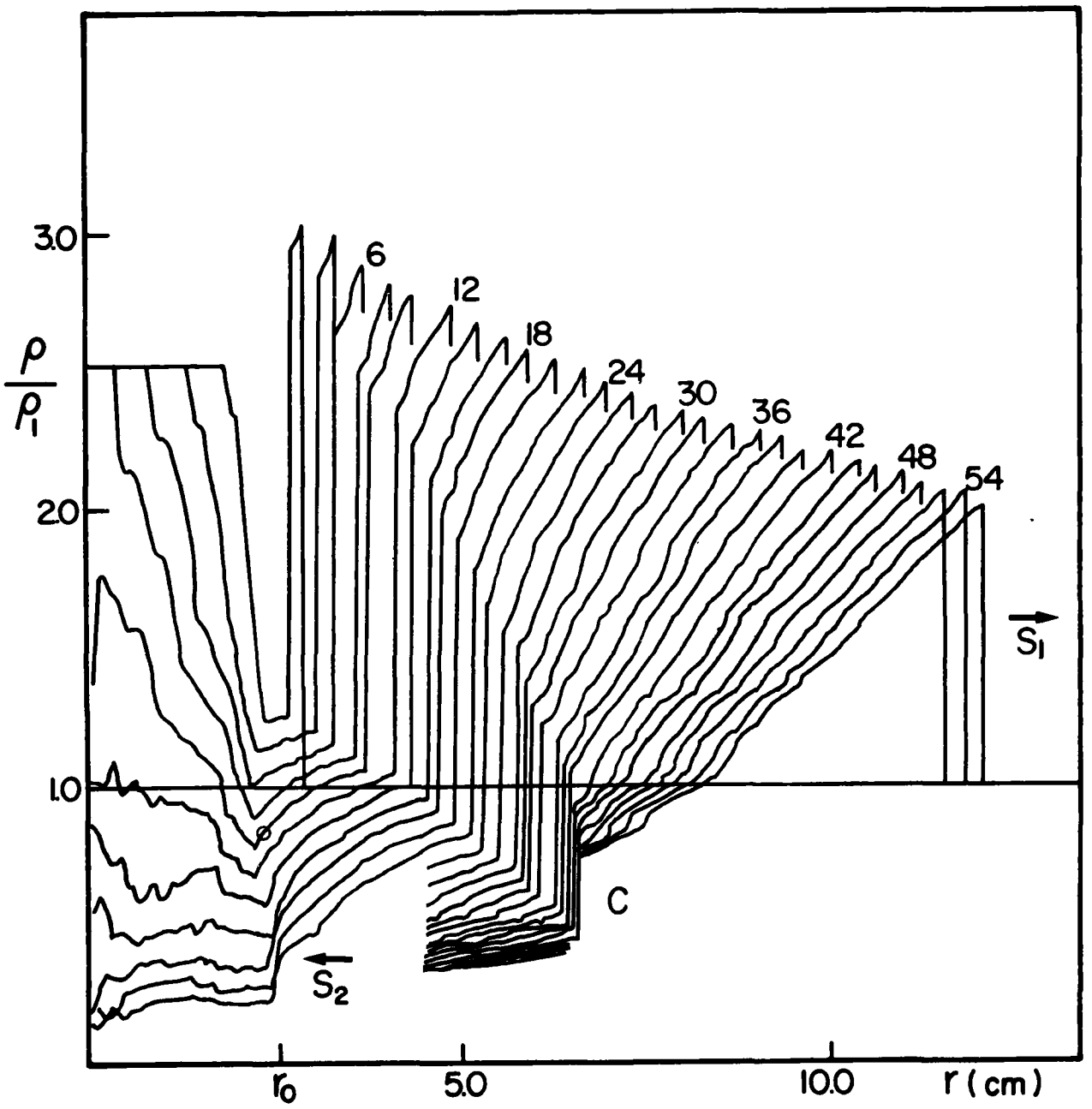

FIG. 13 EXPLOSION OF A HELIUM SPHERE. DENSITY PROFILES vs RADIUS FOR FIXED TIMES. ○ BIRTH POINT OF SECOND SHOCK. TIME NUMBERS: 6 - 16.1 μs, 12 - 31.7 μs, 18 - 47.2 μs, 24 - 62.8 μs, 30 - 78.3 μs, 36 - 93.9 μs, 42 - 109. μs, 48 - 125. μs, 54 - 140. μs.

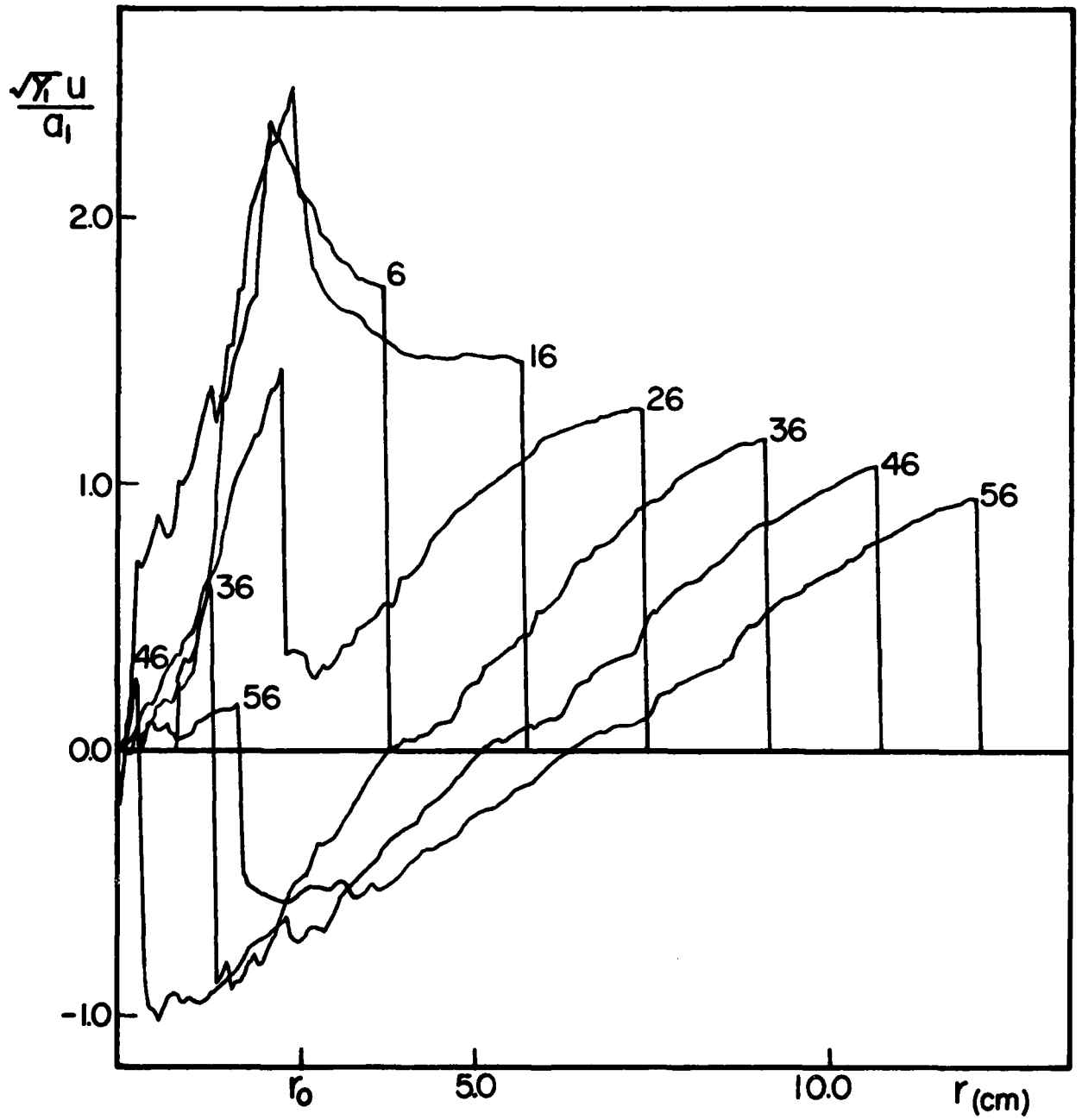

FIG. 14 EXPLOSION OF A HELIUM SPHERE. PARTICLE VELOCITY PROFILES vs RADIUS FOR FIXED TIMES. TIME NUMBERS: 6 - 16.1 μs, 16 - 42.0 μs, 26 - 68.0 μs, 36 - 93.6 μs, 46 - 120. μs, 56 - 146. μs.

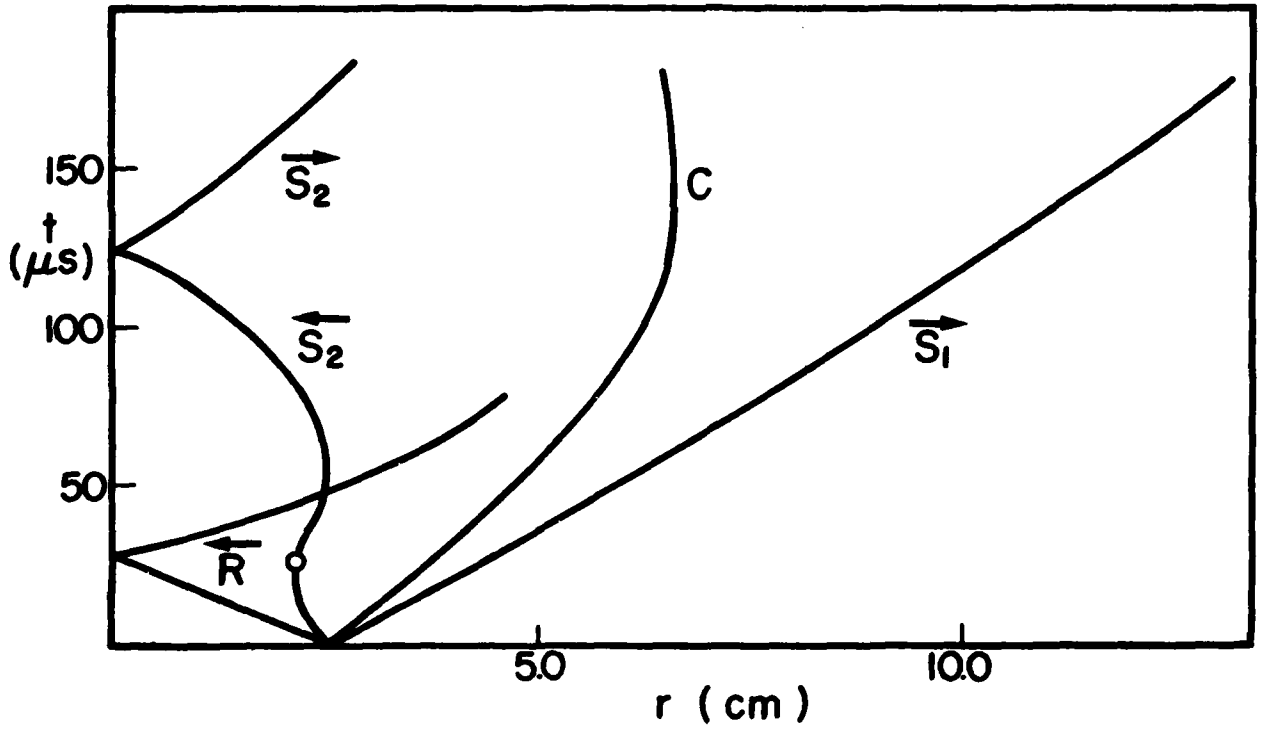

FIG. 15 EXPLOSION WAVE DIAGRAM IN THE (r, t)-PLANE. ○ BIRTH POINT OF SECOND SHOCK.

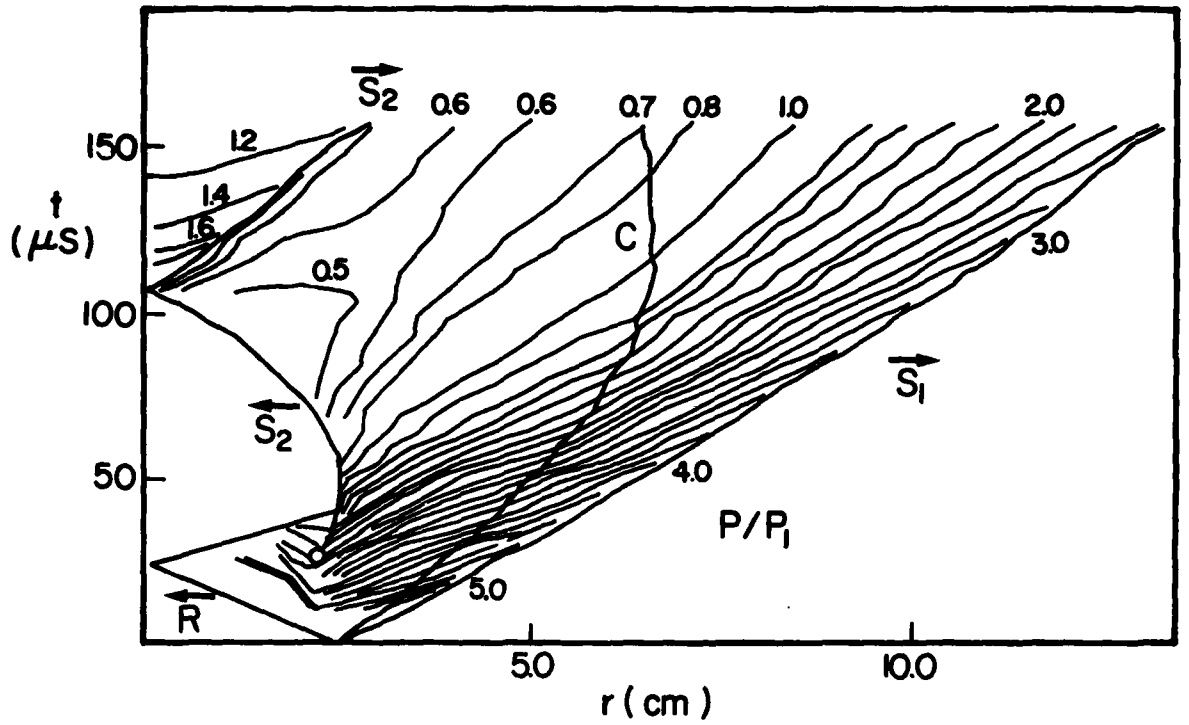

FIG. 16-a ISOBARS IN THE (r, t)-PLANE. ○ BIRTH POINT OF SECOND SHOCK.

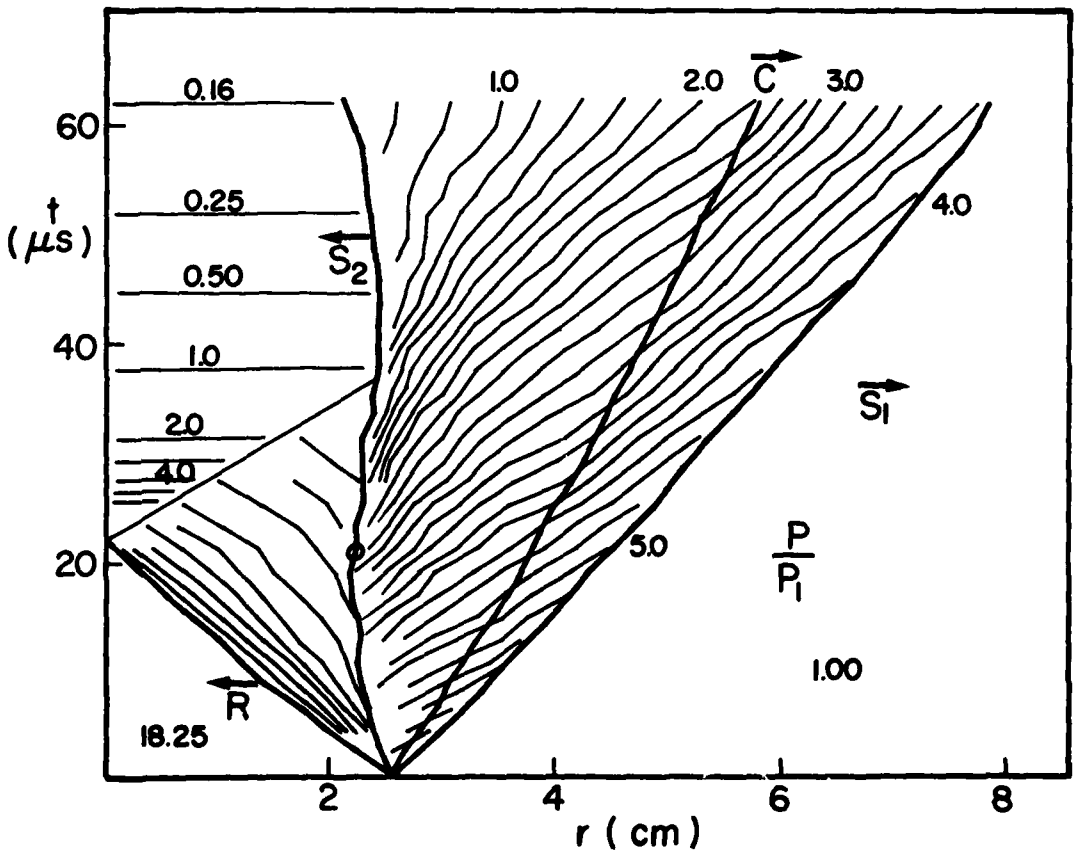

FIG. 16-b DETAILED AREA OF ISOBARS NEAR THE ORIGIN. ○ BIRTH POINT OF SECOND SHOCK.

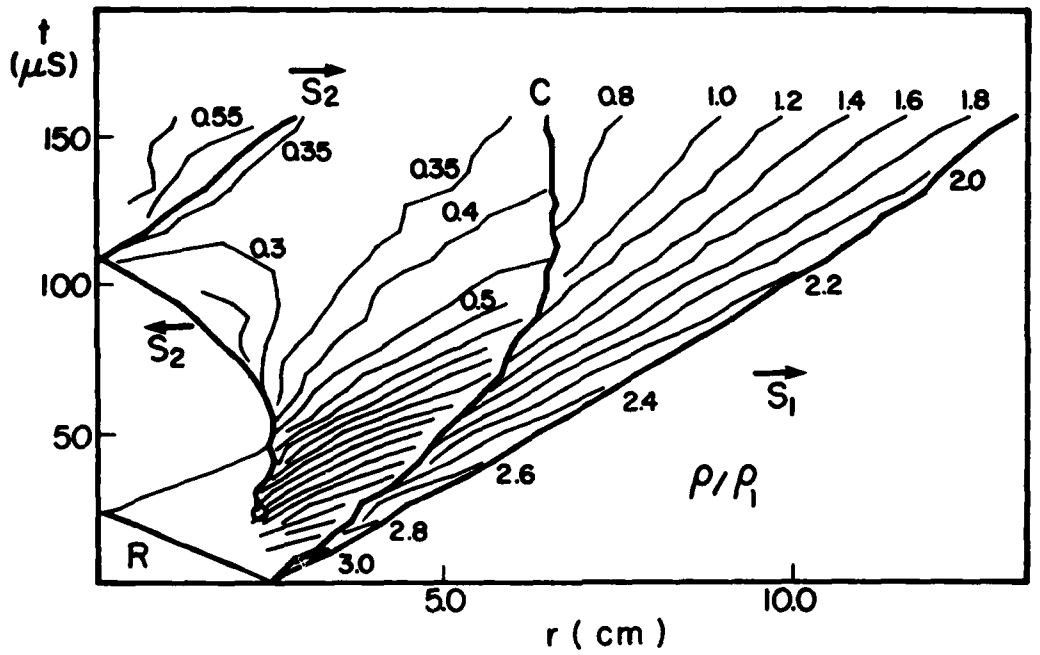

FIG. 17-a ISOPYCNICS IN THE (r, t)-PLANE. o BIRTH POINT OF SECOND SHOCK.

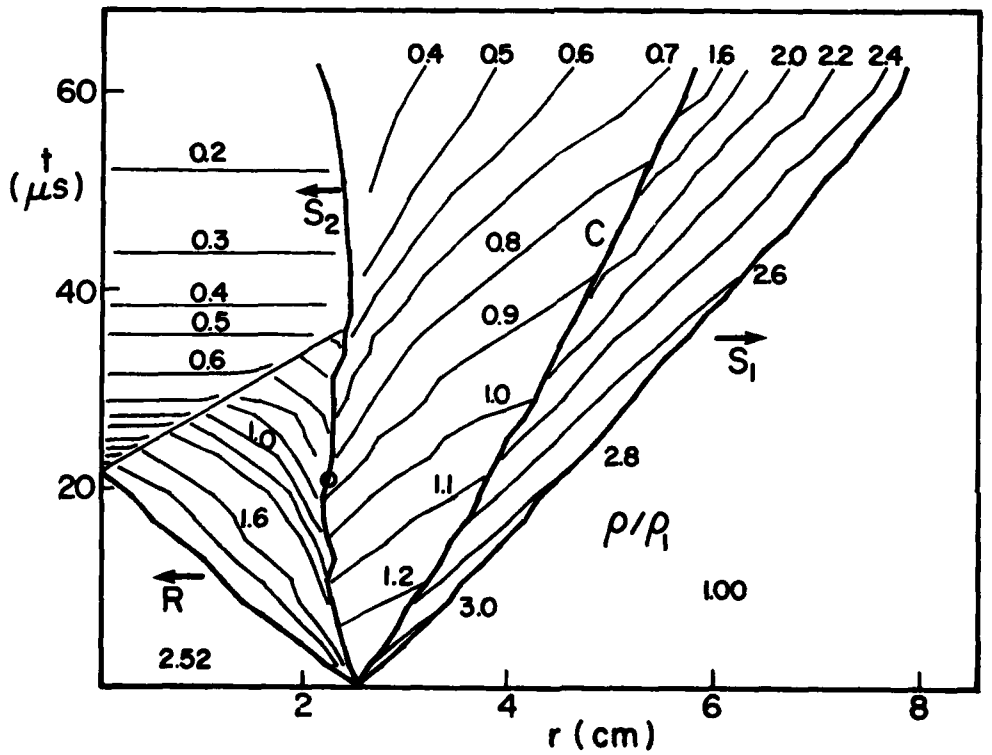

FIG. 17-b DETAILED AREA OF ISOPYCNICS NEAR THE ORIGIN. o BIRTH POINT OF SECOND SHOCK.

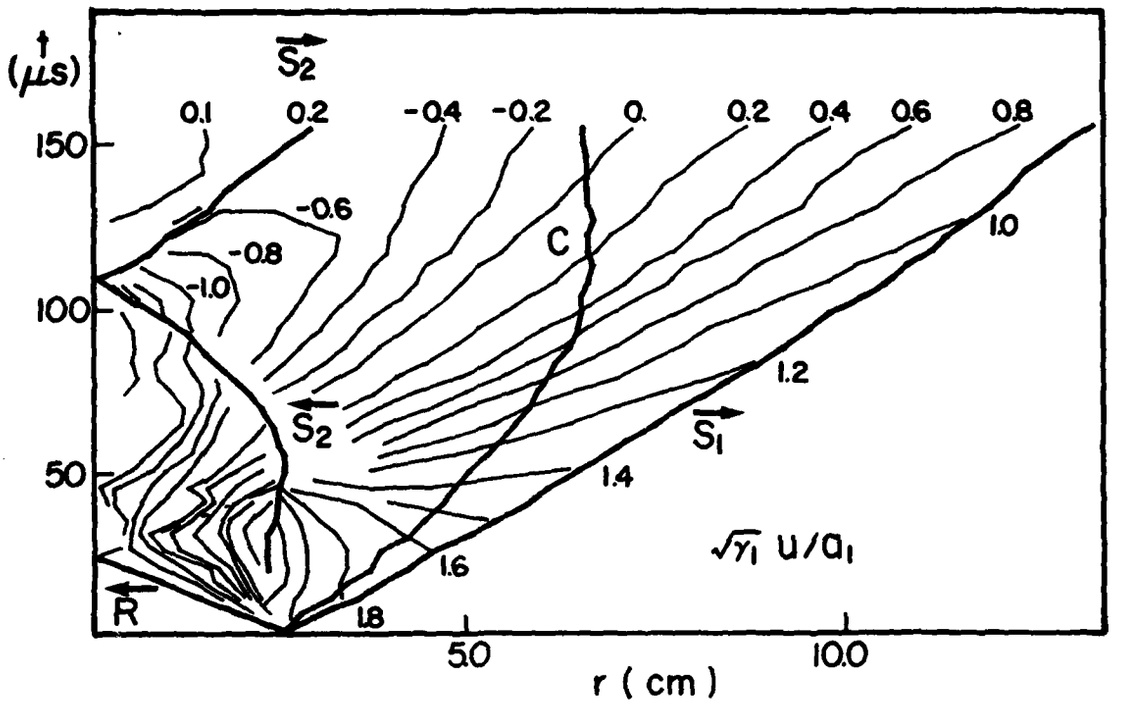

FIG. 18 ISOTACHS IN THE (r, t)-PLANE. o BIRTH POINT OF SECOND SHOCK.

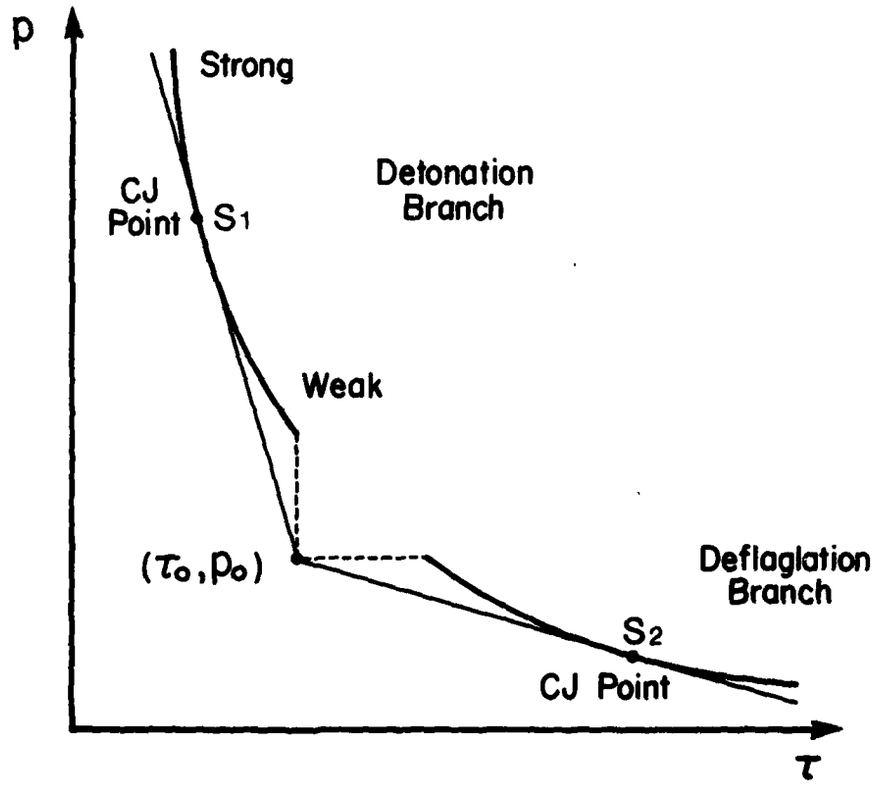

FIG. 19 THE HUGONIOT CURVE FOR EXOTHERMIC GAS FLOW (REF. 7).

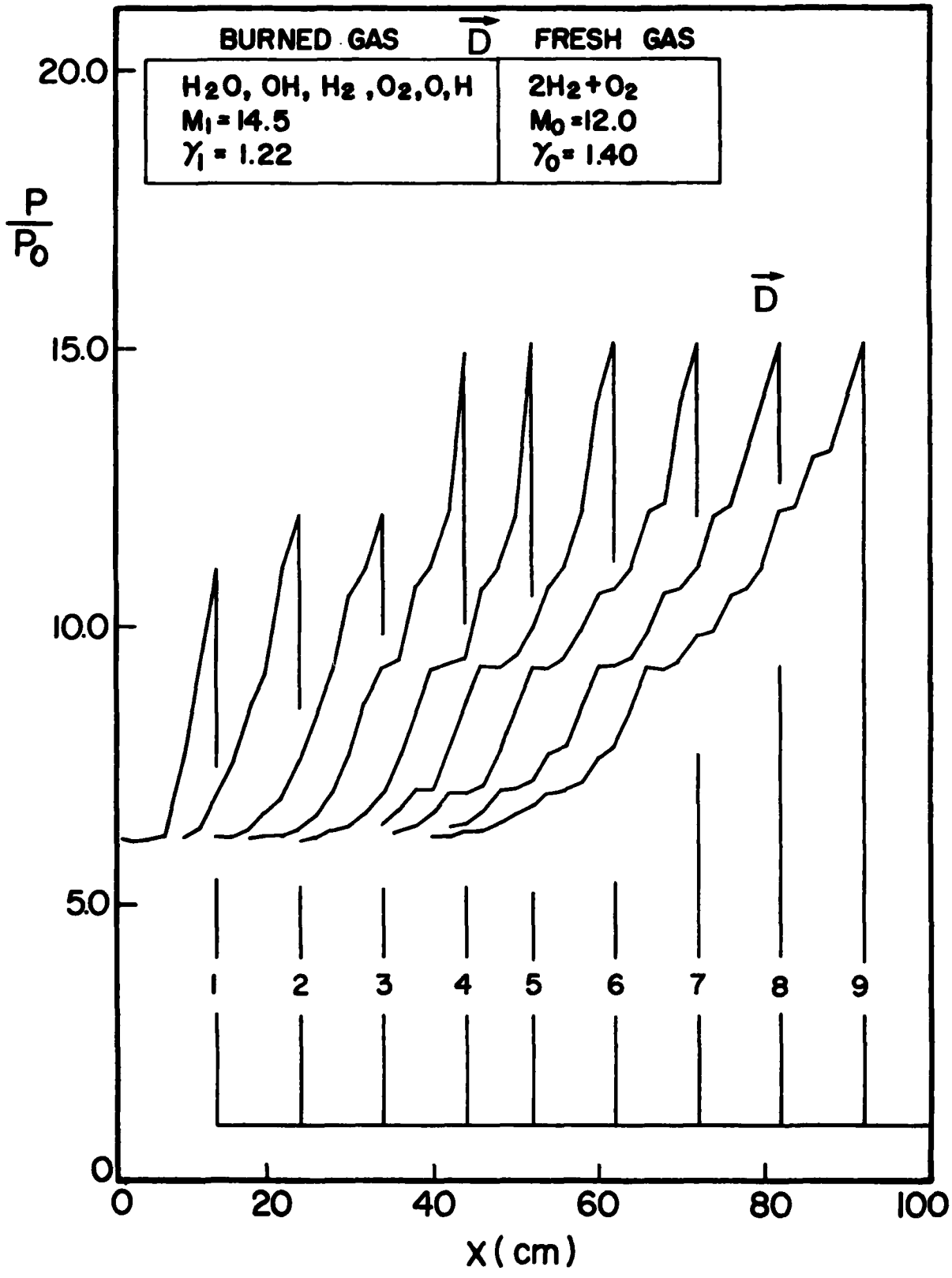

FIG. 20 PROPAGATION OF A DETONATION WAVE (D) IN A MIXTURE OF $2H_2 + O_2$. TIME NUMBERS: 1 - 41.1 μs, 2 - 81.7 μs, 3 - 122. μs, 4 - 162. μs, 5 - 202 μs, 6 - 242 μs, 7 - 282. μs, 8 - 322. μs, 9 - 362. μs.

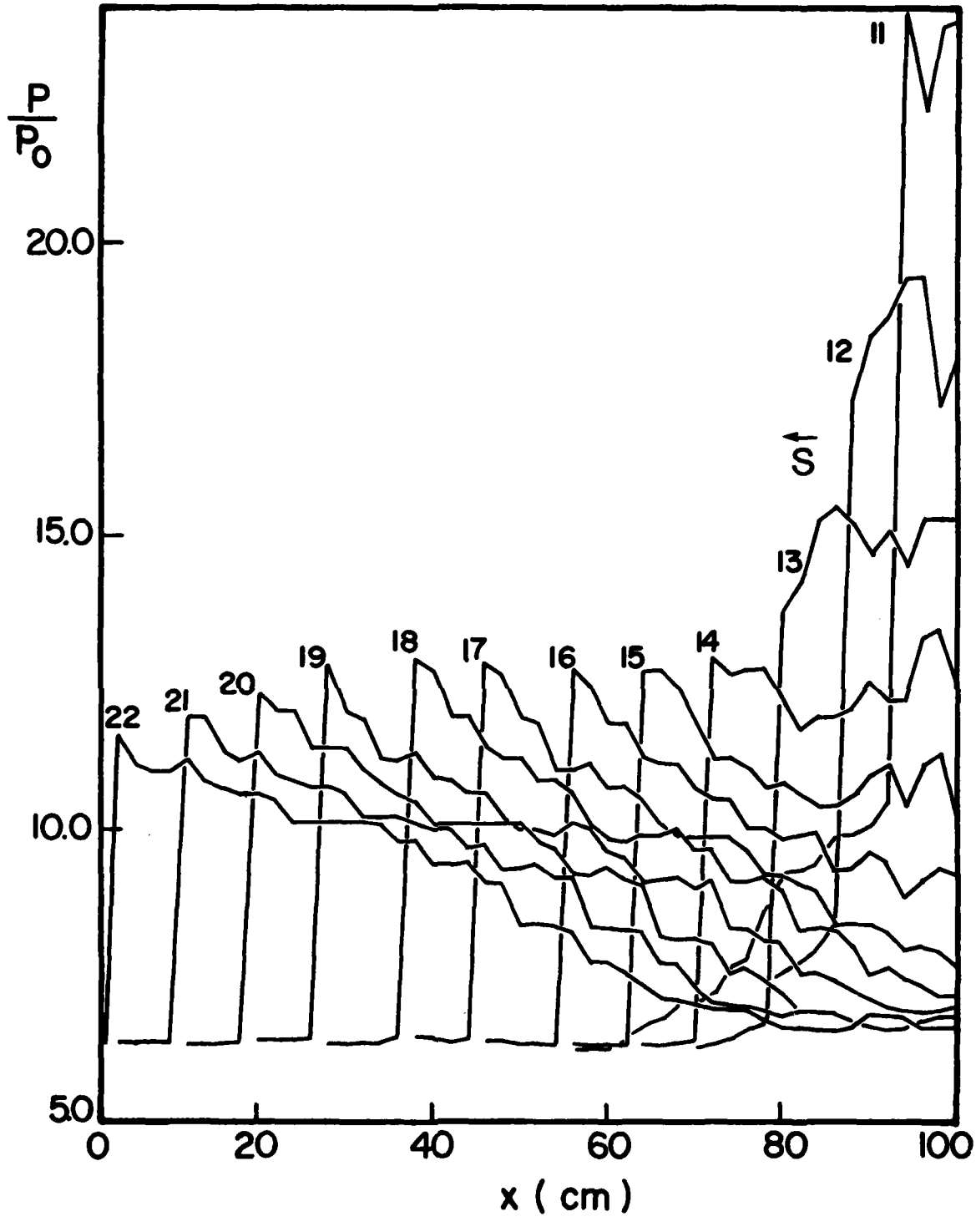

FIG. 21 REFLECTION OF A DETONATION WAVE IN $2H_2 + O_2$ AT THE END WALL OF A TUBE. TIME NUMBERS: 11 - 445. μs, 12 - 498. μs, 13 - 548. μs, 14 - 592. μs, 15 - 637. μs, 16 - 681. μs, 17 - 725. μs, 18 - 770. μs, 19 - 816. μs, 20 - 863. μs, 21 - 911. μs, 22 - 958. μs.

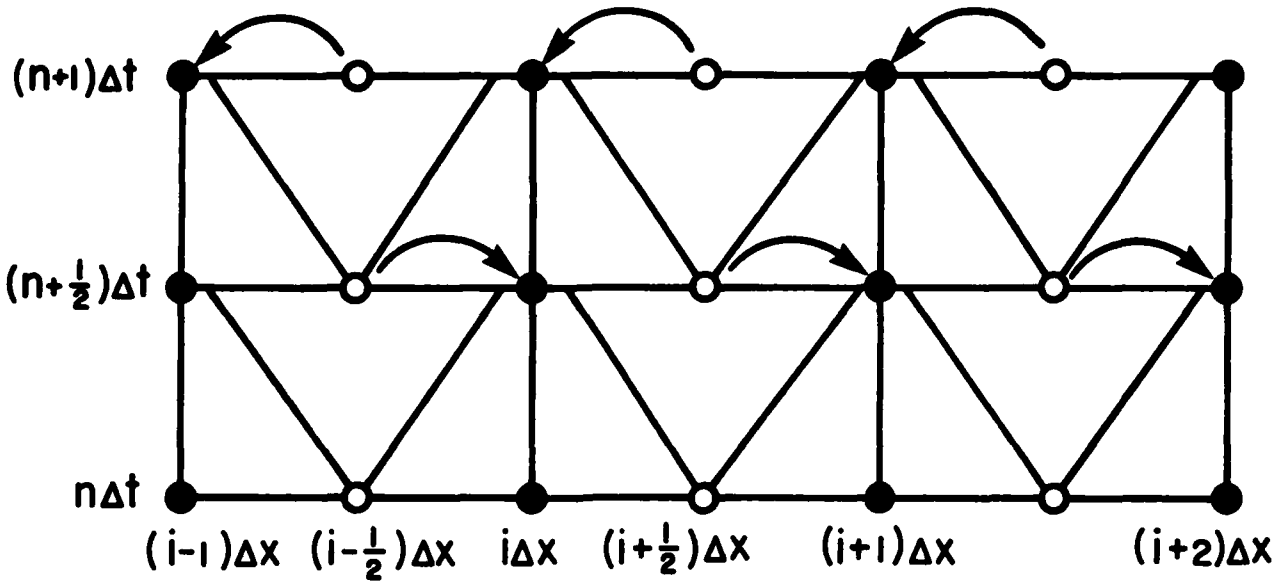

FIG. A-1-a COMPUTATIONAL DOMAIN. ● : ACTUAL GRID POINT; ○ : IMAGINARY GRID POINT.

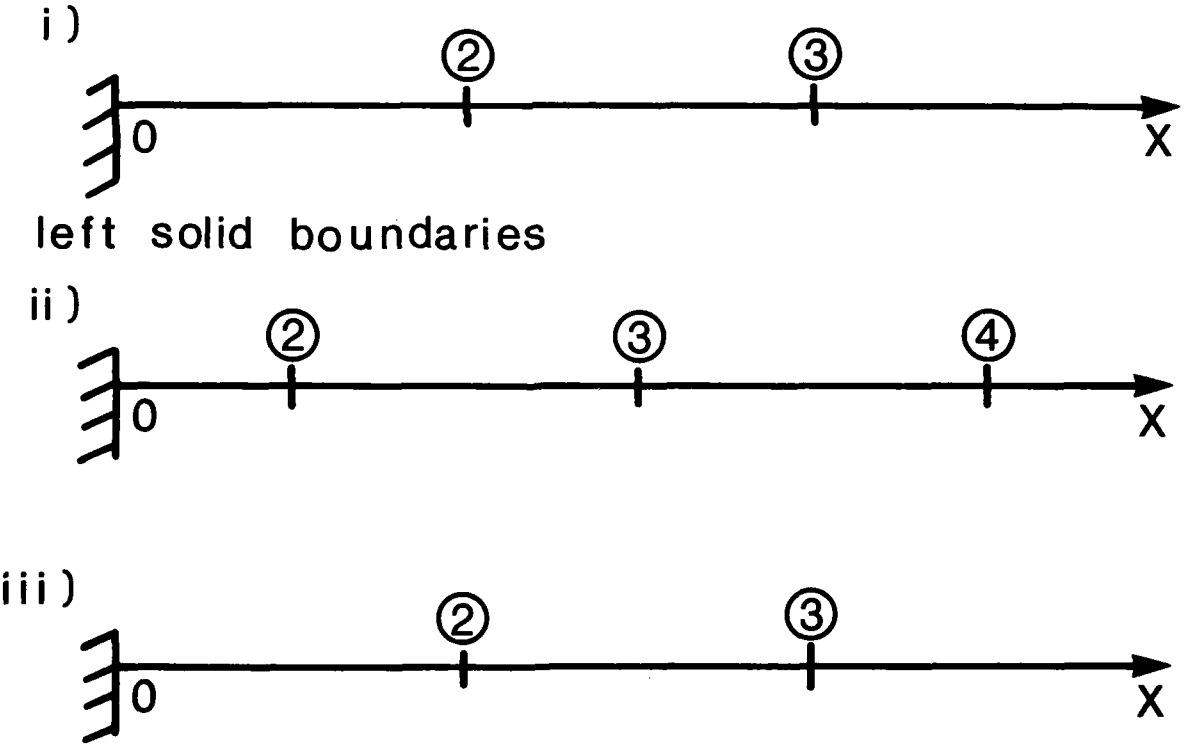

FIG. A-1-b RELATIONSHIP BETWEEN COMPUTATIONAL MESH POINTS AND ACTUAL PHYSICAL LOCATIONS. (i) WHEN CALCULATION STARTS, (ii) AFTER FIRST-HALF-STEP, (iii) AFTER SECOND-HALF-STEP. ②, ③, ... : CORRESPOND MESH POINTS.

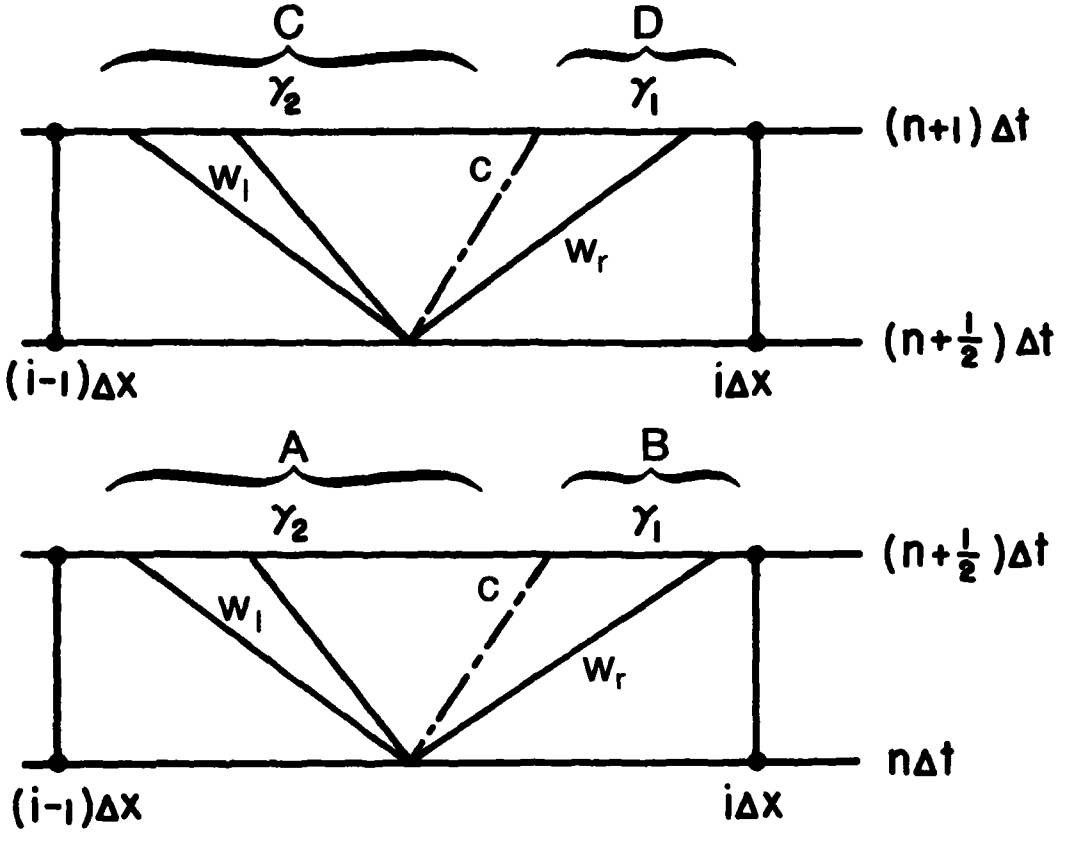

FIG. A-2 FOUR REGIONS WHICH DETERMINE MOVEMENT IN CONTACT SURFACE.
(i) IN FIRST-HALF STEP, (ii) IN SECOND-HALF STEP.

UTIAS REPORT NO. 240

Institute for Aerospace Studies, University of Toronto (UTIAS)
4925 Dufferin Street, Downsview, Ontario, Canada, M3H 5T6

APPLICATIONS OF RANDOM-CHOICE METHOD TO PROBLEMS IN SHOCK AND DETONATION-WAVE DYNAMICS

Saito, T., Glass, I. I.

1. Numerical Methods, 2. Shock waves, 3. Contact surfaces, 4. Rarefaction waves, 5. Blast waves, 6. Detonation waves

I. Saito, T., Glass, I. I. II. UTIAS Report No. 240

Although successful numerical methods exist for solving problems in shock and detonation-wave dynamics, there is still a real need of developing new techniques where the old methods fail to predict important flow properties. For example, it has recently been shown in Ref. 1 that existing methods fail to predict the interferometrically measured isopycnics in regular and single Mach reflections (let alone complex and double-Mach reflections, for which numerical solutions do not even exist). The purpose of the present report is to present eight applications of the Random-Choice Method (RCM) to the solution of problems in shock and detonation-wave dynamics. It is shown that unlike other numerical methods, the RCM yields sharp-fronted shocks and contact surfaces without resorting to artificial and perhaps erroneous means of predicting their locations, which depend more on art than science. It is also a very useful method in showing such fine points as the birth point of the second shock (implosion) wave at the tail of the rarefaction wave in a spherical explosion.

Despite all these advantages the RCM has yet to be developed to cope with problems such as oblique and spherical shock-wave reflections in order to compute the various isolines (pressure, density and velocity) and compare them with available interferometric or other experimental data. For example, isopycnics are much more sensitive indicators of the accuracy of a given numerical method than a comparison of shock shapes (Ref. 1). Undoubtedly, such applications of the RCM will probably take place in the near future, as the need for such numerical methods now exists.

UTIAS REPORT NO. 240

Institute for Aerospace Studies, University of Toronto (UTIAS)
4925 Dufferin Street, Downsview, Ontario, Canada, M3H 5T6

APPLICATIONS OF RANDOM-CHOICE METHOD TO PROBLEMS IN SHOCK AND DETONATION-WAVE DYNAMICS

Saito, T., Glass, I. I.

1. Numerical Methods, 2. Shock waves, 3. Contact surfaces, 4. Rarefaction waves, 5. Blast waves, 6. Detonation waves

I. Saito, T., Glass, I. I. II. UTIAS Report No. 240

Although successful numerical methods exist for solving problems in shock and detonation-wave dynamics, there is still a real need of developing new techniques where the old methods fail to predict important flow properties. For example, it has recently been shown in Ref. 1 that existing methods fail to predict the interferometrically measured isopycnics in regular and single Mach reflections (let alone complex and double-Mach reflections, for which numerical solutions do not even exist). The purpose of the present report is to present eight applications of the Random-Choice Method (RCM) to the solution of problems in shock and detonation-wave dynamics. It is shown that unlike other numerical methods, the RCM yields sharp-fronted shocks and contact surfaces without resorting to artificial and perhaps erroneous means of predicting their locations, which depend more on art than science. It is also a very useful method in showing such fine points as the birth point of the second shock (implosion) wave at the tail of the rarefaction wave in a spherical explosion.

Despite all these advantages the RCM has yet to be developed to cope with problems such as oblique and spherical shock-wave reflections in order to compute the various isolines (pressure, density and velocity) and compare them with available interferometric or other experimental data. For example, isopycnics are much more sensitive indicators of the accuracy of a given numerical method than a comparison of shock shapes (Ref. 1). Undoubtedly, such applications of the RCM will probably take place in the near future, as the need for such numerical methods now exists.

Available copies of this report are limited. Return this card to UTIAS, if you require a copy.

UTIAS REPORT NO. 240

Institute for Aerospace Studies, University of Toronto (UTIAS)
4925 Dufferin Street, Downsview, Ontario, Canada, M3H 5T6

APPLICATIONS OF RANDOM-CHOICE METHOD TO PROBLEMS IN SHOCK AND DETONATION-WAVE DYNAMICS

Saito, T., Glass, I. I.

1. Numerical Methods, 2. Shock waves, 3. Contact surfaces, 4. Rarefaction waves, 5. Blast waves, 6. Detonation waves

I. Saito, T., Glass, I. I. II. UTIAS Report No. 240

Although successful numerical methods exist for solving problems in shock and detonation-wave dynamics, there is still a real need of developing new techniques where the old methods fail to predict important flow properties. For example, it has recently been shown in Ref. 1 that existing methods fail to predict the interferometrically measured isopycnics in regular and single Mach reflections (let alone complex and double-Mach reflections, for which numerical solutions do not even exist). The purpose of the present report is to present eight applications of the Random-Choice Method (RCM) to the solution of problems in shock and detonation-wave dynamics. It is shown that unlike other numerical methods, the RCM yields sharp-fronted shocks and contact surfaces without resorting to artificial and perhaps erroneous means of predicting their locations, which depend more on art than science. It is also a very useful method in showing such fine points as the birth point of the second shock (implosion) wave at the tail of the rarefaction wave in a spherical explosion.

Despite all these advantages the RCM has yet to be developed to cope with problems such as oblique and spherical shock-wave reflections in order to compute the various isolines (pressure, density and velocity) and compare them with available interferometric or other experimental data. For example, isopycnics are much more sensitive indicators of the accuracy of a given numerical method than a comparison of shock shapes (Ref. 1). Undoubtedly, such applications of the RCM will probably take place in the near future, as the need for such numerical methods now exists.

Available copies of this report are limited. Return this card to UTIAS, if you require a copy.

UTIAC REPORT NO. 240

Institute for Aerospace Studies, University of Toronto (UTIAS)
4925 Dufferin Street, Downsview, Ontario, Canada, M3H 5T6

APPLICATIONS OF RANDOM-CHOICE METHOD TO PROBLEMS IN SHOCK AND DETONATION-WAVE DYNAMICS

Saito, T., Glass, I. I.

1. Numerical Methods, 2. Shock waves, 3. Contact surfaces, 4. Rarefaction waves, 5. Blast waves, 6. Detonation waves

I. Saito, T., Glass, I. I. II. UTIAS Report No. 240

Although successful numerical methods exist for solving problems in shock and detonation-wave dynamics, there is still a real need of developing new techniques where the old methods fail to predict important flow properties. For example, it has recently been shown in Ref. 1 that existing methods fail to predict the interferometrically measured isopycnics in regular and single Mach reflections (let alone complex and double-Mach reflections, for which numerical solutions do not even exist). The purpose of the present report is to present eight applications of the Random-Choice Method (RCM) to the solution of problems in shock and detonation-wave dynamics. It is shown that unlike other numerical methods, the RCM yields sharp-fronted shocks and contact surfaces without resorting to artificial and perhaps erroneous means of predicting their locations, which depend more on art than science. It is also a very useful method in showing such fine points as the birth point of the second shock (implosion) wave at the tail of the rarefaction wave in a spherical explosion.

Despite all these advantages the RCM has yet to be developed to cope with problems such as oblique and spherical shock-wave reflections in order to compute the various isolines (pressure, density and velocity) and compare them with available interferometric or other experimental data. For example, isopycnics are much more sensitive indicators of the accuracy of a given numerical method than a comparison of shock shapes (Ref. 1). Undoubtedly, such applications of the RCM will probably take place in the near future, as the need for such numerical methods now exists.

Available copies of this report are limited. Return this card to UTIAS, if you require a copy.

UTIAS REPORT NO. 240

Institute for Aerospace Studies, University of Toronto (UTIAS)
4925 Dufferin Street, Downsview, Ontario, Canada, M3H 5T6

APPLICATIONS OF RANDOM-CHOICE METHOD TO PROBLEMS IN SHOCK AND DETONATION-WAVE DYNAMICS

Saito, T., Glass, I. I.

1. Numerical Methods, 2. Shock waves, 3. Contact surfaces, 4. Rarefaction waves, 5. Blast waves, 6. Detonation waves

I. Saito, T., Glass, I. I. II. UTIAS Report No. 240

Although successful numerical methods exist for solving problems in shock and detonation-wave dynamics, there is still a real need of developing new techniques where the old methods fail to predict important flow properties. For example, it has recently been shown in Ref. 1 that existing methods fail to predict the interferometrically measured isopycnics in regular and single Mach reflections (let alone complex and double-Mach reflections, for which numerical solutions do not even exist). The purpose of the present report is to present eight applications of the Random-Choice Method (RCM) to the solution of problems in shock and detonation-wave dynamics. It is shown that unlike other numerical methods, the RCM yields sharp-fronted shocks and contact surfaces without resorting to artificial and perhaps erroneous means of predicting their locations, which depend more on art than science. It is also a very useful method in showing such fine points as the birth point of the second shock (implosion) wave at the tail of the rarefaction wave in a spherical explosion.

Despite all these advantages the RCM has yet to be developed to cope with problems such as oblique and spherical shock-wave reflections in order to compute the various isolines (pressure, density and velocity) and compare them with available interferometric or other experimental data. For example, isopycnics are much more sensitive indicators of the accuracy of a given numerical method than a comparison of shock shapes (Ref. 1). Undoubtedly, such applications of the RCM will probably take place in the near future, as the need for such numerical methods now exists.

Available copies of this report are limited. Return this card to UTIAS, if you require a copy.

UTIAS REPORT NO. 240

Institute for Aerospace Studies, University of Toronto (UTIAS)
4925 Dufferin Street, Downsview, Ontario, Canada, M3H 5T6

APPLICATIONS OF RANDOM-CHOICE METHOD TO PROBLEMS IN SHOCK AND DETONATION-WAVE DYNAMICS

Saito, T., Glass, I. I.

1. Numerical Methods, 2. Shock waves, 3. Contact surfaces, 4. Rarefaction waves, 5. Blast waves, 6. Detonation waves

I. Saito, T., Glass, I. I. II. UTIAS Report No. 240

Although successful numerical methods exist for solving problems in shock and detonation-wave dynamics, there is still a real need of developing new techniques where the old methods fail to predict important flow properties. For example, it has recently been shown in Ref. 1 that existing methods fail to predict the interferometrically measured isopycnics in regular and single Mach reflections (let alone complex and double-Mach reflections, for which numerical solutions do not even exist). The purpose of the present report is to present eight applications of the Random-Choice Method (RCM) to the solution of problems in shock and detonation-wave dynamics. It is shown that unlike other numerical methods, the RCM yields sharp-fronted shocks and contact surfaces without resorting to artificial and perhaps erroneous means of predicting their locations, which depend more on art than science. It is also a very useful method in showing such fine points as the birth point of the second shock (implosion) wave at the tail of the rarefaction wave in a spherical explosion.

Despite all these advantages the RCM has yet to be developed to cope with problems such as oblique and spherical shock-wave reflections in order to compute the various isolines (pressure, density and velocity) and compare them with available interferometric or other experimental data. For example, isopycnics are much more sensitive indicators of the accuracy of a given numerical method than a comparison of shock shapes (Ref. 1). Undoubtedly, such applications of the RCM will probably take place in the near future, as the need for such numerical methods now exists.

Available copies of this report are limited. Return this card to UTIAS, if you require a copy.

UTIAS REPORT NO. 240

Institute for Aerospace Studies, University of Toronto (UTIAS)
4925 Dufferin Street, Downsview, Ontario, Canada, M3H 5T6

APPLICATIONS OF RANDOM-CHOICE METHOD TO PROBLEMS IN SHOCK AND DETONATION-WAVE DYNAMICS

Saito, T., Glass, I. I.

1. Numerical Methods, 2. Shock waves, 3. Contact surfaces, 4. Rarefaction waves, 5. Blast waves, 6. Detonation waves

I. Saito, T., Glass, I. I. II. UTIAS Report No. 240

Although successful numerical methods exist for solving problems in shock and detonation-wave dynamics, there is still a real need of developing new techniques where the old methods fail to predict important flow properties. For example, it has recently been shown in Ref. 1 that existing methods fail to predict the interferometrically measured isopycnics in regular and single Mach reflections (let alone complex and double-Mach reflections, for which numerical solutions do not even exist). The purpose of the present report is to present eight applications of the Random-Choice Method (RCM) to the solution of problems in shock and detonation-wave dynamics. It is shown that unlike other numerical methods, the RCM yields sharp-fronted shocks and contact surfaces without resorting to artificial and perhaps erroneous means of predicting their locations, which depend more on art than science. It is also a very useful method in showing such fine points as the birth point of the second shock (implosion) wave at the tail of the rarefaction wave in a spherical explosion.

Despite all these advantages the RCM has yet to be developed to cope with problems such as oblique and spherical shock-wave reflections in order to compute the various isolines (pressure, density and velocity) and compare them with available interferometric or other experimental data. For example, isopycnics are much more sensitive indicators of the accuracy of a given numerical method than a comparison of shock shapes (Ref. 1). Undoubtedly, such applications of the RCM will probably take place in the near future, as the need for such numerical methods now exists.

Available copies of this report are limited. Return this card to UTIAS, if you require a copy.

UTIAS REPORT NO. 240

Institute for Aerospace Studies, University of Toronto (UTIAS)
4925 Dufferin Street, Downsview, Ontario, Canada, M3H 5T6

APPLICATIONS OF RANDOM-CHOICE METHOD TO PROBLEMS IN SHOCK AND DETONATION-WAVE DYNAMICS

Saito, T., Glass, I. I.

1. Numerical Methods, 2. Shock waves, 3. Contact surfaces, 4. Rarefaction waves, 5. Blast waves, 6. Detonation waves

I. Saito, T., Glass, I. I. II. UTIAS Report No. 240

Although successful numerical methods exist for solving problems in shock and detonation-wave dynamics, there is still a real need of developing new techniques where the old methods fail to predict important flow properties. For example, it has recently been shown in Ref. 1 that existing methods fail to predict the interferometrically measured isopycnics in regular and single Mach reflections (let alone complex and double-Mach reflections, for which numerical solutions do not even exist). The purpose of the present report is to present eight applications of the Random-Choice Method (RCM) to the solution of problems in shock and detonation-wave dynamics. It is shown that unlike other numerical methods, the RCM yields sharp-fronted shocks and contact surfaces without resorting to artificial and perhaps erroneous means of predicting their locations, which depend more on art than science. It is also a very useful method in showing such fine points as the birth point of the second shock (implosion) wave at the tail of the rarefaction wave in a spherical explosion.

Despite all these advantages the RCM has yet to be developed to cope with problems such as oblique and spherical shock-wave reflections in order to compute the various isolines (pressure, density and velocity) and compare them with available interferometric or other experimental data. For example, isopycnics are much more sensitive indicators of the accuracy of a given numerical method than a comparison of shock shapes (Ref. 1). Undoubtedly, such applications of the RCM will probably take place in the near future, as the need for such numerical methods now exists.

Available copies of this report are limited. Return this card to UTIAS, if you require a copy.